Zeitschrift: Helvetica Physica Acta
Band: 54 (1981)
Heft: 4

Artikel: The electronic structure of hydrogen in elemental metals in the light of muon spin rotation (SR) investigations
Autor: Schenck, Alexander
DOI: https://doi.org/10.5169/seals-115225

Helvetica Physica Acta
Vol. 54, 1981

0018-0238/81/040552-09$1.50+0.20/0
Birkhäuser Verlag, Basel

The electronic structure of hydrogen in elemental metals in the light of muon spin rotation (μSR) investigations[1])

Alexander Schenck, Laboratorium für Hochenergiephysik der ETH Zürich, c/o SIN, CH-5234 Villigen, Switzerland

(26. X. 1981)

Abstract. From a solid state and chemical point of view a positive muon (μ^+) can be considered a light isotope of the proton. Positive muons implanted in metals exhibit therefore properties which are closely related to corresponding properties of hydrogen in metals. Notably the electronic structure around the two particles should be identical to the extent that isotope effects can be neglected. On this premise a comprehensive review on the present status of Knight shift (KS) measurements of μ^+ implanted in elemental nontransition (Li, K, Na, Rb, Cs, Cu, Ag, Be, Mg, Ca, Sr, Ba, Hg, Al, Ga, Pb) and transition (V, Nb, Ta, Pd, paramagnetic Ni) metals is presented. In addition measurements of the electric field gradients exerted on μ^+ nearest neighbor host nuclei will be discussed. The data are compared with existing predictions from nonlinear jellium, cluster and band structure calculations. Certain tendencies of the KS-data from cubic simple metals are used to speculate on possible mechanisms involved. By comparison with proton KS-data in Nb, Ta, V and Pd interesting aspects of isotope effects become evident.

I. Introduction

For several years it has become increasingly evident that the positive muon is a potentially powerful tool [1–5] in the study of the magnetic [6, 7] and electronic properties of metals, in particular at interstitial sites in the material. An interesting aspect of the study of implanted positive muons in metals is that the muon can be considered a light isotope of the proton ($m_\mu \cong \frac{1}{9} \cdot m_p$). Thus by studying its properties in metals one is in fact studying the properties of hydrogen in metals [8, 9] extended to a much smaller isotopic mass. To the extent that isotope effects are unimportant, the positive muon serves as a convenient and often unique hydrogen substitute.

Concerning this substitute aspect, most experimental work so far has concentrated on investigations of the diffusional behavior of positive muons in metals [10, 11]. A wealth of information has been obtained, but it is as yet not clear as to how far it can contribute to a deeper understanding of the diffusion of hydrogen in metals in general. Hydrogen diffusion studies have been performed in most cases at high temperatures [8] (typically $T > \theta_D$), while the muon work has been done at relatively low temperatures ($T \lesssim \theta_D$). The features of the muon diffusion at low temperatures are determined by a hierarchy of traps, which seem to be

[1]) This paper is based on the Habilitationsschrift of the author submitted to the ETH in partial fulfillment for obtaining the venia legendi.

unavoidable even in the extremely pure samples investigated so far [10, 11]. These relatively shallow traps are negligible at higher temperatures. It therefore seems that one is studying quite different mechanisms by observing either the diffusion of protons at high temperatures or the diffusion of muons at low temperatures, and it is not possible at the moment to relate the results to each other.

However, aside from this incongruity in the motional aspects of the two 'hydrogen' isotopes, there are other aspects where muons and protons seem to behave analogously. In particular the two 'isotopes' seem to show a preference to reside at the same types of interstitital sites, e.g. in fcc-Cu at the octahedral interstitial site [12, 13], in fcc-Al at the tetrahedral interstitial site [14, 15], in bcc-Nb [8, 16], -Ta [8, 17], and -V [8, 18] at the tetrahedral interstitial sites. Some partial occupation of octahedral interstitial sites in Al, Nb, Ta and V by muons cannot be ruled out [15, 18]. In the case of Al the tetrahedral site occupation of both muons [15] and protons [14] seems to be related to trapping. This can be taken as an indication, that the most basic property, i.e. the local electronic structure of the impurity-metal complex is identical for both particles within the limits of the Born–Oppenheimer approximation. In vacuum the atoms hydrogen and muonium (μ^+e^-) have binding energies and Bohr radii which differ by only $\sim$0.5% as a result of the slightly different effective masses of the 1*s*-electrons.

It is this close identity expected for the electronic structure of protons and muons in metals, and on the other hand the scarcity of experimental information on the electronic structure of hydrogen in metals which has motivated and stimulated corresponding investigations with muons.

For hydrogen in metals most information stems from magnetic susceptibility and specific heat measurements as a function of hydrogen concentration [8]. The Pauli part of the magnetic susceptibility and the electronic contribution to the specific heat are both proportional to the density of states at the Fermi energy and are therefore more reflecting changes in the bulk electronic properties of the metal-hydrogen system rather than revealing details about the local electronic structure of the hydrogen-metal complex. It should be emphasized at this point that a detailed understanding of the local electronic structure is basic to a detailed understanding of other important properties, such as the nature of localization or delocalization of the hydrogen, the site of localization, the amount and symmetry of a local lattice distortion or small polaron formation, hydrogen diffusion (activation energies etc.), the occurrence of tunneling states, interaction with traps etc. [8, 19–22].

More direct information on the local electronic structure is contained in the measurement of the Knight shift of the proton magnetic resonance (NMR) frequency in metals which is proportional to the local spin density at the impurity site. The local spin density reflects a particular property of the established electronic structure. In addition, other effects might produce a shift in the resonance frequency, which can also be related to the local electronic structure. In particular one might expect to obtain hints on the presence or absence of bound states (H, H^+, H^-) and/or bonding states in the local hydrogen-metal complex or cluster, and on the relative contribution of scattering (Bloch) states to the total screening of the positive proton or muon charge. So far only a few photo emission studies have given indications that well localized impurity states are formed, for instance in PdH_x [22], in NbH_x [23] and in VH_x [24].

Despite the importance of 'Knight shift' measurements of the proton-NMR frequency in metals only very few such measurements have been performed so far [25–28] probably because of a variety of experimental problems. In contrast it is relatively easy to measure the Knight shift with implanted positive muons in any kind of metal or alloy, independent of whether its hydrogen solubility is high or low, whether it is in the form of a single crystal or polycrystalline and independent of size and shape. (The shape matters only in so far, as corrections for demagnetization fields may become difficult to calculate.) In this respect positive muons seem to be ideal substitutes for protons and the information obtained should be representative of the electronic structure of hydrogen in metals in general.

In view of this a series of Knight shift measurements using positive muons have recently been performed in elementary nontransition (simple) and transition metals. Nontransition metals investigated were: all members of the alkali and alkaline earth series and Cu, Ag, Al, Ga, Zn, Cd, Hg and Pb [29–31]. Some of the metals were investigated both in the solid and in the liquid phase (Rb, Cs, Ga, Hg) [30] (see Table 7). Measurements in transition metals were performed in V, Nb, Ta [32], Pd [33] and paramagnetic Ni [34] (see Tables 9–11). We will also mention some measurements in the semi metal Sb, which yielded results of a quite different type [35]. We will not discuss results that have been obtained in the composite systems $LaNi_5H_x$ [36], MnSi [37] and CeTh [38].

Quite interesting and complementary information was obtained from the measurement of electric field gradients exerted by the muon on the nearest neighbor host nuclei in Cu [13] and Al [15]. While the Knight shift depends only on the spin density at the impurity site, measurements of the electric field gradient at some distance from the impurity will give information on the spatial structure of the charge distribution around the impurity.

It is the aim of this report to review these measurements and to discuss the results in the frame work of recent theoretical calculations on the electronic structure of hydrogen in metals. Since this field, concerning both experiment and theory, is in a state of rapid development, this report should be considered as a status report only.

Since all studies, discussed here, were performed in the infinite dilute limit (only one 'hydrogen' present at a time) the discussion will address itself to those aspects that concern the impurity and its immediate surroundings only, while bulk properties, which remain unchanged from the pure host metal are not considered. This means in particular that the discussion will be done on the basis of local theories of the electronic structure of the hydrogen-metal complex and of the screening of the impurity. Since most local theories refer to protons or muons in 'simple' metals, the bulk of the Knight shift measurements have been performed in nontransition metals too.

In the following Chapter II we will first present a short treatise of the muon spin rotation (μSR) technique by means of which the measurements were performed. In Chapter III a short introduction to the contact hyperfine interaction in metals and the Knight shift will be given, followed in Chapter IV by a survey over existing theories on the electronic structure of hydrogen in metals. The experimental results from various measurements are collected in Chapter V and Chapter VI contains the discussion of the data and the comparison with theoretical predictions. The paper closes with a summary in Chapter VII.

II. The principles of the μSR method

2.1. *Introduction*

μSR stands for muon spin rotation, relaxation, resonance etc. The mnemonic acronym emphasizes the close correspondence to nuclear magnetic resonance (NMR) and electron spin resonance (ESR). The method is further completely analogous to γe or $\gamma\gamma$ perturbed angular-correlation and distribution measurements. The technique rests on the asymmetric distribution of the decay electrons with respect to the muon spin which follows from the parity violation in the muon decay. A necessary practical prerequisite for exploiting this effect, namely the availability of spin polarized muon beams, is also given since muon beams naturally show a high degree of polarization due to the way in which these beams are formed from pions decaying in flight. As is well known, muons are 100% spin polarized with respect to their momentum in the rest frame of the pion. Muon beams with a polarization of 70% or more are quire common. It is also an established fact that practically no depolarization occurs during the rapid slowing down process of muons in matter [1, 2]. The implanted muons show therefore the full polarization of the used muon beam at the moment of thermalization.

The μSR-technique allows to monitor the subsequent evolution of the muons polarization which is determined by local magnetic fields at the muon's site. In this way it becomes possible to study properties of these local fields which are related to characteristic features of the host material and also to the further behavior of the implanted muons.

2.2. *The decay of the positive muon and* μSR

The muon decays weakly in the following way:

$$\mu^+ \rightarrow e^+ + \nu_e + \bar{\nu}_\mu$$

with an average lifetime of

$$\tau_\mu = 2.19712(8) \cdot 10^{-6}\,\text{sec}$$

Other properties of the muon are listed in Table 1. The positron spectrum is given by the following expression that can be derived rigorously from the 4 fermion current–current interaction:

$$\begin{aligned}\frac{dN(w,\theta)}{dw\,d\Omega} &= \frac{w^2}{2\pi}[(3-2w)-P(1-2w)\cos\theta] \\ &= \frac{c}{2\pi}[1+A\cdot\cos\theta]\end{aligned} \tag{2.2.1}$$

where $w = E/E_{\max}$ is the positron energy measured in units of the maximal possible energy $E_{\max} = m_\mu/2 = 52.8\,\text{MeV}$. The expression in the brackets shows the asymmetric distribution of the positrons, where θ is the angle between the spin of the decaying muon and the positive trajectory. On the average the spin direction is given by the spin polarization vector **P**.

Table 1
Properties of the muon

Mass	$105.6595(3)\ \mathrm{MeV/c^2} = 206.7684(6) \cdot m_e = 0.1126 \cdot m_p$
charge:	$+e, -e$
spin:	1/2
Mag. Moment	$\mu_\mu = \frac{1}{2}\frac{e\hbar}{mc} gS_z = 3.1833448(29) \cdot \mu_p$
Gyromag. ratio	$\gamma_\mu = 13.55 \cdot 10^3$ Hz/Gauss
average lifetime	$\tau_\mu = 2.19712(8)\ \mu$sec
decay	$\mu^+ \to e^+ + \nu_e + \bar{\nu}_\mu$
	$\mu^- \to e^- + \bar{\nu}_e + \nu_\mu$
angular distribution of e^+, e^-	$dN_e \pm \cong (1 \pm A \cdot \cos\theta)\, d\Omega$
	$A \sim 0.3, \theta = \sphericalangle(\mathbf{S}_\mu, \mathbf{P}_e \pm)$
production	$\pi^\pm \to \mu^\pm + \nu_\mu(\bar{\nu}_\mu)$
	$\tau_\pi = 2.6 \cdot 10^{-8}$ sec

The asymmetry parameter A is a function of the positron energy

$$A = P\frac{2w-1}{3-2w} \tag{2.2.2}$$

with $P = |\mathbf{P}|$ degree of the spin polarization of the decaying muons.

In practice, the positrons are detected with an efficiency $\varepsilon(w)$ which will not be constant over the entire range due to absorption and scattering in the target and the counters as well as to the effect of an external magnetic field on the positron trajectories.

The observed probability distribution is then (integrated over energy)

$$\frac{dN(\theta)}{d\Omega} = \int_0^1 \left[\frac{dN(\theta, w)}{dw\, d\Omega}\right] \cdot \varepsilon(w)\, dw$$

$$= \frac{1}{4\pi} N_0 \cdot (1 + P\bar{a}\cos\theta) \tag{2.2.3}$$

If all positrons were detected with the same efficiency, the observed average asymmetry $\bar{a}$ would be $\frac{1}{3}$. Usually the low energy positrons have only a reduced detection efficiency which results in an $\bar{a}$ greater than $\frac{1}{3}$. In practice, however, this effect is counterbalanced by a reduction of the average asymmetry due to the finite detection angle. The resulting effective asymmetry $\bar{a} \cdot P$ at the instant of thermalization varies in the different experiments from about 0.18 to 0.3.

The measurement of the positron distribution will determine the direction and, except for the factor $\bar{a}$, the value of the polarization $|\mathbf{P}|$ of the observed muon ensemble. This is the basic principle of the μSR-method.

2.3. *The time differential μSR-method*

The implanted muons will interact with internal or external magnetic fields which cause the muon spins to precess in a very characteristic manner, i.e. the polarization **P** will become time-dependent. To make this time dependence visible

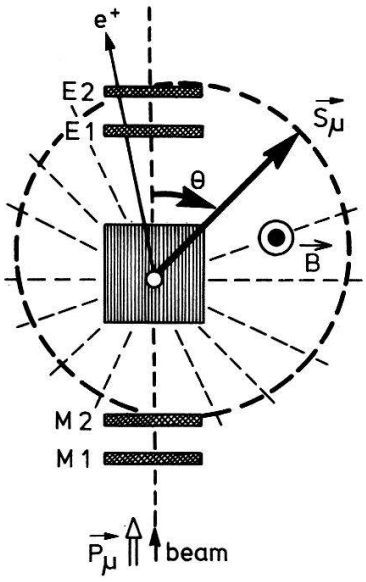

Figure 1
Schematic experimental arrangement in a transverse field. The asymmetric decay pattern is rotating past the position telescope $E_1 \cdot E_2$.

the decay positron rate has to be monitored in some fixed direction **r** as a function of the time that the muons have spent in the target:

$$dN(\theta, t) = \frac{1}{4\pi\tau_\mu} e^{-t/\tau_\mu}(1 + \bar{a}\,|\mathbf{P}(t)|\cos\theta(t))\,d\Omega\,dt \tag{2.3.1}$$

$\theta(t)$ = angle between **r** and $\mathbf{P}(t)$.

The exponential factor is due to the decay of the muon.

Experimentally one has to measure for each implanted muon its individual life time and to form a rate versus time histogram [39, 40]. In the following we will only consider an experimental arrangement in which an applied magnetic field is oriented perpendicular to the beam axis or the initial muon polarization, respectively (transverse field technique). This implies that the stopped muons will start to precess in a plane perpendicular to the direction of the magnetic field. The precision or Larmor frequency is given by

$$\nu = \frac{2\mu_\mu B}{h} = \frac{g_\mu e B}{4\pi m_\mu c} \simeq 13.55\,\frac{\text{kHz}}{\text{gauss}} \times B \tag{2.3.2}$$

The experimental arrangement for making the precession visible is shown in Fig. 1. The spin polarization vector, or the asymmetric positron distribution, respectively, rotates in the plane of the diagram. Observing the positrons with the detector telescope ($E1 \cdot E2$) the average angle between the spin polarization vector and the positron trajectories, will change according to

$$\theta = \omega t$$

and the distribution of positrons in time is recorded like

$$dN(t) \simeq \frac{1}{\tau_\mu} \exp(-t/\tau_\mu)(1 + \bar{a}P(t)\cos(\omega t + \phi))\,dt \tag{2.3.4}$$

ϕ is a phase that indicates the angle between the initial muon polarization $\mathbf{P}(0)$

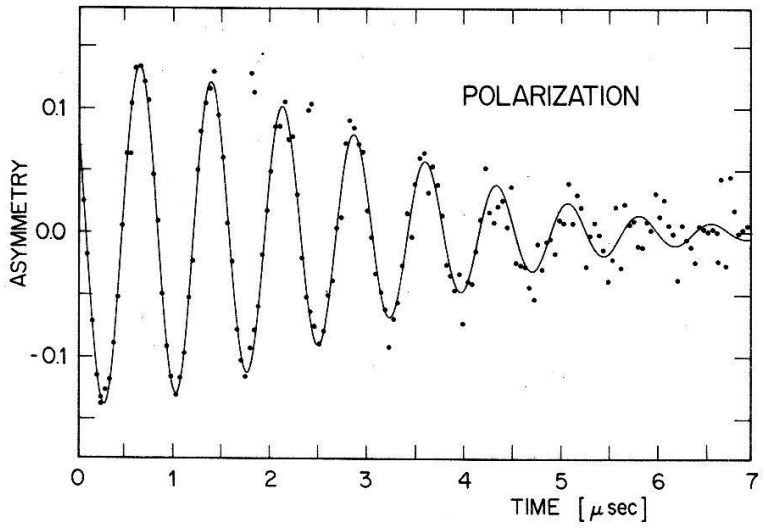

Figure 2
Experimental precession signal $a \cdot P(t) \cos \omega t$ from muons in Cu at low temperature. The exponential decay due to the muon life time has been removed. The decrease in polarization or precession amplitude, respectively is in this instance described by a Gaussian function $P(t)$.

and the axis of the positron detector telescope. Equation (2.3.4) shows that the precession manifests itself by a cosine modulation of the time dependent positron rate. The polarization P may show an intrinsic time dependence $P(t)$.

A decrease of $P(t)$ in time is a consequence of some spin depolarization or relaxation processes. Depolarization in a transverse field is a consequence of the loss of phase coherence between the precessing spins. No energy exchange need to be involved. The loss of phase coherence always takes place when the magnetic field strength is not infinitely sharp but instead shows a certain distribution in space about some average value. The corresponding spread in muon precession rates will lead after some time, to the presence of a random distribution of spin directions in the muon ensemble. As an example Fig. 2 shows the oscillatory part of an experimental spectrum (the exponential decay is removed) which displays a decreasing $P(t)$ (in this instance $P(t)$ is given by a Gaussian relaxation function).

Inspecting equation (2.3.4) we see that the interesting and characteristic information is contained in the parameters ω (=average local magnetic field at the μ^+), $\bar{a}$ (=fraction of μ^+ which precess at ω), ϕ (=phase of initial polarization $\mathbf{P}(0)$ of μ^+ precessing with ω with respect to the axis of the positron telescope) and in the specific details of the time dependence of $P(t)$, the relaxation function. With respect to Knight shift measurements we are particularly interested in a precession determination of the parameter ω.

The time differential method requires the observation of individual muon decays. This limits the muon stopping rate to about several 10^4/sec. Otherwise the identification of individual decay events is increasingly impossible. In view of the high stopping rates at the meson factories ($>10^6 \mu^+$/sec at SIN) this is a very undesirable property of the time differential μSR-method. An alternative integral technique is discussed in the next section.

2.4. *The stroboscopic method*

This method was used for all the Knight shift measurements to be discussed. It can be applied if the intensity of the muon beam can be modulated periodically.

The principle of the method consists in letting the muons precess with a frequency close to an integral multiple of the frequency Ω with which the intensity of the muon beam is modulated [3].

Muons entering the target thus have almost the same spin phase as the ones that have already spent some time in the target. In effect, most muons, independent of their arrival time, will precess more or less coherently. The coherence is strongest at

$$\omega_\mu = n\Omega \qquad (n = 1, 2, \ldots)$$

and vanishes for

$$|\omega_\mu - n\Omega| > \frac{1}{\tau_\mu}$$

The degree of coherence is detected by measuring the positron rate in a time window (gate) of suitable length and suitable phase with respect to the beam intensity modulation. This will be called the stroboscopic signal.

Such a method has been first applied by Christiansen et al. in a $\gamma\gamma$PAD experiment [41] and was first applied to muons by Camani et al. [42].

The stroboscopic signal and its line shape can be derived as follows assuming the beam to display a periodic burst structure [43]. The stopping rate of positive muons is given by the burst structure of the beam: $F(t) = F(t+nT)$, $n = 1, 2, \ldots, 2\pi/T = \Omega$. The positrons are recorded in time windows that are synchronous with the burst structure. The time structure of the windows or gates may be described by $G(t) = G(t+nT)$, $n = 1, 2, \ldots$. The gated positron rate accumulated between times t_A and t_E is then given by (assuming no depolarization)

$$\begin{aligned}\langle N_e + \rangle &= \frac{1}{\tau_\mu} \int_{t_A}^{t_E} dt G(t) \int_{-\infty}^{t} dt_s F(t_s) e^{-(t-t_s)/\tau_\mu} [1 + \tilde{A} \cos(\omega(t-t_s) + \tilde{\phi})] \\ &= \frac{1}{\tau_\mu} \int_{t_A}^{t_E} dt G(t) \int_{0}^{\infty} dt' F(t-t') e^{-t'/\tau_\mu} [1 + \tilde{A} \cos(\omega t' + \tilde{\phi})] \end{aligned} \tag{2.4.1}$$

The wiggles on A and ϕ indicate that proper averages due to the experimental conditions have been taken.

The function

$$S(t') = \frac{1}{t_E - t_A} \int_{t_A}^{t_E} dt G(t) F(t-t') \tag{2.4.2}$$

is called the stroboscopic structure function. Clearly it is a periodic function of time.

We express $S(t)$ by its Fourier expansion

$$S(t) \sum_{\nu=-\infty}^{\infty} C_\nu(S) e^{+i\nu\Omega t} \tag{2.4.3}$$

with

$$C_\nu(S) = \frac{1}{T} \int_0^T S(t) e^{-i\nu\Omega t} \tag{2.4.4}$$

Equation (2.4.1) can now easily be evaluated

$$\frac{\langle N_{e^+}\rangle}{t_E - t_A} = S(\omega) = \frac{1}{\tau_\mu}\int_0^\infty dt \sum_\nu C_\nu(S) e^{(i\nu\Omega - 1/\tau_\mu)t}(1 + \tilde{A}\cos(\omega t + \tilde{\phi}))$$

$$= \text{const} + \tilde{A}\sum_\nu \left[\text{Re}\{C_\nu(S)e^{i\tilde{\phi}}\}\cdot \frac{1}{1+(\omega-\nu\Omega)^2\tau_\mu^2}\right.$$

$$\left. + \text{Im}\{C_\nu(S)e^{i\phi}\}\cdot \frac{\omega - \nu\Omega}{1+(\omega-\nu\Omega)^2\tau_\mu^2}\right] \qquad (2.4.5)$$

$S(\omega)$ is called the normalized stroboscopic signal. It consists of a constant and a resonance term. The latter one is a superposition of Lorentzian and dispersion curves. The real and imaginary parts of $C_\nu(s)e^{i\tilde{\phi}}$ contain all the information on the beam structure, the time windows and the telescope position. The line width is solely determined by the μ^+ lifetime and is given by $\Delta\omega_0 = 2/\tau_\mu$.

It can be shown that e.g. for $\omega \cong 2\Omega$ all terms with $\nu \neq 2$ contribute only negligibly to the signal [43].

The signal, or the line shape $S(\omega)$ is presented in a completely parameterized analytical expression into which the actual beam structure and the position and width of the time windows is absorbed. It is obvious, since the method involves only counting of positrons, that there is no limitation on the event rate, at least as far as the method in principle is concerned.

A second advantageous feature of this method was realized in its application at SIN. Here the beam burst structure is the result of the acceleration, involving *rf* cavities. The *rf*-frequency (= 50.63 MHz) is derived from a quartz master oscillator which exhibits a stability of the order of 10^{-8}. The beam burst structure exhibits then the same repetition frequency with a corresponding stability and accuracy. The stroboscopic method involves therefore a comparison of the muon Larmor frequency with an extremely well known reference frequency. In the actual experiment the Larmor frequency was chosen to correspond to twice the beam burst repetition frequency.

In the experiment the stroboscopic signal is observed by changing the external magnetic field or the muon Larmor frequency ω_μ, respectively, over the resonance condition $\omega_\mu = 2 \cdot \Omega$. An example is shown in Fig. 3.

So far it was assumed that the muon's polarization was not subject to relaxation. If relaxation is present the shape and/or the width of the normalized stroboscopic signal $S(\omega)$ will be changed. This can be easily implemented into the above line shape theory by replacing the constant $\tilde{A}$ by $\tilde{A} \cdot P(t)$ in equation (2.4.1).

2.5. *Static dipolar depolarization and the manifestation of electric field gradients*

In this section we mention a particular relaxation mechanism, which can reveal much of the muon's local environment in a lattice and which is exploited for determining the site of localization, the local lattice distortion and, in an indirect way, the magnitude of possible electric field gradients at the neighbor host nuclei.

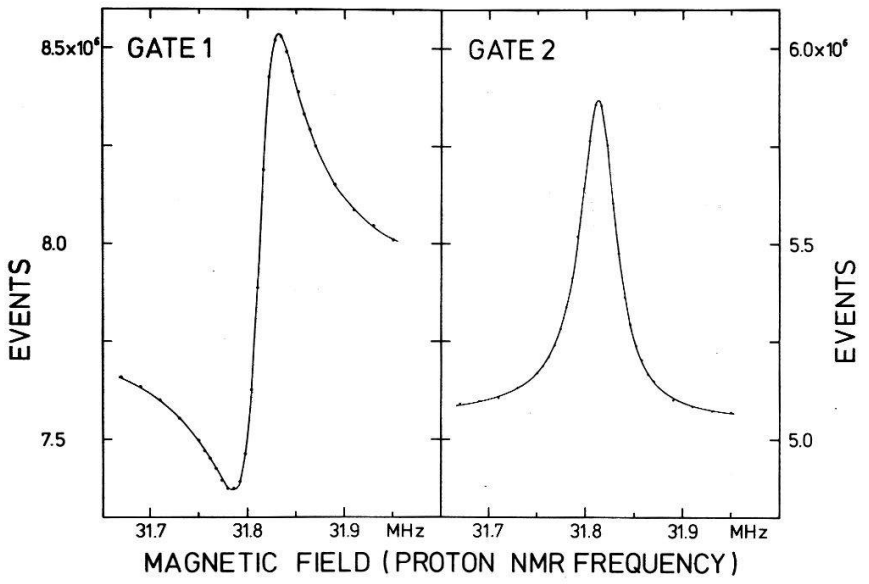

Figure 3
Example of stroboscopic signals from two different gates (from Ref. 43). Plotted is the normalized countrate $S(\omega_\mu)$ versus the proton NMR-frequency ω_p, which measures the field and which is proportional to the muon precession frequency ω_μ (see also equations (5.1.2) and (5.1.3)). The field was choosen such that $\omega_\mu \sim 2\Omega$ (= second harmonic of the beam burst repetition frequency).

This relaxation mechanism is present under the following conditions.

(i) The host lattice atoms must possess nuclei with nonzero magnetic moments or local electronic magnetic moments. Any dynamics of this system of moments or spins, respectively, must be slow compared with the muon life time (this excludes electronic moments in the paramagnetic state).

(ii) The muon must remain at some particular lattice site for times long compared with $\langle \Delta\omega^2 \rangle^{-1/2}$, where $\langle \Delta\omega^2 \rangle$ is the average quadratic spread of nuclear or electronic dipole fields at the muon position; that is, the muon diffusion must be slow or absent.

Because of the spread in dipole field components from site to site, adding to the applied external magnetic field, the ensemble of muons, sampling over the different possible sites, will show a spectrum of frequencies, centered around the frequency ω_0 determined by the external magnetic field. The superposition of all these frequencies will lead to a depolarization which can be well approximated by a Gaussian function [44]

$$A(t) = A_0 \cdot \exp(-\sigma^2 t^2) \tag{2.5.1}$$

The corresponding effect in Nuclear Magnetic Resonance will be a line broadening (dipolar line broadening), which has been treated theoretically by Van Vleck [45, 44].

Under the assumption that the applied external magnetic field is much larger than the nuclear dipole fields, which we will only consider henceforth ($\omega_0 \gg \Delta\omega$), the damping constant σ is given by [44]

$$\sigma^2 = \langle \omega^2 \rangle = \tfrac{1}{2} M_2 \tag{2.5.2}$$

where M_2 is the second moment of the dipolar field spread. For a single crystal

M_2 is given by

$$M_2 = \tfrac{1}{3} I(I+1)\hbar^2 \gamma_\mu^2 \gamma_I^2 \sum_i \frac{(1-3\cos^2\theta_i)^2}{r_i^6} \tag{2.5.3}$$

I = host nuclear spin, γ_μ = gyromagnetic ratio of muon, γ_I = gyromagnetic ratio of host nucleus, θ_i = angle between external magnetic field (z-direction) and the vector $\mathbf{r}_i$ connecting the muon and the ith-neighbor nucleus. The sum extends over all host nuclei (lattice sum).

M_2 will depend on the orientation of the crystal with respect to the external magnetic field. It is independent of the strength of the external magnetic field (as long as $\Delta\omega \ll \omega_0$). The orientation dependence of σ or M_2, respectively can be used to determine the site of the probe, i.e. of the muon. A deviation of an experimental σ from the prediction of equation (2.5.3), assuming a rigid lattice, is indicative of a lattice distortion around the probe site, i.e. the muon site.

It has been shown by Meier [46] that the second moment is not changed if the muon charge is distributed spherically around the center of an interstitial site as long as there is no overlap with the neighboring host nuclei. An extended μ^+-wave function is always to be expected on account of its zero point motion in the interstitial potential well.

So far it was implicitly assumed that the nuclear spins were only subjected to a Zeeman interaction. The direction of the external magnetic field provided a convenient axis of quantization and the expectation values for the nuclear spins along this direction were readily evaluated. This situation changes, if the following third condition is fulfilled.

(iii) The host nuclei possess spin $I \geq 1$ and a nonzero electric quadrupole moment.

The presence of some electric field gradient (EFG) will give rise to a quadrupole interaction which is in competition with the Zeeman interaction. Evaluation of the expectation values of the nuclear spins requires now a diagonalization of the total Hamiltonian acting on the nuclear spins. In effect one will obtain not only a static expectation value in the z-direction but also a static one in the x-direction [47]. The second moment will then read

$$M_2 = \hbar^2 \gamma_\mu^2 \gamma_I^2 \sum_i \left(\overline{\langle S_z \rangle_i^2} \frac{(1-3\cos^2\theta_i)^2}{r_i^6} + \overline{\langle S_x \rangle_i^2} \frac{9\sin^2\theta_i \cos^2\theta_i}{r_i^6} \right) \tag{2.5.4}$$

where $\overline{\langle S_z \rangle_i^2}$ and $\overline{\langle S_x \rangle_i^2}$ are the average squared expectation values in z and x direction for the ith nuclear spin. $\overline{\langle S_z \rangle^2}$ and $\overline{\langle S_x \rangle^2}$ will now depend on the strength of the external magnetic field. For very strong external magnetic fields the quadrupole interaction will become quenched and one obtains

$$\overline{\langle S_z \rangle^2} = \frac{I(I+1)}{3} \quad \text{and} \quad \overline{\langle S_x \rangle^2} = 0$$

which will reduce equation (2.5.4) to the Van Vleck expression equation (2.5.3). This behavior has been envisioned and treated theoretically for the first time by O. Hartmann [47].

Measurement of the field dependence of the second moment or of the

damping of the muon precession amplitude, respectively will allow the determination of the magnitude of the EFG acting on the neighbor host nuclei.

The origin of the field gradient may be the screened potential of the muon itself, in which case the electric field gradient will fall off quickly with distance, or may be a local lattice distortion, which in cubic metals destroys the cubic symmetry locally, thereby producing an electric field gradient.

III. Hyperfine interaction, Knight shift and diamagnetic screening

Positive muons or protons in a metal will interact electrostatically strongly with the conduction electrons and perhaps also with more localized core electrons. This interaction will determine the electronic structure of the screened impurity and in particular the density of electrons around and at the impurity.

In so far the electrons have s-character with respect to the muon or proton there will be a magnetic interaction of the Fermi contact type. This hyperfine interaction will result in a net magnetic hyperfine field if the electrons at the impurity site possess a net spin polarization. In addition, if the spin polarized electrons around the muon are distributed nonspherically a net dipolar field contribution at the impurity will result. This effect which of course will only be observable in single crystal samples will manifest itself in an anisotropic behavior. Finally, one has to consider diamagnetic screening resulting from currents induced by an external magnetic field.

Most generally the contact hyperfine field at the impurity (r_μ) can be written as [48]

$$B_{hf}(r_\mu)=\frac{8\pi}{3}\mu_B(n^+(r_\mu)-n^-(r_\mu)) \tag{3.1.1}$$

$n^\pm(r_\mu)$ are the density of (conduction) electrons at the impurity (r_μ) with spin up (+) or spin down (−), respectively. The difference $n^+(r_\mu)-n^-(r_\mu)$ is the spin density at the impurity (local spin density). The nonzero spin density is supposed to be induced by an external magnetic field (B_{ext}). $B_{hf}(r_\mu)$ is thus an additional field acting on the muon or proton. This additional field is defined as the direct Knight shift.

We may therefore write

$$B_{hf}(r_\mu)=K\cdot B_{ext}$$

where K is the Knight shift constant. This constant may more properly be defined as

$$K=\frac{dB_{hf}(r_\mu)}{dB_{ext}}=\frac{8\pi}{3}\mu_B\frac{d(n^+(r_\mu)-n^-(r_\mu))}{dB_{ext}} \tag{3.1.2}$$

The spin density can be expressed as follows [48]

$$n^+(r_\mu)-n^-(r_\mu)=\frac{1}{N}\sum_{\mathbf{k}}(f^+(\varepsilon_{\mathbf{k}})\,|\psi^+_{\mathbf{k}}(r_\mu)|^2-f^-(\varepsilon_{\mathbf{k}})\,|\psi^-_{\mathbf{k}}(r_\mu)|^2) \tag{3.1.3}$$

N is the total number of conduction electrons, $\psi^\pm_{\mathbf{k}}(r)$ are one electron wave functions, normalized to unity over the volume $\Omega_e=V/N=1/n_0$, $f^\pm(\varepsilon_{\mathbf{k}})$ are the corresponding occupation probabilities (Fermi–Dirac function).

Applying equation (3.1.2) one obtains for the Knight shift constant

$$K=\frac{8\pi}{3}\mu_B\frac{d}{dB_{\text{ext}}}\left[\frac{1}{N}\sum_{\mathbf{k}}\left(f^+(\varepsilon_{\mathbf{k}})\,|\psi^+_{\mathbf{k}}(r_\mu)|^2-f^-(\varepsilon_{\mathbf{k}})\,|\psi^-_{\mathbf{k}}(r_\mu)|^2\right)\right]$$
$$=\frac{8\pi}{3}\mu_B\frac{d}{dB_{\text{ext}}}\Omega_e\int_0^\infty\left[d\varepsilon\frac{1}{(2\pi)^3}\int\frac{dS^+_\varepsilon}{\text{grad}_{\mathbf{k}}\,\varepsilon}|\psi^+_{\mathbf{k}}(r_\mu|^2 f^+(\varepsilon)\right.$$
$$\left.-\frac{1}{(2\pi)^3}\int\frac{dS^-_\varepsilon}{|\text{grad}_{\mathbf{k}}\,\varepsilon|}|\psi^-_{\mathbf{k}}(r_\mu)|^2 f^-(\varepsilon)\right] \tag{3.1.4}$$

Here $dS^\pm_\varepsilon$ are elements of area on a surface of constant ε in $\mathbf{k}$-space (momentum space). Explicitly only the occupation functions $f^\pm(\varepsilon_{\mathbf{k}})$ are field dependent

$$f^\pm(\varepsilon_{\mathbf{k}})=\left(\exp\left[(\varepsilon_{\mathbf{k}}\pm\mu_B\cdot B_{\text{ext}}-\mu)\frac{1}{kT}\right]+1\right)^{-1} \tag{3.1.5}$$

(μ = chemical potential which for $T\to 0K$ is the Fermi energy ε_F).

Implicitely also the wave functions $\psi^\pm(r)$ may depend on the applied field by way of spin dependent exchange and correlation potentials.

Neglecting the latter possibility for the moment equation (3.1.4) can be simplified by noting that for a paramagnetic metal

$$|\psi^+_{\mathbf{k}}(r_\mu)|^2=|\psi^-_{\mathbf{k}}(r_\mu)|^2=|\psi_{\mathbf{k}}(r_\mu)|^2 \tag{3.1.6}$$

and

$$\frac{dS^+_\varepsilon}{|\text{grad}_{\mathbf{k}}\,\varepsilon|}=\frac{dS^-_\varepsilon}{|\text{grad}_{\mathbf{k}}\,\varepsilon|}\quad\text{for}\quad\varepsilon<\varepsilon_F\ (\text{Fermienergy}) \tag{3.1.7}$$

consequently

$$K_s=\frac{8\pi}{3}\mu_B^2\Omega_e\int_{\varepsilon_F}\frac{dS_{\varepsilon_F}}{|\text{grad}_{\mathbf{k}}\,\varepsilon_F|}|\psi_{\mathbf{k}_F}(r_\mu)|^2. \tag{3.1.8}$$

The integral is taken over the Fermi surface. For a spherical Fermi surface one obtains simply:

$$K_s=\frac{8\pi}{3}\Omega_e\langle|\psi_{\mathbf{k}_F}(r_\mu)|^2\rangle_F\chi_F. \tag{3.1.9}$$

$\langle|\psi_{\mathbf{k}_F}(r_\mu)|^2\rangle_F$ is an average over the Fermi surface and (for noninteracting electrons)

$$\chi_F=\frac{2}{(2\pi)^3}\mu_B^2\int_{\varepsilon_F}\frac{dS_{\varepsilon_F}}{\text{grad}_{\mathbf{k}}\,\varepsilon_F}=\mu_B^2\cdot N(\varepsilon_F) \tag{3.1.10}$$

is the Pauli spin susceptibility. $N(\varepsilon_F)$ is the total density of states at the Fermi energy [cm^{-3}].

For a nonspherical Fermi surface and strongly varying $|\psi_{\mathbf{k}_F}(r_\mu)|^2$ over the Fermi surface, the factorization in equation (3.1.9) is not applicable strictly and one would have to resort to equation (3.1.8) (see e.g. Ref. 59). In what follows we will always assume that equation (3.1.9) is sufficiently accurate to be used in the analysis of the data.

For interacting electrons $\varepsilon_{\mathbf{k}}$ (the single particle energy at wave vector $\mathbf{k}$) will depend implicitly on χ too. In this case the enhanced susceptibility can be represented by the following expression

$$\chi_p = \frac{\mu_B^2 N(\varepsilon_F)}{1 - N(\varepsilon_F) I} \tag{3.1.11}$$

where I represents an exchange integral.

From the derivation of equation (3.1.9) it is seen that the Knight shift or the induced hyperfine field, respectively, are a consequence of the Pauli spin paramagnetism of the conduction electrons. Repopulation of the spin up and spin down states at the Fermi energy in the presence of an external magnetic field, leads to a spin polarization of the Fermi surface electrons, which then can produce a net contact hyperfine field at the muon or proton site. The dependence of the induced hyperfine field on the actual electronic structure at the impurity site in the presence of the muon or proton is seen from equation (3.1.9) by noting that $1/\Omega_e = n_0$ is the average conduction electron density. Hence

$$K_s = \frac{8\pi}{3} \frac{\langle |\psi_{k_F}(r_\mu)|^2 \rangle_F}{n_0} \chi_p = \frac{8\pi}{3} \eta_F(r_\mu) \chi_p \tag{3.1.12}$$

where $\eta_F(r_\mu)$ is a charge density enhancement factor concerning Fermi surface electrons.

With the chosen normalization of the one electron wave functions, χ is measured in [emu/cm^3]. Alternatively one may use a normalization over the atomic volume Ω_a

$$\int_{\Omega_a} |\psi(r)|^2 \, dv = 1. \tag{3.1.13}$$

Equation (3.1.2) would then read

$$n^+(r_\mu) - n^-(r_\mu) = \frac{\Omega_a}{V} \sum_{\mathbf{k}} (f^+(\varepsilon_{\mathbf{k}}) \, |\psi_{\mathbf{k}}^+(r_\mu)|^2 - f^-(\varepsilon_{\mathbf{k}}) \, |\psi_{\mathbf{k}}^-(r_\mu)|^2) \tag{3.1.14}$$

and equation (3.1.9) would become

$$\begin{aligned} K_s &= \frac{8\pi}{3} \langle |\psi_{\mathbf{k}_F}(r_\mu)|^2 \rangle_F \Omega_a \chi_p \\ &= \frac{8\pi}{3} \langle |\psi_{\mathbf{k}_F}(r_\mu)|^2 \rangle_F \chi_p^a. \end{aligned} \tag{3.1.15}$$

χ_p^a is now the atomic susceptibility. The Knight shift can also be expressed in terms of a hyperfine field per unpaired electron in some given volume Ω: $B_{hf}^{\Omega}(r_\mu)$

$$B_{hf}(r_\mu) = K \cdot B_{\text{ext}} = B_{hf}^{\Omega}(r_\mu)(n^+ - n^-)_\Omega \tag{3.1.16}$$

where $(n^+ - n^-)_\Omega$ is the total number of unpaired electrons in the volume Ω.

If $\Omega = \Omega_a$ we write

$$(n^+ - n^-)_{\Omega_a} = \frac{1}{\mu_B} \chi_p^a \cdot B_{\text{ext}} \tag{3.1.17}$$

or

$$K_s = \frac{1}{\mu_B} B_{hf}^{\Omega_a}(r_\mu)\chi_p^a \tag{3.1.18}$$

with

$$B_{hf}^{\Omega_a}(r_\mu) = \frac{8\pi}{3}\mu_B \langle|\psi_{\mathbf{k}_F}(r_\mu)|^2\rangle_F. \tag{3.1.19}$$

K_s is principally a positive number.

We will now allow also the wave functions to become field dependent, i.e. the spatial distribution of spin up and spin down electrons is supposed to change in different ways such that

$$\frac{d}{dB_{ext}}(|\psi_{\mathbf{k}}^+(r_\mu)|^2 - |\psi_{\mathbf{k}}^-(r_\mu)|^2) = \frac{dF_{\mathbf{k}}(B_{ext})}{dB_{ext}} \neq 0$$

This will lead to an additional term of the form

$$K_{cp} = \frac{8\pi}{3}\mu_B \frac{1}{N}\sum_k f(\varepsilon_k)\frac{dF_k(B_{ext})}{dB_{ext}} \tag{3.1.20}$$

The shift is now no longer determined solely by the properties of the wave functions at the Fermi energy, but involves other states with $k < k_F$ as well. The driving force behind this mechanism are exchange interactions with Fermi surface electrons, which are spin polarized by the external field ($\sim\chi_p \cdot B_{ext}$). This effect is usually named core polarization (CP) associated with the presence of core states in the atomic species used in conventional NMR investigations.

Although the muon does not possess an electron core in the usual sense one may, nevertheless, speak in this respect of something analogue to the well studied mechanism of core polarization. The next chapter will show that wave function distortions are indeed predicted by theoretical calculations.

It is also conceivable that core polarization of the host atoms may contribute to the Knight shift of an interstitial muon in so far as the tails of the relevant core states produce different densities of spin up and spin down electrons at the muon site.

Experience from nuclear Knight shift measurements shows that $dF_k(B_{ext})/dB_{ext} \sim \chi_p^*$ or

$K_{cp} \sim \chi_p^*$, with χ_p^* the proper spin susceptibility.

In analogy to equation (3.1.18) one may introduce another hyperfine field per unpaired electron, e.g.

$$K_{cp} = \frac{1}{\mu_B} B_{hf}^{\Omega_a}(r_\mu)_{cp}\chi_p^{a*} \tag{3.1.21}$$

In contrast to K_s, K_{cp} may assume positive as well as negative values. The star in χ_p^* is meant to indicate that different types of electrons, contributing to the total spin paramagnetism, may be responsible for K_s and K_{cp}. In transition metals χ_p^* may be identified with χ_d, where χ_d is the susceptibility associated with the d-electrons. In non transition metals the Pauli spin susceptibility originates only from the s-type conduction electrons.

For comparison with theory in the case of simple (nontransition metals) it is sometimes convenient to write the sum of K_s and K_{cp} in the following way by use of equations (3.1.1) and (3.1.17)

$$K' = K_s + K_{cp} = \frac{8\pi}{3}\mu_B \frac{n^+(r_\mu) - n^-(r_\mu)}{n_0^+ - n_0^-} \cdot \frac{n_0^+ - n_0^-}{B_{ext}}$$
$$= \frac{8\pi}{3}\rho_s(r_\mu)\chi_p \tag{3.1.22}$$

Here $\rho_s(r_\mu)$ is the so called spin density enhancement factor, resulting from the presence of the muon and $n_0^+ - n_0^-$ is the average undisturbed spin density of the conduction electrons.

If local moments are present as in rare earth metals or in certain alloys the conduction electrons may aquire a spatially varying spin polarization, due to the RKKY exchange interaction, on top of the polarization induced directly by the external field. This can be accounted for by introducing an effective field B_{eff} instead of just using B_{ext} [49]:

$$B_{eff} = B_{ext}\left(1 + J_{sf}\frac{g_J - 1}{g_J}\frac{\chi_f}{2\mu_B^2}\right) \tag{3.1.23}$$

where

$$J_{sf} = 6\pi z J(0) \sum_i F(2k_F\,|\mathbf{R}_i - \mathbf{r}_\mu|) \tag{3.1.24}$$

Here g_J is the Landé g factor of the local moment, χ_f is the susceptibility due to the local moments (e.g. due to 4*f*-electrons), z is the number of conduction electrons per atom and $J(0)$ is an *s*-*f*-electron exchange integral for wave vector $\mathbf{q} = 0$. The function

$$F(2k_F\,|\mathbf{R}_i - \mathbf{r}_\mu|) = (2k_F\,|\mathbf{R}_i - \mathbf{r}_\mu|\cos(2k_F\,|\mathbf{R}_i - \mathbf{r}_\mu|)$$
$$-\sin(2k_F\,|\mathbf{R}_i - \mathbf{r}_\mu|))/(2k_F\,|\mathbf{R}_i - \mathbf{r}_\mu|)^4 \tag{3.1.25}$$

accounts for the famous RKKY oscillations of the spin polarization.

Concerning now diamagnetic contributions to the total frequency shift one has to consider in principal two contributions. Firstly, there is the contribution from the Landau diamagnetism of the conduction electrons at the Fermi surface

$$\sigma_{Landau} = -\frac{1}{3}\cdot\frac{8\pi}{3}\cdot\left(\frac{m}{m^*}\right)^2\chi_p \tag{3.1.26}$$

where m and m^* are the free and effective electron masses, respectively, χ_p is the Pauli spin susceptibility. This term is usually negligibly small but may acquire nonnegligible values in certain exotic cases. Secondly, the local electronic structure around the muon or proton may give rise to diamagnetic screening analogous to the familiar chemical shift in molecules. This may be particularly important if bound electron states at the impurity or local bonding states with the host neighbors exist. This contribution can be calculated from the Lamb expression [50]

$$\sigma_{Lamb} = -\frac{e^2}{3mc^2}\langle 0|\frac{1}{r}|0\rangle \tag{3.1.27}$$

It involves calculation of the expectation value of $1/r$ for the electronic ground state configuration $|0\rangle$. In contrast to the contact hyperfine contributions the entire charge distribution around the muon determines the effect. This implies also, that states below the Fermi level are involved. The chemical shift depends therefore in a very condensed form on many features of the established electronic structure around the muon or proton and deserves therefore much attention. In conventional nuclear Knight shift measurements diamagnetic effects are usually below the level of observability, but may be of a sizeable fraction in the case of interstitial muons or protons.

The total Knight shift may now be written as follows (neglecting σ_{Landau})

$$K = K_s + K_{cp} + \sigma_{\text{Lamb}} \tag{3.1.28}$$

It is obvious that a measurement of K in some given host metal will not allow directly to deduce properties of the electronic structure around the muon. Rather this has to be accomplished by some indirect procedure. On the basis of some model, theoretical calculations will predict numbers for the various contributions to K, which can then be checked against the experimentally obtained Knight shift. The comparison will benefit from a systematic study of the experimental Knight shift in many different host metals and as a function of other parameters like the temperature. Some of the contributions to K may become distinguishable and certain trends may show up, which in turn could lead to an improved understanding, etc.

An inherent difficulty should be pointed out here. Both the direct Knight shift and possible "core polarization" contributions contain electronic bulk properties (via χ_p, $N(\varepsilon_F)$, and local properties (via $\langle|\psi(r_\mu)|^2\rangle_F$, $\rho_s(0)$), entering as a product in the corresponding relations. In order to extract the information on the local properties from measured K data it is necessary to know with some confidence the relevant Pauli spin susceptibility. Such knowledge is reliably available only in a limited number of cases.

IV. Electronic structure of hydrogen in metals

4.1. *Introduction*

The electronic structure of hydrogen in metals has been pictured on the basis of three phenomenological models. These are:

(i) The hydride-anion model in which an electron is transferred from the metal atom to hydrogen, resulting in the formation of an H^--ion.
(ii) The covalent-hydrogen model, in which it is assumed, that the hydrogen atoms are covalently bonded to the metal atoms and
(iii) the screened proton model, in which it is assumed that hydrogen donates its electron to the conduction band (unfilled states of the host) and that the screening of the positive charge is a cooperative effect of all conduction electrons, which are scattered by the impurity potential.

The first model is thought to be applicable to alkali hydrides such as LiH [51], the second model may be of importance for hydrogen in transition metals

Table 2
Collection of results from nonlinear jellium calculations

r_s	1	2	2.07 (A1)	3	4	5	6	Ref.
	5.16	17.5	—	45.6	97.4	—	303.2	91
	—	—	20	45	95	170	—	93
$\frac{n(0)}{n_0}$	5.12	17.2	—	44.8	95	180	300	92
	—	—	~16	—	—	—	—	79
	~5	~12	—	~44	~91	~169	—	96*
$\frac{n(0)^{***}}{n_H}$	3.85	1.62	—	1.25	1.12	1.09	1.05	92
	—	—	7.38	11.97	18.40	23.14	—	93
$n_F(0)$	—	7.2	—	12.1	19.2	28.0	39.6	79
	—	~7	—	~12	~17.5	~23	—	98**
	—	~7	—	10	13	14	14	98**
$\rho_s(0)$	—	7	—	9.6	12.5	14	13.8	100

*) The charge density $n(0)$ changes less than 4% between $\zeta_0 = 0$ and $\zeta_0 = 0.6$.
**) The polarization was fixed at $\zeta_0 = 0.1$, but $\rho_s(0)$ is expected to be insensitive to small values of ζ_0 [98].
***) $n_H = 2.14 \cdot 10^{24}/\text{cm}^3$

[52] and the third model, which is the most simple one, may provide a good approximation to hydrogen in simple, free electron gas metals such as Na.

The calculation of the electronic structure of hydrogen in metals has followed three different techniques. (1) For transition metal hydrides with high hydrogen concentrations in stoichiometric and nonstoichiometric order electronic band structure calculation were performed. More adequate to the dilute concentration situation are the two other methods. These are (2) linear or nonlinear screening calculations, the so called jellium calculations and, on the other hand, (3) atomic cluster calculations. In approach (2) the conduction electrons are approximated by a free electron gas with a homogeneous positively charged compensating background representing the positive ion cores (jellium model). The electronic structure of the impurity is derived from the response of the free electron gas to the positive impurity charge. Possible influence of the host ion cores and related effects, such as lattice distortions etc. as well as of the band structure of the electronic states are usually neglected in most calculations, but can be taken into account at least approximately. The third (3) approach, which appears to be the most realistic and the most basic one reduces the problem of dealing with the impurity in an essentially infinite lattice to one in which the impurity is 'only' surrounded by a few layers of host atoms (the cluster) and where the rest is taken into account by proper boundary conditions for the cluster.

Calculations on the basis of the jellium approach were the first ones applied to the problem of hydrogen in metals and are still the most commonly used ones due to their relative simplicity. It is obvious that the screened proton model finds its most adequate representation in the jellium approach. Cluster calculations have just recently been applied for the first time to hydrogen in metals and although there are as yet only a few results available this technique appears most promising for future work. The hydride anion and the covalent hydrogen model

should be well accommodated by a cluster description or, by applying special techniques, by band structure theory. Being of the nature of first principles calculations, these techniques off course go beyond the phenomenological models. They demonstrate that none of the phenomenological models is a very good approximation to the actual electronic structure of hydrogen in metals indeed and that a more realistic description contains aspects of all three models. In particular the 'simple' screened proton model appears to be too naive. Nevertheless, because most theoretical calculations that pertain to the dilute concentration limit have adopted the jellium or free electron gas model, this approach will be discussed in somewhat more detail in the following, while the two other methods will find less coverage.

4.2. *Band structure calculations*

A review of band structure calculations of (transition) metal hydrides has been recently given by Switendick [53], who was also the first one to apply energy band theory to metal hydrides [54]. Usually it is assumed that the metal hydride compound possesses a stoichiometric composition. An extension to disordered, substoichiometric PdH_x has recently been worked out by Faulkner [55, 56] and Gelatt et al. [57], by either adopting the coherent potential approximation of Soven [58] or the average t-matrix approximation in conjunction with the KKR (Kohn–Korringer–Rostoker) method, respectively.

These calculations by their nature produce mainly results that concern the overall electronic structure of the metal hydride system and corresponding observables, such as the electronic specific heat, the magnetic susceptibility and in particular the electron spin susceptibility, and the heat of solution. The calculations indicate the formation of low lying hydrogen induced states which are a manifestation of bonding and antibonding between hydrogen and the host atoms, and between the hydrogen interstitials themselves. These states have s-character with respect to hydrogen. Generally it is found that only those states of the pure host are affected which have s-character at the hydrogen site [57].

To our knowledge band structure calculations so far have not been used to predict the Knight shift for protons in metals or other specific local properties of the hydrogen metal complex, e.g. such as the occupied interstitial lattice site with three exceptions: Firstly Gupta and Freeman [59] have calculated the spin-lattice relaxation time T_{1e} of protons in stoichiometric PdH. A partial density of states analysis at the hydrogen site shows that practically only states with s-symmetry are present. The density of states with s-character at the hydrogen site at the

Table 3
Results of nonlinear jellium calculations adopting the spherical solid model (SSM) (Nieminen and Manninen [102, 103].

		$\eta_F(r_\mu)$		$\rho_s(r_\mu)$	
Metal	r_s	octahedral	tetrahedral	octahedral	tetrahedral
Al	2.07	6.9	4.5	6.3	3.4
Cu	2.67	11.1	10.3	10.4	8.6
Na	3.93	14.6	14.8	10.1	10.1

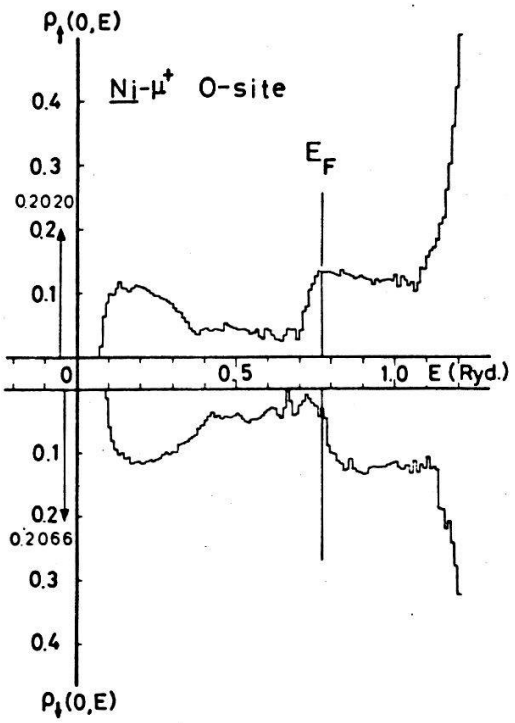

Figure 4
The local density of states seen by μ^+ at an octahedral interstitial site in ferromagnetic Ni. Arrows near the bottom of the conduction band indicate bound states, whose spectral weights are 0.2020 for the up spin band and 0.2066 for the down spin band (from Ref. 61).

Fermi energy is calculated to be $N_s^H(\varepsilon_F) \cong 0.2550$ states/Ry spin until cell and the charge density at the hydrogen site for states with $k = k_F : \langle|\psi(0)|^2\rangle_F = 0.18 \cdot |\psi(0)|^2_{\text{free hydrogen}}$. $T_{1e} \cdot T$ is calculated from the unfactorized Korringa relation [48]

$$T_{1e} \cdot T = \left[\frac{\Omega^2}{9\pi^3} \gamma_e^2 \gamma_p^2 k_B \hbar^3 \left(\int_{FS} |\psi_k^s(0)|^2 \frac{dS_{\varepsilon_F}}{\text{grad}_{\mathbf{k}}\, \varepsilon_F} \right)^2 \right]^{-1}$$
$$= 43 \text{ sec} \cdot K \qquad (4.2.1)$$

The electronic relaxation rate has been determined experimentally between 3 K and 77 K by Wiley et al. [60]. The result for $PdH_{0.995}$ is $T_{1e} \cdot T = 48 \pm 0.6 \text{ sec} \cdot K$. This is in very good agreement with the predicted value.

Secondly the hyperfine field at a positive muon in ferromagnetic Ni has been calculated from a band structure approach by Katayama et al. [61] on the basis of the coherent potential approximation of Soven [58]. As in the case of other band structure calculations the formation of bonding states below the conduction band is observed. The relevant results are shown in Fig. 4 which displays the local spin density $\rho_\sigma(r_\mu, E)$ of majority and minority electrons at the μ^+ as a function of band energy. A particular feature is the dip in $\rho_\sigma(r_\mu, E)$ at $E = 0.69$ Ry for $\sigma = \uparrow$ and at $E = 0.73$ Ry for $\sigma = \downarrow$ which is a consequence of an interference among the μ^+ induced states and certain host states (Fano effect [62]). As Fig. 4 immediately shows, the bonding states produce a net negative spin density at the $\mu^+(-2.41 \text{ kG})$, while the band states contribute a positive spin density, resulting in a total predicted hyperfine field of [61]

$$B_\mu = \frac{8\pi}{3} \mu_B \int_0^{\varepsilon_F} (\rho_\uparrow(r_\mu, E) - \rho_\downarrow(r_\mu, E)\, dE = -720G$$

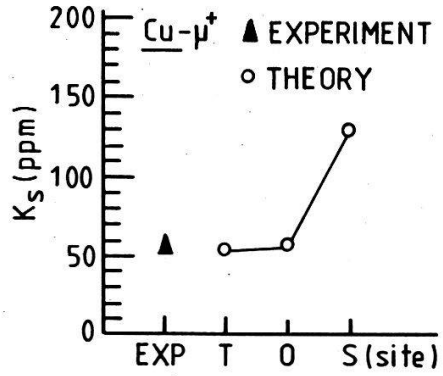

Figure 5
Predictions for the Knight shift of positive muons at octahedral (O), tetrahedral (T) and substitutional sites (S) in Cu (from Ref. 63).

or $B_{hf}^{\Omega_a}(r_\mu) = B_\mu/M(T=0) = -1.2\ \text{kG}/\mu_B$ where $M(T=0)$ is the bulk magnetization at $T=0$ K. The bonding level is a result of hybridization between the muonium $1s$ state and Ni $3d$-states, which also produces antibonding states above the d-band. More recently this type of calculation has also been extended to muons in Cu. The results for various site assignments are displayed in Figure 5.

Thirdly Jepsen et al. [64] have applied a supercell approach to hydrogen in ferromagnetic Ni by considering a five layer film geometry with the muons or protons occupying the octahedral interstitial position in the central layer (this corresponds to a substoichiometric Ni_5H compound). Previous investigations of the same authors had shown that already the central layer of a three layer film behaves bulk like. Density of states curves were obtained for a hydrogen free film and for a hydrogen loaded film. As in the other band structure calculations a low lying band shows up in the hydrogenated Ni film which originates from the lowest pure Ni sp conduction band and is split off to form a Ni—H bonding band in Ni_5H. Another remarkable result is a lowering of the Ni magnetic moments adjacent to the hydrogen impurity. As a result the spin density at the octahedral site in the central layer changes only little upon hydrogenation. Finally, the hyperfine field at the muon or proton is calculated to be $B_{hf}(r_\mu) = -0.463$ kG or $B_{hf}^{\Omega_a}(r_\mu) = -0.77\ \text{kG}/\mu_B$.

4.3. *Free electron gas models*

4.3.1. *Linear screening*

The screening of a point impurity in an electron gas has been treated first by Mott [65] and Friedel [66] in the so called linear response scheme. For more recent work see Aldred [67], Patterson and Falicov [68], Popovic and Stott [69] and Prakash [70].

In this scheme it is assumed that the change in charge density distribution is small compared to the undisturbed case and that the dielectric function description provides an adequate tool to calculate the response of the electron gas to the impurity charge. According to this scheme the Fourier transformed screened impurity potential is given by:

$$V(k) = e^2 \frac{4\pi}{k^2} \frac{1}{\varepsilon(k)} \tag{4.3.1}$$

where $\varepsilon(k)$ is the static dielectric function.

The static dielectric function for a free electron gas is given by the well known Lindhard [71] expression:

$$\varepsilon(k) = 1 + \frac{k_s^2}{k^2}\left(\frac{1}{2} - \frac{k_F}{2k}\left(1 - \frac{k^2}{4k_F^2}\right)\ln\left|\frac{2k_F - k}{2k_F + k}\right|\right) \tag{4.3.2}$$

and $k_s = 4k_F/\pi a_B$, $n_0 =$ average electron density and $a_B =$ Bohr radius.

Corrections to this expression due to exchange and correlation effects have been calculated by e.g. Singwi et al. [72, 73], Hubbard [74], Sham [75] and Vashishta and Singwi [76].

From the Poisson equation follows that the induced screening charge $n(k)$ is given by $n(k) = [(\varepsilon(k) - 1)/\varepsilon(k)] \cdot 1$ and after performing a Fourier transformation back to r-space:

$$n'(r) = \int \frac{d^3k}{(2\pi)^3} e^{i\mathbf{k}\cdot\mathbf{r}}\left(\frac{\varepsilon(k) - 1}{\varepsilon(k)}\right) \tag{4.3.3}$$

Usually this integral has to be evaluated numerically (but see also Aldred [67, 77]). In the long wave length Thomas Fermi limit (k small) $\varepsilon(k)$ is given by

$$\varepsilon(k) \simeq 1 + \frac{1}{2}\frac{k_s^2}{k^2} \tag{4.3.4}$$

The screened potential can then be evaluated explicitely:

$$V(r) = \frac{1}{r}\exp(-\lambda r) \tag{4.3.5}$$

with $\lambda = (4\pi N(\varepsilon_F))^{1/2}$.

$N(\varepsilon_F)$ is the density of states at the Fermi limit and $1/\lambda$ is called the screening length (see e.g. Kittel [78]).

A remarkable result in the general case is that the induced electron-density shows an oscillatory behavior (Friedel oscillations) which can be traced back to the almost step like change of the electron density at the Fermi surface. This step like change causes the logarithmic divergence of the first derivative of $\varepsilon(k)$ at $k = 2k_F$ (Meier [79]).

The dielectric function approach has also been applied to a point charge impurity in a ferromagnetic electron gas by Kim [80] using the spin dependent dielectric function of Kim et al. [81].

An interesting result is that for a parabolic hole band (as in Ni or Co) a reversal of the relative density of states for majority and minority spins close to the impurity is observed. This does not necessarily mean, however, that also the magnetization changes its sign locally. For a parabolic electron band no such reversal of the relative density of states is observed.

The linear screening approach, of course, does not include the possibility of the formation of bound states. The electrons, contributing to the screening cloud, are to be described by scattering (Bloch) states.

4.3.2. *Nonlinear screening*

In view of the fact that the Coulomb potential of a positive point impurity, such as a proton or a muon, presents a rather strong perturbation to the electronic

system, particularly close to the origin, one has started to doubt the validity of the linear response assumption in the treatment of the screening of a proton or muon. Theoretical schemes that go beyond the linear response approach have therefore been developed (Sjölander and Stott [82], Bhattacharyya and Singwi [83]). All more recent nonlinear calculations are based on the Hohenberg–Kohn–Sham (HKS) density functional formalism (Hohenberg and Kohn [84], Kohn and Sham [85]) or on the spin density functional (SDF) formalism (Barth and Hedin [86], Rajogopal and Callaway [87], Gunnarson and Lundquist [88]) which allow a self consistent treatment of the screening of a proton, muon, positron etc. in an electron gas. The possible occurrence of bound states is a natural phenomenon in these approaches.

According to the HKS formalism one writes the energy functional of the particle density $n(\hat{r})$ as

$$E[n(\hat{r})] = T_0[n(\hat{r})] + \int d\hat{r} n(\hat{r}) V_0(\hat{r}) + \frac{1}{2} \int\int \frac{n(\hat{r}) n(\hat{r}')}{1\hat{r} - \hat{r}'1} d\hat{r}\, d\hat{r}' + E_{xc}[n(\hat{r})] \tag{4.3.6}$$

$T_0[n(\hat{r})]$ is the kinetic energy of a system of noninteracting electrons, $E_{xc}[n(r)]$ is the exchange-correlation energy, $V_0(\hat{r}) = e/r$ is the impurity potential. The true ground state density $n_0(\hat{r})$ will correspond to a minimum in the total energy $E[n(\hat{r})]$. Applying this variational principle one obtains the following set of self consistent equations

$$\{-\nabla^2 + V_{\text{eff}}[n(\hat{r}), r]\}\psi_i(\hat{r}) = \varepsilon_i \psi_i(\hat{r}) \tag{4.3.7}$$

$$n(\hat{r}) = \sum_i |\psi_i(\hat{r})|^2 \tag{4.3.8}$$

$$V_{\text{eff}}[n(\hat{r}), r] = \phi(r) + V_{xc}[n(\hat{r})] \tag{4.3.9}$$

with

$$\phi(r) = -\frac{e}{r} + e \int dr' \cdot \frac{n(\hat{r}')}{|\hat{r} - \hat{r}'|} \tag{4.3.10}$$

and

$$V_{xc}[n(\hat{r})] = \frac{\delta E_{xc}[n(\hat{r})]}{\delta n(\hat{r})} \tag{4.3.11}$$

The problem in solving this set by equations is related to the exchange and correlation potential V_{xc} which is not known in general.

For slowly varying densities approximate expressions for V_{xc} may be taken from the theory of the homogeneous electron gas. For strongly varying $n(\hat{r})$, as in the neighborhood of a proton or muon, V_{xc} will not only depend on $n(\hat{r})$ (local approximation) but also on the gradient of $n(r)$ (nonlocal dependence).

The solutions of equations (4.3.7)–(4.3.9) are scattering states or bound states of electrons in the spherically symmetric potential V_{eff}. The requirement that the total impurity charge is screened leads to a condition on the asymptotic terms of the scattered waves, which is expressed in the famous Friedel sum rule (Friedel

[89]) for the phase shifts of the partial waves at the Fermi wave number k_F

$$Z = \frac{2}{\pi} \sum_l (2l+1)\delta_l(k_F)$$
$$Z = 1 \quad \text{for} \quad \mu^+ \text{ or } p \tag{4.3.12}$$

The HKS-formalism was first applied by Popovic and Stott [69] to the screening of a proton in Al and Mg. $V_{xc}(n(\hat{r}))$ was taken from the results of Singwi et al. [73] in the parametrized form proposed by Hedin and Lundquist [90]. (Local density approximation.) Subsequently the screening of a proton or a muon was treated in the HKS-formalism for a wide range of typical metallic densities by Almbladh et al. [91], Zaremba et al. [92] and Jena and Singwi [93].

Almbladh et al. [91] and Zaremba et al. [92] used for the exchange-correlation potential again the parametrized version of Hedin and Lundquist [90]. Jena and Singwi went one step further in also including a first gradient correction to the exchange-correlation energy:

$$E_{xc}[n(\hat{r})] = \int d\hat{r} n(\hat{r}) \varepsilon_{xc}[n(\hat{r})] + \frac{1}{2} \int d\hat{r} g_{xc}^{(2)}[n(\hat{r})] |\nabla n(\hat{r})|^2 \tag{4.3.13}$$

The exchange-correlation energy ε_{xc} (per particle) for a homogeneous electron gas was taken from Vashishta and Singwi [76] and the coefficient $g_{xc}^{(2)}$ from the work of Rasolt and Geldart [94].

A nonlinear but nonself-consistent calculation of the screening of a positron, muon or proton in jellium has been performed by Meier [79] who uses a modelform for the effective potential and applies the theory of potential scattering. The modelform for the effective potential was choosen to be the Hulthen potential

$$V_{\text{eff}} = -e^2 \frac{\lambda}{e^{\lambda r} - 1} \tag{4.3.14}$$

Enhancement factors were calculated explicitly by use of the Jost function [95]. The occurrence of bound states is a natural ingredient of the applied formalism.

Meier has not taken any exchange and correlation effects into account. It is expected that this does not effect very much the density of electrons at the impurity site as for small distances the exchange-correlation potential is only a small fraction of the total potential. However, for larger distances this forms a significant part of the potential and the Hulthen potential of Meier may be a very inaccurate representation of the actual spatial screening charge distribution.

Calculation of the screening of a proton or a muon in a spin polarized electron gas in the spin density functional (SDF)-formalism have been performed by Jena et al. [96] and by Petzinger and Munjal [97, 98] in the local density approximation. In all cases the spin dependent exchange correlation potential was taken from the work of Gunnarson et al. [99] (see also Gunnarson and Lundquist [88]).

The HKS and SDF treatments lead to rather similar results as far as the electronic structure is concerned. The picture that emerges from the calculations is the following: For densities with $r_s > 1.9$[2]) the electronic structure resembles

[2]) The density parameter r_s is related to the conduction electron density n by the relation $n = (4\pi/3)(r_s a_0)^3$. Hence r_s in units of the Bohrradius a_0 is the radius of a sphere containing just one electron.

that of a very extended H^- ion accompanied by an equally extended hole in the continuum density [93].

The doubly occupied bound states that show up for $r_s > 1.9$ are extremely shallow with binding energies of -0.0043 eV, at $r_s = 2.07$ (Al) and -0.218 eV at $r_s = 5$ in the local density approximation[93]. These numbers should be compared with the vacuum binding energies of atomic hydrogen and of the hydrogen ion H^- of -13.5 eV and -0.7 eV respectively.

It is also interesting to note that, due to the H^--like structure at lower electron densities, an excess in screening charge can be found in a certain volume around the impurity, which has a radius between 2 Å and about 4 Å (Jena and Singwi [93]), a region, into which often the nearest neighbour host sites are falling.

As an illustration Fig. 6 shows the number of electrons $Z(R)$ contained in a sphere of radius R around the proton for an average electron density corresponding to $r_s = 2.7$ (solid curve). Also shown is the same curve for free atomic hydrogen (dashed curve) (taken from Jena [100]). It clearly shows the build up of an excess screening charge in a certain volume around the proton or muon and indicates the onset of a charge depletion in the continuum further out. In reality this excess charge could arise from a charge transfer from the metal ions to the proton or muon, as pictured in the hydride-anion model.

In any case the total charge of the proton or muon is screened within a Radius $R \simeq 2 \cdot a_0$, whereas the bound states extends over a much larger distance of roughly $\sim 20 \cdot a_0$. Nevertheless the bound states contribute, within the screening radius, about 25% of the screening charge for $r_s = 2.07$ (Al) and as much as

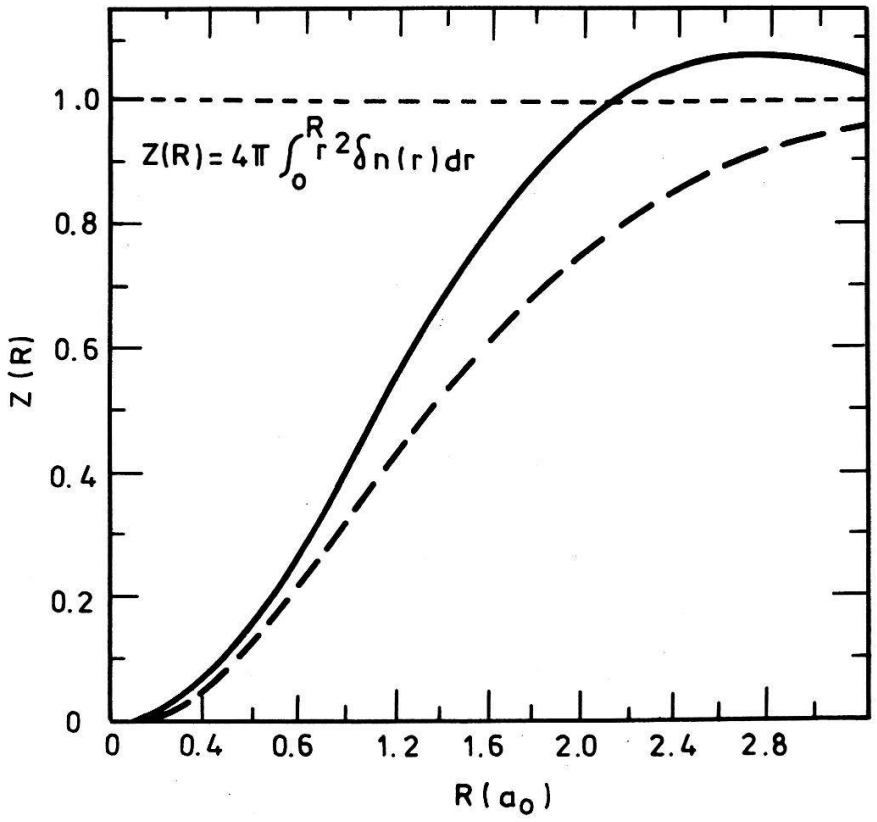

Figure 6
The number $Z(R)$ of electrons contained in a sphere of radius R around a proton or muon in a jellium of $r_s = 2.7$ (solid curve). The dashed curve shows the same for atomic hydrogen or muonium in free space (from Ref. 100).

80% of the screening charge for $r_s = 5$. The missing fraction to complete the screening is provided by scattering continuum states.

The shallowness of the bound states and their overlap with the neighbor ion cores raises the question as to the survival of these bound states, resulting from a jellium model, in a more realistic approach. Indeed their significance is at this stage of the discussion not at all clear [100].

The increase of the total charge density at the proton or muon over the unperturbed one as given by the various authors is collected in Table 2. As can be seen there is very good agreement between the various calculations including the nonself-consistent one of Meier [79]. It is also evident that the spin polarization has a negligible effect on the total charge density accumulated at the impurity.

It is instructive to calculate the total charge density at the proton or muon in units of the charge density in free atomic hydrogen (see Table 2). Except for the highest electron concentrations ($r_s \leq 2$) the density approaches quickly the density in free atomic hydrogen.

The calculated total charge density enhancement finds some experimental verification by observed positron annihilation rates in metals.

The annihilation rate is given by

$$\Gamma = \frac{n(0)}{n_0}\Gamma_0, \qquad \Gamma_0 \simeq \frac{12}{r_s^3} \cdot 10^9\,\mathrm{sec}^{-1} \tag{4.3.15}$$

Figure 7 displays a comparison between theoretical results calculated by Meier [79] and experimental numbers. The tendency of the experimental numbers is

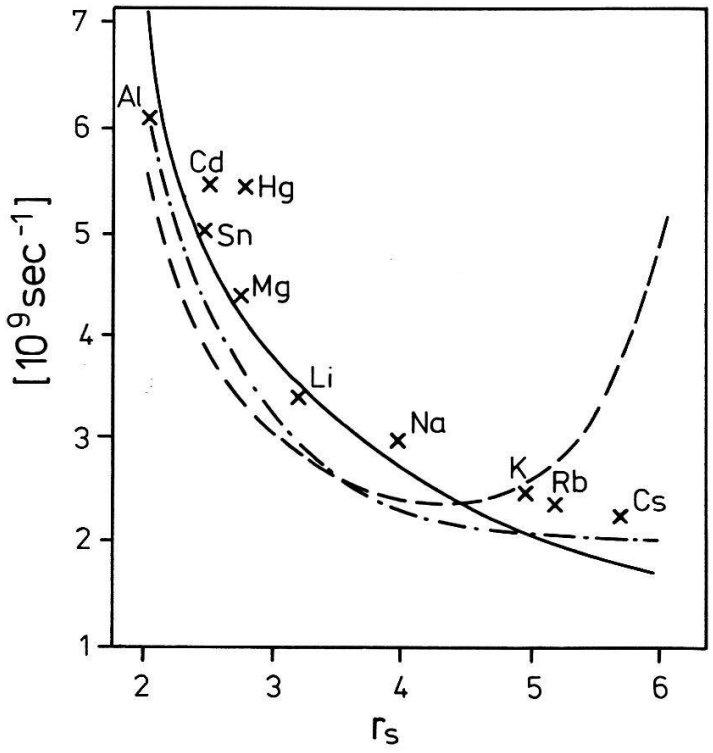

Figure 7
Comparison of experimental positron annihilation rates with theoretical predictions. The solid line is the prediction of the nonlinear model calculation by Meier [79], the dashed line is due to Sjölander and Stott [82] and the dashed dotted line due to Bhattacharyya and Singwi [83] (from Ref. 79).

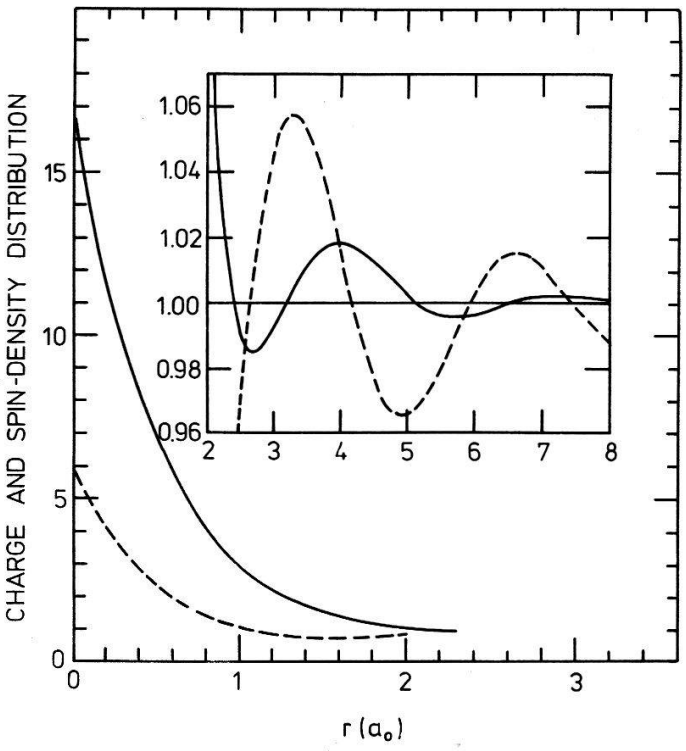

Figure 8
Charge and spin density distribution around a positive muon in a spin polarized electron gas with $r_s = 2$ and $\zeta_0 = 0.17$. The solid and dashed curves correspond respectively to $n(r)/n_0$ and $\rho_s(r)$ (from Ref. 100).

rather well reproduced by theory and also the absolute numbers are quite close to each other.

The actual charge distribution around a positive muon or proton, as resulting from a jellium calculation is illustrated in Fig. 8 for $r_s = 2.0$, taken again from Jena [100] (solid line). Quite visible is the huge charge pile up at the impurity. For large distances the charge density shows oscillations around the average density which are the famous Friedel oscillations.

With regard to hyperfine fields and Knight shifts we are particularly interested in the quantities (see Chapter III)

$$\eta_F(r_\mu) = \frac{\langle|\psi(r_\mu)|^2\rangle_F}{n_0} \tag{4.3.16}$$

and

$$\rho_s(r_\mu) = \frac{n^+(r_\mu) - n^-(r_\mu)}{n_0^+ - n_0^-} \tag{4.3.17}$$

With regard to the first one, all HKS and SDF calculations, including again the nonself-consistent treatment of Meier [79] agree very well with each other (see Table 2).

The SDF calculations[3]) (Petzinger and Munjal [98], Jena [100]) show,

[3]) An earlier discrepancy between the results of Ref. 96 and Ref. 98 has been resolved in favor of Ref. 98 [100].

Table 4
Diamagnetic shielding of muons in metals

Metal	r_s	σ[ppm] (Ref. 108)	σ[ppm] (Ref. 126, 128)
Li	3.25	−18	
Na	3.96	−20	
K	4.86	−21	
Rb	5.20	−22	
Cs	5.64	−22	
Be	1.88	−14	−27
Mg	2.65	−16	
Ca	3.27	−18	
Sr	3.56	−19	
Ba	3.69	−19	
Cu	2.67	−16	−10
Al	2.07	−15	

however, that

$$\rho_s(r_\mu) < \eta(r_\mu) \quad \text{for} \quad r_s > 1.9$$

The results of the SDF calculation of Petzinger et al. [98] are displayed in Fig. 9. $\rho_s(0)$ rises much weaker than $\eta_F(r_\mu)$ with increasing r_s and becomes almost independent of concentration beyond $r_s = 4.5$.

Petzinger and Munjal [98] trace the deviation between $\rho_s(r_\mu)$ and $\eta_F(r_\mu)$ back to the occurrence of bound states. Below $r_s = 1.9$, where no bound states are shown to exist: $\rho_s(r_\mu) = \eta_F(r_\mu)$. Above $r_s = 1.9$ the minority spin bound state is always more tightly bound than the majority spin bound state because of the now spin dependent exchange and correlation potential. This results in a negative contribution to the total spin density at the origin (see also Ref. 101).

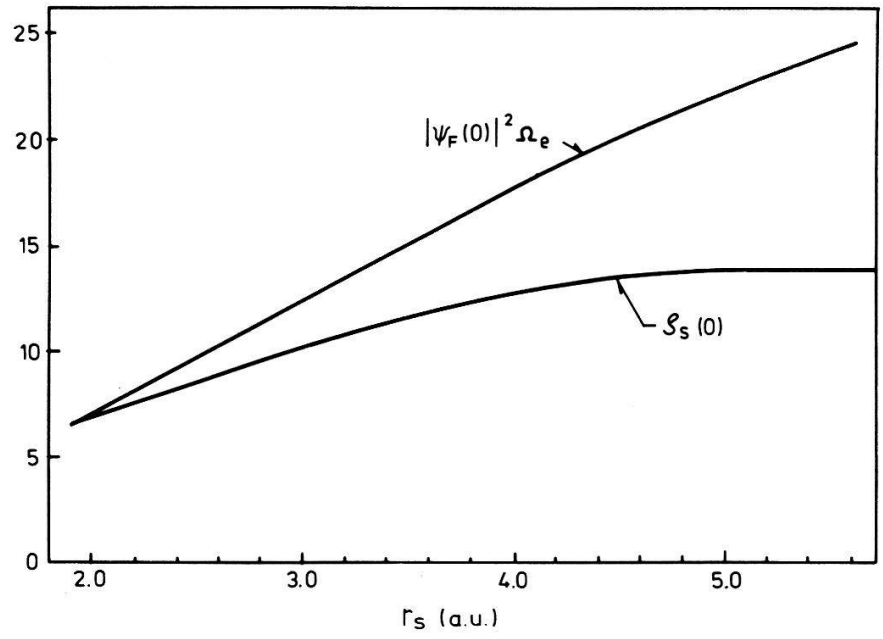

Figure 9
Plot of $\eta_F(0)$ and $\rho_s(0)$ from the nonlinear SDF jellium calculation of Munjal and Petzinger [98] versus the electron density parameter $r_s = ((3/4\pi)(1/\eta))^{1/3}/a_B$.

The spatial distribution of the spin density around a muon or proton is illustrated also in Fig. 8. The spin density shows likewise oscillations, but the oscillations are not in phase with the charge density oscillations.

4.3.3. *Spherical solid model*

So far the discrete structure of the lattice environment of a proton or a muon has been completely neglected. The pure jellium calculations are therefore certainly only of a limited value, even for nearly free electron gas metals, since any possible site dependence of the electronic structure will be outside the focus of such calculations. On the other hand it is precisely the correlation of site and electronic structure, that will allow us to understand why hydrogen occupies a certain lattice site and, e.g., to predict the corresponding heat of a solution.

A step forward in this direction on the basis of nonlinear response jellium calculations has recently been taken by Nieminen and Manninen [102, 103]. The influence of the neighbor ion potentials was approximated by forming a spherical average (called the spherical solid model (Almbladh and v. Barth [104], but see also Keller [123, 124])) with the proton or muon at the center and incorporating it into the SDF-equations as an external host potential. The host ion potential was represented by a pseudo ion potential of the Ashcroft form [105]. These calculations were applied to muons or protons in bcc Na and fcc Al and Cu, assuming the muon or proton to occupy the octahedral or tetrahedral interstitial position or a substitutional position (a host vacancy).

Some of the results are given in Table 3. Again it was found that $\rho_s(r_\mu) < \eta_F(r_\mu)$. As can be seen, particularly for Al, different site assignments lead to considerably different predictions for $\rho_s(r_\mu)$.

Another result of these calculations are predictions for the heat of solution (ΔH). According to these, one would expect to find the proton or muon at the tetrahedral site in Na ($\Delta H = -0.12$ eV) and at the octahedral site in Al ($\Delta H = 0.19$ eV), while no trapping at substitutional vacancies is indicated. The experimental value for ΔH in Al is 0.65 eV (Eichenauer [106]). (See also Jena and Singwi [93].)

4.3.4. *Pseudo jellium model*

A different approach to a more realistic application of nonlinear response jellium theory has been devised by Jena et al. [107]. It is intended to describe the screening of the proton in a nonfree electron gas like metal such as Pd. In this model the ambient charge density distribution in the perfect host is obtained from superposing atomic charge densities centered at the host nuclei. The screening of the proton at some arbitrary site in the lattice is then calculated from jellium theory, by assuming the local charge density to respond to the presence of the positive impurity charge as if there were a homogeneous electron gas of the same density. In particular it is then possible to calculate the effect of zero point motion on the average spin density at the impurity and corresponding isotope effects.

For protons or muons in Pd, held fixed at the center of the octahedral interstitial position, Jena et al. [107] find a spin density enhancement factor of $\rho_s(r_\mu) = 10.7$. It should be pointed out that this model treats s, p and d-electrons as essentially equal. In particular no distinction is made with respect to the spin paramagnetism of these electrons, their different spatial distribution and different contributions to the screening of the proton. Since the interstitial charge density is

mainly of s-electron origin also in Jena et al.'s prescription their calculated spin density enhancement factor might be a useful number in calculating the corresponding s-electron induced Knight shift only.

4.3.5. *Diamagnetic screening*

Zaremba and Zobin [108] have recently presented a very elegant treatment of the diamagnetic screening of positive muons in a jellium. The field at the muon resulting from the diamagnetic current $\langle e\mathbf{J}(\mathbf{r})\rangle$ induced by the external field is given by

$$\mathbf{B}(r_\mu)=\frac{1}{c}\int_0^\infty d\mathbf{r}\,\frac{(\mathbf{r}-\mathbf{r}_\mu)\langle e\mathbf{J}(\mathbf{r}-\mathbf{r}_\mu)\rangle}{|\mathbf{r}-\mathbf{r}_\mu|^3} \tag{4.3.5.1}$$

The diamagnetic current is calculated from a linear response theory. The change of $\mathbf{B}(r_\mu)$ on implantation of the muon is denoted by $\Delta\mathbf{B}(r_\mu)$. The diamagnetic shielding constant may then be written as follows ($r_\mu=0$)

$$\sigma=\frac{\Delta B(0)}{B_{\text{ext}}}=-\frac{e^2}{3mc^2}\int_0^\infty\frac{dr}{r}4\pi r^2\,\Delta n(r)$$
$$+\frac{e}{3mc^2}\int_0^\infty\frac{dr}{r}\frac{2k_F}{\pi}\sum_{l=1}^{\infty}l(l+1)(2l+1)[R^2_{lk_F}(r)-j_l^2(k_Fr)] \tag{4.3.5.2}$$

Here $\Delta n(r)$ is the change of the charge distribution from the ambient one around the muon and $R_{lk_F}(r)$ are radial wave functions and $j_l(k_Fr)$ are free particle Bessel functions. $\Delta n(r)$ and $R_{lk_F}(r)$ are obtained from a nonlinear response jellium calculation. The first term in equation (4.3.5.2) may be identified with the Lamb term equation (3.1.27). The second term is a new contribution arising from the presence of a continuum of occupied states at the Fermi energy. In a sense it corresponds to the Landau term equation (3.1.26).

Some results for various electron densities corresponding to the indicated metals are collected in Table 4. It is seen that almost independent of the electron density parameter r_s the shielding constant stays close to -20 ppm. This is close to the value for atomic hydrogen of $\sigma_H=-17.8$ ppm and reflects essentially a basic similarity of the charge distribution in free atomic hydrogen and around a proton embedded in an electron gas. It is interesting to note that the second term in equation (4.3.5.2) turns out to be positive for $r_s<4.5$ and becomes negative for $r_s>4.5$. Except for very high electron densities its value is always small compared with the Lamb term contribution.

4.3.6. *Electric field gradients* (EFG)

In a perfect cubic metal lattice there will be no electric field gradients at the host nuclei due to crystalline fields. In the presence of a muon or proton an electric field gradient at a neighbor host nucleus is, however, to be expected and can be of two origins.

First, due to a local lattice distortion induced by the impurity, the cubic symmetry will be destroyed locally giving rise to a nonvanishing EFG at the neighbor hosts (size effect). No estimates of the possible magnitude of such induced field gradients are as yet available for interstitial protons or muons. In the case of substitutional impurities in copper alloys Beal-Monod and Kohn [109] find

that strain induced EFG are very small. More recently Sagalyn and Alexander [110] have found that, on the contrary, size effects may contribute significantly to the total EFG. Their result may be rewritten for an interstitial impurity [111]. On the basis of the point charge model the EFG at the nearest neighbor to an interstitial impurity at the octahedral site in a fcc lattice along the distance **d** is calculated to be

$$q_{zz} = -\frac{9 \cdot \sqrt{2}\,\lambda\,\Delta V}{\pi \gamma_E a^3 d^3} \tag{4.3.16}$$

where $\gamma_E = 1.44$ for Cu. λ is a dimensionless parameter which relates the experimental EFG to the EFG which would be observed if the distorted lattice were made up of unshielded point charges ($\lambda \simeq -15$ for Cu, Sagalyn and Alexander [110]). ΔV is the change in volume per impurity. This expression may be used to give an order of magnitude estimate for the strain induced EFG due to interstitial protons or muons.

Second, and perhaps most important, the screened proton or muon potential will itself be the source of an electric field gradient at the neighbor host sites.

The EFG at a host nucleus at a distance $\mathbf{r}_n$ from the impurity is related to the perturbed charge density distribution $\delta' n(\mathbf{r}) = n'(\mathbf{r}) - n_0(\mathbf{r})$ ($(n_0(\mathbf{r}) =$ unperturbed charge density distribution) by the following relation (Kohn and Vosko [112])

$$q(\mathbf{r}_n) = \frac{V_{zz}(\mathbf{r}_n)}{e} = -\int \frac{\delta' n(\mathbf{r}_n + \mathbf{r}')}{r'^3} (1 + \gamma(r'))(3\cos^2\theta' - 1)\, d^3 r' \tag{4.3.17}$$

where $\mathbf{r}' = \mathbf{r} - \mathbf{r}_n$, $\theta' =$ angle between $\mathbf{r}'$ and $\mathbf{r}_n$. The z-axis is taken along $\mathbf{r}_n$. $\gamma(r')$ is the so called antishielding factor which accounts for core polarization effects (Sternheimer effect [113]). The charge density distribution $\delta' n(\mathbf{r})$ introduced here is not the one calculated in the free electron gas approximation, Section 4.3.2, denoted by $\delta n(r)$, where the electrons are represented by plane waves.

Rather, dealing now with the host atoms of the metal lattice, the conduction electrons have to be represented by the appropriate Bloch wave functions $\psi_k(r)$, reflecting the periodic structure of the crystal potential.

In the following it is neglected that the $\psi_k(r)$ are distorted by the presence of the muon or proton and the $\psi_k(r)$ are taken to be the Bloch wave functions of the undisturbed lattice.

For $\mathbf{r}$ not too small equation (4.3.17) can be factorized in the following way (Kohn and Vosko [112]):

$$q(\mathbf{r}_n) = \frac{8\pi}{3}\, \alpha(\mathbf{k}_F)\, \delta n(\mathbf{r}_n) \tag{4.3.18}$$

where $\alpha(\mathbf{k}_F)$ is the so called Bloch enhancement factor.

$$\alpha(\mathbf{k}_F) = \frac{\int d^3 r' \psi^2_{k_F}(\mathbf{r}') P_2(\cos\theta') \frac{1}{r'^3} (1 + \gamma(r'))}{\int d^3 r' e^{2 \cdot \mathbf{k}_F \cdot \mathbf{r}'} P_2(\cos\theta') \frac{1}{r'^3}} \tag{4.3.19}$$

and $\delta n(\mathbf{r}_n) = n(\mathbf{r}_n) - n_0$ is the perturbation in the bulk electron density at $\mathbf{r}_n$, the

quantity, that is calculated in the free electron gas model. $\mathbf{k}_F$, the Fermi momentum, is taken in the direction of $\mathbf{r}_n$. Kohn and Vosko have shown that $\gamma(r')$ plays only a minor role for the value of α in the case of Cu. In fact $\gamma(r)$ has been neglected altogether in a recent calculation of α by Jena et al. [114].

It should be emphasized that equation (4.3.18) is written in a form which allows its use in conjunction with jellium type calculations of the screening of protons or muons in a metal, as treated in Section 4.2.2.

The Bloch enhancement factor which measures the increase of $q(\mathbf{r})$ over its value in a pure plane wave theory, depends on the direction of the Fermi momentum $\mathbf{k}_F$ or $\mathbf{r}_n$, respectively. For Cu $\alpha(\mathbf{k}_F)$ has been calculated by Jena et al. [114] with the result: $\alpha(\mathbf{k}_F|\,|\langle 100\rangle) = -6.5$, $\alpha(\mathbf{k}_F|\,|\langle 110\rangle) = 0.2$ and $\alpha(\mathbf{k}_F|\,|\langle 111\rangle) = -8.2$. The Bloch electron was represented by a linear combination of atomic orbitals (LCAO) in conjunction with *ab initio* APW band calculations of Burdick [115].

For protons or muons at the octahedral interstitial site in a fcc metal $\mathbf{k}_F$ will be along a $\langle 100\rangle$ direction for all six nearest neighbors.

As pointed out by Williams [116] the results of Jena et al. [114] for $\alpha(\mathbf{k}_F)$ have to be taken with caution. Applied to substitutional impurities in Cu one would expect to find only an extremely small EFG at the nearest host neighbors due to the screened potential of the impurity since $\mathbf{r}$ or $\mathbf{k}_F$, respectively, will coincide with the $\langle 110\rangle$-direction. This is in disagreement with the NMR-measurements in Cu of Jensen et al. [117].

In the older calculation of α in Cu by Kohn and Vosko [112] the Bloch electron was approximated by a single orthogonalized plane wave with no reference to the crystal periodic potential. This lead to an isotropic value for α which came out to be 25.6.

The Bloch enhancement factor was also calculated in Al [118, 119]. We mention here only results of Holtham and Jena [119], which were obtained by explicitely solving the one electron band structure Hamiltonian for aluminium using the model potential of Ashcroft. The results are:

$$\alpha(\mathbf{k}_F|\,|\langle 100\rangle) = 6.4; \qquad \alpha(\mathbf{k}_F|\,|\langle 111\rangle) = 8.3; \qquad \alpha(\mathbf{k}_F|\,|\langle 110\rangle) = 7.8$$

It is obvious that the measurement of EFG's at nuclei next to a proton or muon is indeed of much interest as it contains information on the spatial structure of the electron distribution around the impurity via $\delta n(r)$. However, to extract this information form μSR-data a better theoretical understanding of enhancement effects is clearly called for.

4.4. *Cluster-models*

The principal limitations of the applicability of the free electron gas model and its refinements are obvious as the actual electronic and geometrical structure of a real lattice is not accounted for in detail. Such details as lattice relaxation in relation to a certain site occupation, modifications of the electronic structure of the neighbors, bandstructure effects, local modifications of the bandstructure are certainly important in obtaining a realistic picture of the true electronic structure around a proton or a muon in a metal.

It seems that cluster calculations with respect to these details, at least

partially, may allow a much better approach. It may turn out, in fact, that it does not make much sense to ask for the electronic structure of just the impurity alone. One may rather have to consider the electronic structure of the impurity plus its neighborhood as one conceptually unseparable problem. This may reveal how a proton or muon is chemically bonded inside a metal lattice.

Despite the promise that cluster calculations seem to hold, only a few such calculations have actually been performed so far.

To our knowledge the first ones who have tried to perform cluster calculations on hydrogen in metals were Stoneham and Mainwood [120, 121].

They applied molecular orbital techniques in an approximation called Complete Neglect of Differential Overlap (CNDO). Calculations were presented for hydrogen in liquid alkalis and for hydrogen in solid Na, Li, Cu, Al and V. In the solids the potential energy surface for hydrogen was obtained which allowed a prediction of the site of localization and of the height of potential barriers between different sites, thus indicating possible diffusion paths. In some instances the local displacement of the nearest neighbor host atoms were calculated.

Generally it was found, in accord with experimental results, that the tetrahedral interstitial site is the most stable one for body centered cubic (bcc) metals (Na, Li, V) while for face centered cubic-(fcc-) metals (Cu, Al) the octahedral interstitial position is the favored one.

A molecular orbital cluster calculation for HMe_6 (Me = Metal: Ti, Ni, Pd) has also been performed by Adachi et al. [122]. As in the case of the cellular cluster calculations, to be discussed below, an energetically low lying state is formed which is of a covalent bonding nature, involving hydrogen $1s$ and metal $3d$ and $4p$ orbitals. In addition some antibonding resulting from the interaction of hydrogen $1s$ and metal $4s$ orbitals tends to weaken the covalency which effect is strongest for the HNi_6 cluster.

Results on a molecular orbital cluster calculation for hydrogen in Palladium have also been reported by Jena [107]. These calculations were mainly intended to check on the validity of the pseudo jellium calculations [107]. It was found that results from both approaches are quite similar, the pseudo jellium calculations apparently overestimating the charge density enhancement around the proton systematically to a moderate degree. Besides placing the proton at the center of the octahedral cluster Pd_6H the proton was also allowed to be displaced from that center along the $\langle 100 \rangle$ direction. Results for the charge density distribution around the proton at these various sites are shown in Fig. 10. These results again can be used to calculate some effective spin density at the proton averaged over its vibrational spread.

Most elaborate cluster calculations based on the self consistent multiple scattering cellular method [123] have recently been extended by Keller [124] and co-workers to positive muons in metals with the primary goal of calculating hyperfine fields and Knight shifts for muons in ferromagnetic and nonmagnetic metals [125–128]. For details of the technique see Refs. 123, 124. The potentials entering the calculation are obtained self-consistently from charge densities using the local exchange $X_{\alpha\beta}$-technique. The potential outside the cluster considered is represented by spherical averages over additional layers using either atomic potentials or pseudopotentials [123, 124].

A common feature of these cellular cluster calculations with respect to muons or protons in metals is the occurrence of cluster bonding and antibonding states

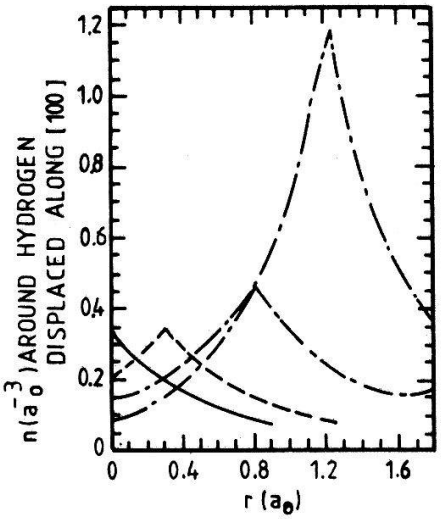

Figure 10
Charge distribution around the μ^+ at various positions displaced along the ⟨100⟩ direction from the center of the octahedral interstitial site in Pd (from cluster calculations [107]).

which are composed of hydrogen-like 1*s*-states and of the host valence states. The bonding states segregate to lower energies while the antibonding states move up on the energy scale. The relevance of these states depends on their relative position with respect to the conduction band and the Fermi energy. Bonding states well below the bottom of the conduction band represent localized cluster-states, which are of particular interest with regard to possible effects on hyperfine fields and Knight shifts. They seem to correspond to the hydrogen induced impurity bands found in bandstructure calculations [57].

Using equation (3.1.29) and the wavefunctions from a cellular cluster calculation, Keller and Schenck [126] have calculated for the first time the diamagnetic shielding or chemical shift constant for muons in a metal, i.e. in Be: $\sigma_{\mu^+\mathrm{Be}} = -27$ ppm. This result will be further discussed in Chapter VI. The cellular cluster technique has also been applied to a calculation of the lattice dilation around a μ^+ in [127, 128]. Above all, these calculations were very successful in reproducing measured hyperfine fields at positive muons in Ni [125], Fe, Co, and Gd [124], but were, however, unsuccessful in the case of Dy [124].

V. Results

5.1. *Knight shift measurements*

5.1.1. *Some experimental details*

The stroboscopic measurements in general and the used apparatus are described in detail in Ref. 43. The external field was chosen such that the muons precessed at the second harmonic of the beam burst repetition rate (≃101 MHz corresponding to 7.47 kG). The stroboscopic signal is then given in a simplified form following from equation (2.4.5)

$$S_i(\omega_\mu) = N\left(1 + \frac{A_{\mathrm{eff},i}}{1+(\omega_\mu - 2\Omega)^2\tau_\mu^2}\left(\cos\psi_i + (\omega_\mu - 2\Omega)\tau_\mu \sin\psi_i\right)\right) \tag{5.1.1}$$

The index i denotes a particular time window. The field was scanned forth and back over the stroboscopic resonance in 25 steps (corresponding to four line

width), each field setting was controlled by two independent proton (H_2O) NMR systems. At about the center of the resonance the target was moved out by remote control and a third NMR probe was inserted to measure the field at the center of the target position. A homogeneous field map over the target volume of ± 1 ppm was achieved with special shim coils which corrected for linear and quadratic field gradients. In terms of the external field the muon Larmor frequency consists of the following contributions [3].

$$\omega_\mu = 2\pi\gamma_\mu\left(1+K-\chi_b N+\frac{4\pi}{3}\chi_b\right)B_{\text{ext}} \tag{5.1.2}$$

Here γ_μ is the gyromagnetic ratio of the muon, K the Knight shift constant, $-\chi_b N B_{\text{ext}}$ the demagnetization field, N the demagnetization factor and $(4\pi/3)\chi_b B_{\text{ext}}$ the Lorentz field. χ_b is the bulk magnetic susceptibility of the sample.

The external magnetic field is measured in terms of the proton NMR frequency, using a cylindrical probe

$$\omega_p = 2\pi\gamma_p(1-\sigma^*_{H_2O})B_{\text{ext}} \tag{5.1.3}$$

γ_p is the proton gyromagnetic ratio and $\sigma^*_{H_2O}$ is mainly given by the diamagnetic shielding constant for protons in water ($\sigma = 25.64$ ppm). It includes small corrections due to the shape of the probe and the admixture of paramagnetic ions into the probe solution with the result $\sigma^* = -25.28$ (16) ppm.

Equation (5.1.1) will be fitted to the obtained data in a particular gate resulting in a determination of ω_p at the resonance $\omega_\mu = 2\Omega$. The Knight shift constant K is then obtained by combining equations (5.1.2) and (5.1.3)

$$K = \left(\frac{\mu_\mu}{\mu_p}\right)^{-1}\frac{2\Omega}{\omega_p}(1-\sigma^*_{H_2O})+\left(N-\frac{4\pi}{3}\right)\chi_b - 1 \tag{5.1.4}$$

Here $\mu_\mu/\mu_p = \gamma_\mu/\gamma_p$ is the ratio of the muon and proton magnetic moments which number is extremely well known [43] ($\mu_\mu/\mu_p = 3.1833441 \pm 0.53$ ppm). It is obvious that the sample shape and the bulk magnetic susceptibility enter critically into the actual evaluation of K. To circumvent this problem from the beginning we used with a few exceptions only spherical targets where the demagnetization field and the Lorentz field cancel ($N = 4\pi/3$).

For measurements below room temperature down to about 20 K a temperature stabilized He-flow cryostat was used. From room temperature up to 900 K an oven was developed in which the target was exposed to a flow of hot nitrogen gas.

Some typical errors related to the magnetic field are shown in Table 5.

Table 5
List of errors related to the magnetic field

Uniformity of field map in time and space	±0.5 ppm
Weighted field average	±(0.2–0.5) ppm*
NMR probe calibration	±0.2 ppm
Average of field measurements at target center for one run (4–6 individual measurements)	±(0.5–1.0) ppm
Total error	±(0.8–1.25) ppm

*) Depending on target size

5.1.2. *Knight shift results in nontransition (simple) metals*

All elementary nontransition (simple) metal samples investigated so far are listed in Table 6 together with information on sample shape, -condition and -purity. Generally the measurements were done at room temperature with the exception of solid Hg (−50°C) and a number of measurement in Cu ranging from 30 K to 800 K. Liquid Rb, Cs and Ga were investigated at temperatures about 10°C above the melting point (i.e. at 49°C, 39°C and 40°C respectively).

The results on the Knight shift constant K are collected in Table 7. The indicated errors are mainly determined by statistics. Other contributions included concern the magnetic field (see Table 5) and background. Where necessary the listed numbers contain also a correction for a stroboscopic background signal. The values for K in Na and K are also corrected for the nonspherical shape of the sample. For comparison Table 7 contains also the results of an older study by Hutchinson et al. [129]. Agreement for the alkali metals and Cu is good while the results for Mg and Ca are certainly incompatible.

In the case of muons in Cu the Knight shift was systematically measured as a function of temperature. The results are displayed in Fig. 11. No temperature dependence is visible. This will be discussed further in Section 6.1.2. In the case of muons in Be the Knight shift was measured in two different samples, one consisting of fine Be-powder of only marginal purity, the other one was machined out of bulk Be with much improved purity. No effect of sample purity and condition on the muon Knight shift is visible.

5.1.3. *Knight shift results in transition metals*

So far measurements have been performed in paramagnetic Ni, in Pd and in V, Nb and Ta. Information on the samples is given in Table 8. The Knight shift in V and Ta has only been measured at room temperature. The Knight shift in Ni was measured from just above T_c to 906 K (see Table 9 and Fig. 12) in Pd, from

Table 6
Target samples (nontransition metals)

Element	Crystal struct.	Sample shape	Sample form	Purity %
Li	bcc	sphere	single piece	99.98
Na	bcc	thick disk	single piece	>99.95
K	bcc	thick disk	single piece	>99.95
Rb*	bcc	sphere	single piece	99.9
Cs*	bcc	sphere	single piece	99.99
Cu	fcc	sphere	single piece	
Cu	fcc	cylinder	single x-tal	99.999
Ag	fcc	flat disk	single piece	99.999
Be	hcp	sphere	powder	>99
Be	hcp	sphere	single piece	>99.94
Mg	hcp	sphere	small grains	>99.8
Ca	fcc	sphere	grains	99.5
Sr	fcc	sphere	single piece	>99
Ba	bcc	sphere	single piece	99.5
Hg		sphere	single piece	99.9999
Al	fcc	sphere	single piece	>99.999
Ga	complex	sphere	single piece	>99.9999
Pb	fcc	flat disk	single piece	puriss.

*) Contained in sealed off spherical quartz vessels

Table 7
Knight shift results in nontransition elemental metals at room temperature (except where indicated)

Element	Knight shift (ppm) this measurement, Ref. [29, 30]	Knight shift (ppm) Ref. [129]*
Li	8.6±4.0	9.5±19*
Na	76.5±5.0	55 ±11*
K	63.2±4.5	64 ±11*
Rb solid	66.1±4.3	—
Rb liquid	79.9±5.5 (~49°C)	
Cs solid	31.0±4.0	
Cs liquid	32.0±6.0 (~39°C)	
Cu	60 ±2.5 (average)	55 ±11
Ag	94 ±3.5	
Be powder	−48.4±5.3	
Be single piece	−44.9±2.8	
Mg	20.6±6.5	63 ±11*
Ca	21.2±6.2	400 ±15*
Sr	−18.4±6.8	
Ba	29.6±5.0	
Hg solid	117 ±11 (−50°C)	
Hg liquid	205 ±6	
Al	79.6±4.0	
Ga solid	−17.0±3.5	
Ga liquid	97.6±4.0 (~40°)	
Pb	105.2±3.5	110 ±13

*) The results quoted in Ref. 129 were obtained with respect to water. The numbers in this table include a correction for the diamagnetic screening of muons in water (−25.6 ppm) and a correction for demagnetization effects.

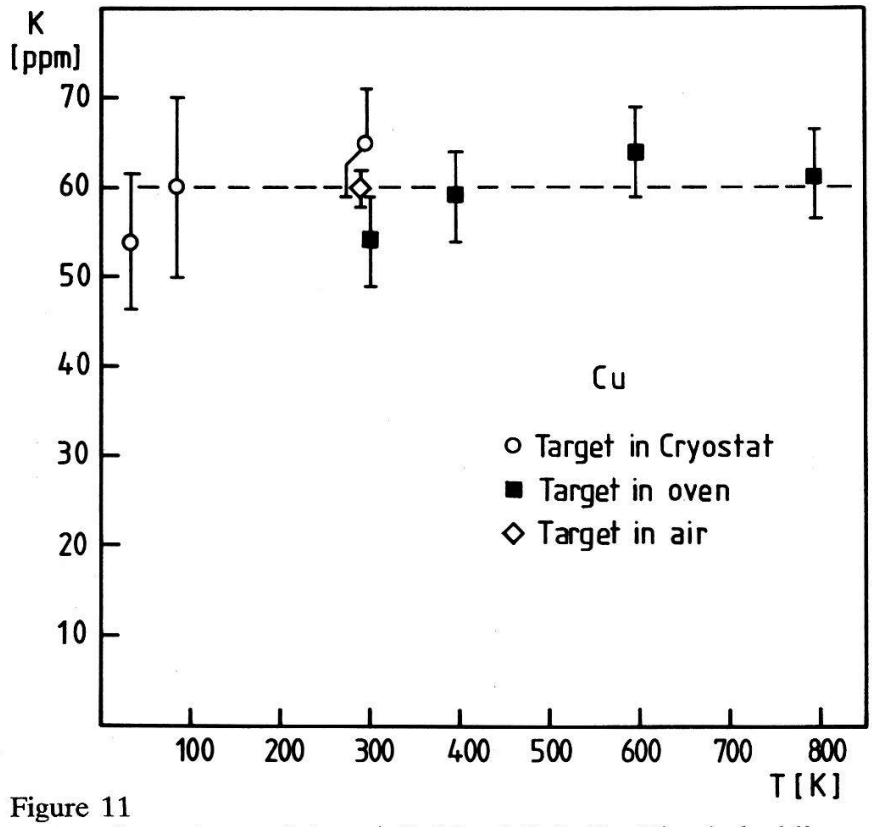

Figure 11
Temperature dependence of the μ^+ Knight shift in Cu. The dashed line represents the average of all data.

Table 8
Target samples (transition metals)

Element	Crystal struct.	Sample shape	Purity (main impurities)
V	bcc	polycrystalline sphere	99.9%
Nb	bcc	polycrystalline sphere	99.95% (Ta: 200 ppm)
Ta	bcc	polycrystalline sphere	99.95% (Nb: 280 ppm)
Ni	fcc	single crystal sphere	99.999%
Pd	fcc	polycrystalline sphere	99.999% (Si 5 ppm, Fe: 2 ppm)

Table 9
Knight shift results in paramagnetic Ni (single crystal sphere) in an external field of 7.47 KG (Ref. 34)

T(K)	$\chi\left(\frac{\text{emu}}{\text{g}}\right)^*$	K (ppm)
637 (±2)	$3.3 \cdot 10^{-3}$	−19025(90)
643 (±2)	$1.18 \cdot 10^{-3}$	−13346(58)
648(±1)	$0.72 \cdot 10^{-3}$	−9099(56)
651 (±1)	$0.57 \cdot 10^{-3}$	−6954(65)
653 (±2)	$0.50 \cdot 10^{-3}$	−6709(42)
$662\binom{+4}{-2}$	$0.29 \cdot 10^{-3}$	−4332(37)
680 (±1.5)	$0.173 \cdot 10^{-3}$	−2222(46)
685 (±2)	$0.153 \cdot 10^{-3}$	−1909(46)
703 (±2)	$0.106 \cdot 10^{-3}$	−1335(35)
752 (±3)	$0.057 \cdot 10^{-3}$	−664(35)
803 (±2)	$0.037 \cdot 10^{-3}$	−446(26)
$855\binom{+1}{-3}$	$0.028 \cdot 10^{-3}$	−307(23)
$906\binom{+1}{-3}$	$0.022 \cdot 10^{-3}$	−263(22)

*) From Refs. 163 and 164. The temperature scale in Ref. 163 has been shifted up by 5 K, fixing T_c at 632.5 K.

20 K to 883 K (see Table 10 and Fig. 13) and in Nb at 100 K, 293 K and 450 K (see Table 11). The numbers quoted for Ni include a correction which accounts for the additional field produced by the Ni-sphere at the NMR regulation probe.

The muon Knight shift in Pd at room temperature has also been measured by Imazato et al. [130] (see Table 10) and is in agreement with the other results.

5.2. *Electric field gradients*

5.2.1. EFG *in* Cu

As discussed in Chapter II the EFG at the host nuclei next to an interstitial muon can be determined from the field dependence of the low temperature

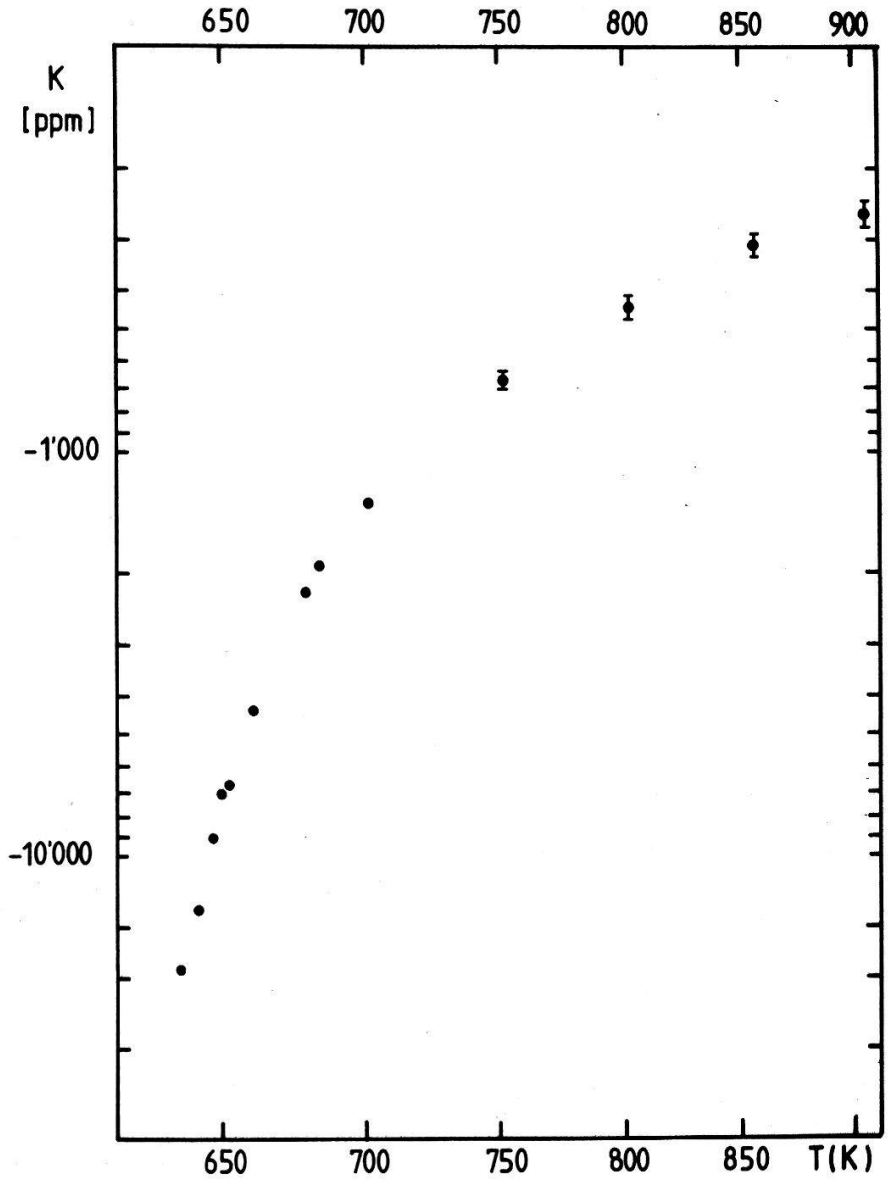

Figure 12
μ^+ Knight shift in paramagnetic Ni as a function of temperature [34]. (log-log plot)

depolarization rates in single crystal samples. The data to be reviewed here (Schilling et al. [18]), were obtained from three single crystals of Cu of high purity (5 N), obtained from Metals Research Ltd. The samples had a cylindrical shape with the cylinder axis coinciding with the ⟨100⟩-, ⟨110⟩-, ⟨111⟩-crystal axis, respectively. The crystals were mounted such that the external field was in each case parallel to the cylinder axis.

The depolarization rates obtained at 20 K and 80 K as a function of applied field strength are shown in Fig. 14. The damping of the μSR-signal was in all instances well represented by a Gaussian function. There is no difference in the results, obtained at the two temperatures, indicating that the muons at these temperatures are well frozen in at some interstitial site, i.e. that the diffusion rate is slow compared with the muon decay rate (10^4 sec^{-1}), thus justifying the use of a Gaussian damping function.

Table 10
Muon Knight shift in Pd (external field = 7.47 kG)
(Ref. 33,† Ref. 130)

Temp [K]	$\chi_{Pd}\left[\frac{emu}{mol}\right]$*	K_μ [ppm]**
19.8	$7.35 \cdot 10^{-4}$	−276.5 ± 11 (7)
34.8	$7.45 \cdot 10^{-4}$	−290.3 ± 9 (5)
50.6	$7.63 \cdot 10^{-4}$	−287.7 ± 9 (5)
60	$7.75 \cdot 10^{-4}$	−282.8 ± 9 (5.5)
75	$7.82 \cdot 10^{-4}$	−285.2 ± 10 (6)
82.5	$7.87 \cdot 10^{-4}$	−285.6 ± 13 (10)
100	$7.87 \cdot 10^{-4}$	−290.3 ± 11 (6.5)
190	$6.85 \cdot 10^{-4}$	−244.9 ± 10 (6)
293	$5.5 \cdot 10^{-4}$	−187.3 ± 11 (7)
293	$5.5 \cdot 10^{-4}$	−214 ± 9 (5.3)
293	$5.5 \cdot 10^{-4}$	−177.9 + 9 (4)
293†	$4.9 \cdot 10^{-4}$	−223 + 80
459	$4.07 \cdot 10^{-4}$	−122 ± 23 (21)
628	$3.17 \cdot 10^{-4}$	−87.8 ± 10 (5.5)
673	$2.98 \cdot 10^{-4}$	−83.3 ± 10 (7)
823	$2.51 \cdot 10^{-4}$	−82.9 ± 16 (4)
883	$2.34 \cdot 10^{-4}$	−64.7 ± 18 (4)

*) The susceptibility data were taken from Ref. 165.
**) The error in parenthesis is the statistical error only. The quoted total error includes contribution from background correction and a contribution from small field shifts inside the cryostat and the oven.

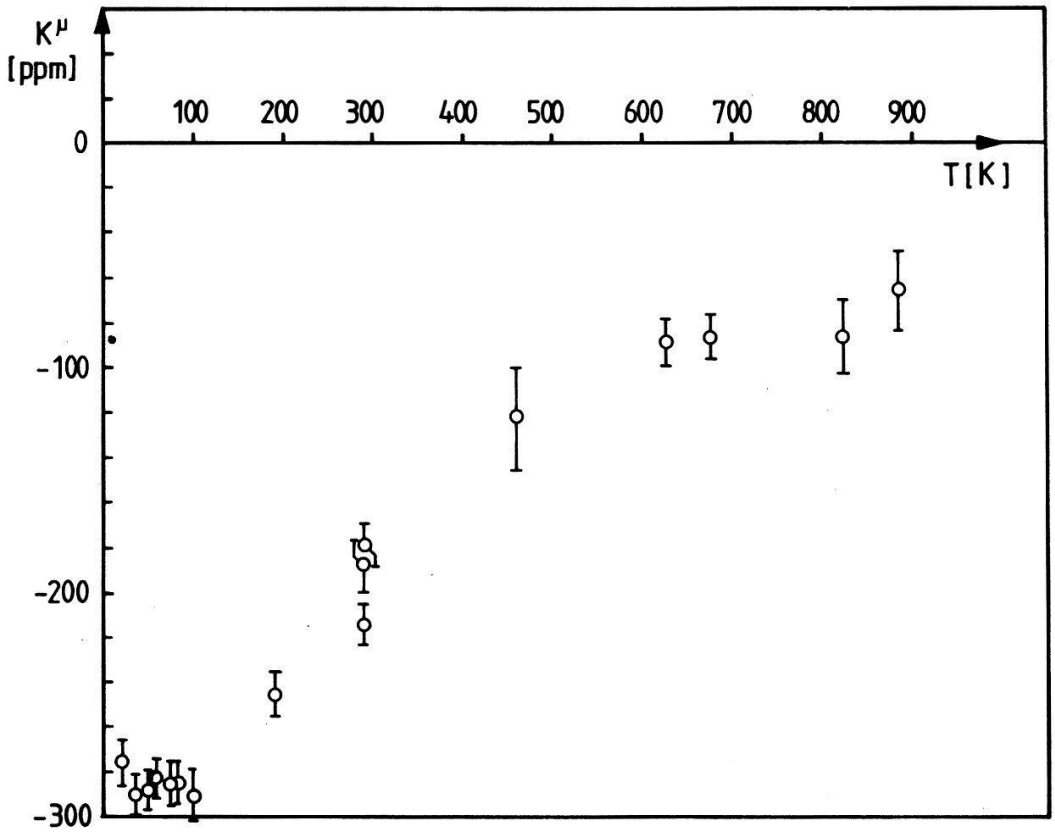

Figure 13
μ^+ Knight shift in Pd as a function of temperature (from Ref. 33).

Table 11
Muon Knight shift in group V *B* metals

Element	Temp [K]	K_μ [ppm]	
V	~290	−(88±8)	
Nb	100	−(14.9±5.8)	average
Nb	~290	−(16.4±4.5)	−(15.6±3.0)
Nb	423	−(15.0±4.5)	
Ta	~290	+(5.5±10)	

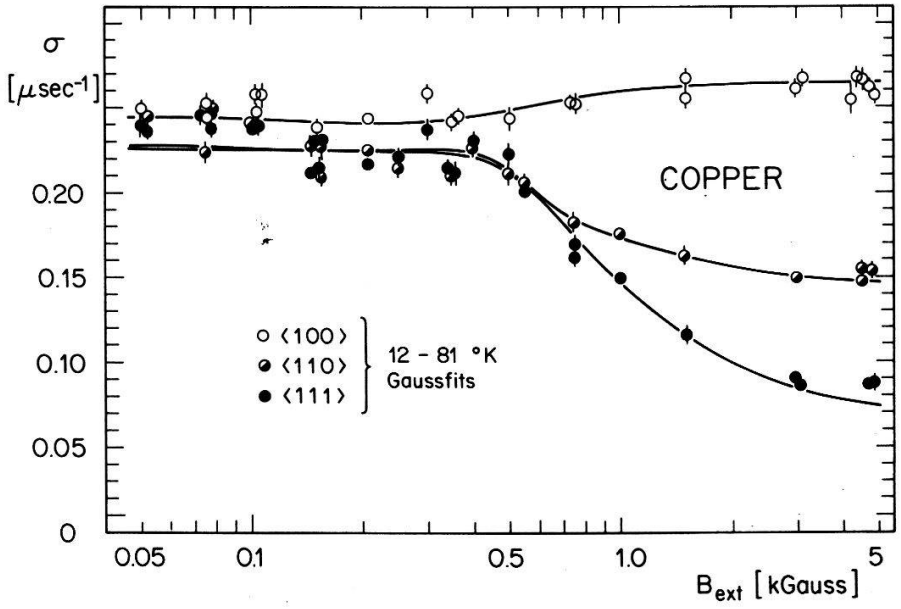

Figure 14
Experimental damping constant σ of the μSR-signal in single crystals of Cu versus magnetic field and for different orientations of the crystals with respect to the field. The solid curves were calculated from the Hartmann model [47] for an octahedral site assignment of the muon and include a dilation of the nearest neighbor by ~5% (from Ref. 18).

The data were analyzed according to Hartmanns theory [47] under the assumption that the EFG was radially directed from the muon and that only the nearest neighbors were affected by it, while the next nearest and further neighbors were treated according to the Van Vleck theory [44].

The muon was placed either in the octahedral or in the tetrahedral interstitial position. Only the octahedral site assignment was compatible with the dependence of the data on the orientation and strength of the applied field.

The electric quadrupole interaction strength at the nearest neighbors was determined to be

$$\frac{\omega_e}{2\pi} = \frac{eQ}{h}\frac{|V_{zz}|}{4S(S+1)} = 0.18 \pm 0.02\ \text{MHz} \qquad (5.2.1)$$

where Q is the electric quadrupole moment of Cu, V_{zz} the EFG at the nearest neighbors and S the nuclear spin of Cu ($S = \frac{3}{2}$). Natural copper is composed of the two isotopes $_{29}Cu^{63}$ and $_{29}Cu^{65}$ with natural abundances of 69.1% and 30.9%,

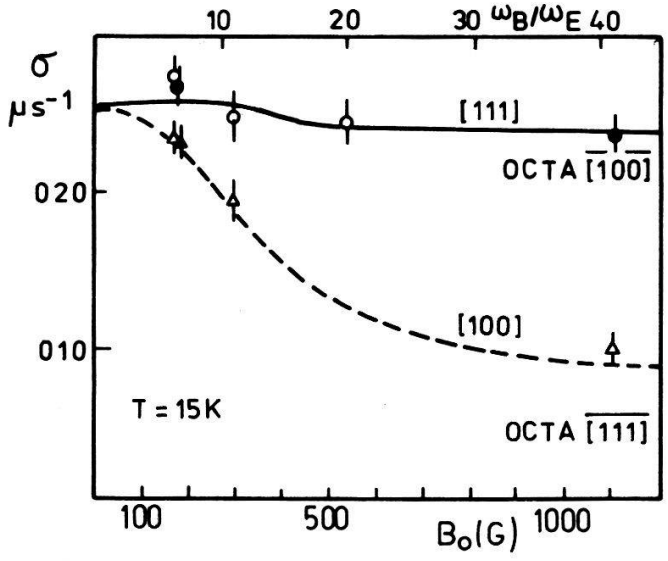

Figure 15
Experimental field dependence of σ in Al at 15 K. The solid and the dashed curves represent theoretical calculations for the different crystal orientations placing the muon at the tetrahedral interstitial site and allowing for a local lattice dilation of +7.7% (from Ref. 15).

respectively. The quadrupole moments of these two isotopes are not too well known and there is quite a scatter of values from different determinations (see e.g. Fuller and Cohen [178]). In any case the quadrupole moments of the two isotopes are quite close to each other. In calculating the EFG from equation (5.2.1) we use for both isotopes[4])

$$Q \approx 0.206 \text{ barn}$$

The EFG is then calculated to be

$$q \approx \frac{|V_{zz}|}{e} = 0.30 \pm 0.03 \text{ Å}^{-3}$$

Note, that the sign of the EFG cannot be determined by the present method. The quoted error reflects only the uncertainty in $\omega_e/2\pi$.

Another result of the analysis is, that the nearest neighbors are displaced radially away from the muon by ~5%, while the next nearest neighbors do not show a displacement, within the present statistical accuracy.

In the analysis the finite extent of the muon wave function in the interstitial site has been neglected. This seems to be justified in view of the discussion in Chapter II.5.

5.2.2. EFG *in* Al

Hartmann et al. [15] have studied the diffusion and localization of positive muons in single crystals of Al doped with a small amount (550 ppm and

[4]) In Ref. 18 an average $Q = 0.20$ barn was used, which results in $q = 0.27$ Å^{-3}.

1300 ppm) of Mn. The doping with Mn was necessary in order to be able to sufficiently slow down the muon motion at low temperatures. The presence of Mn impurities gives rise to strain fields which seem to facilitate the self trapping of positive muons at an ordinary interstitial site somewhere in the vicinity of the impurity.

The field dependence of σ at a temperature of 15 K was measured for the ⟨100⟩- and ⟨111⟩-crystal axes parallel to the applied field. Analysis of the results (see Fig. 15) leads to a tetrahedral site assignment at $T = 15$ K and an estimated EFG at the nearest Al neighbors of $q \simeq 0.18$ Å^{-3}. All four nearest neighbors seem to be Al-atoms, indicating that the immediate environment of the muon is that of the pure host lattice [15].

VI. Discussion

6.1. *Muon in nontransition (simple) metals*

The discussion of the measured Knight shifts is confronted with the problem of knowing with some confidence the electron spin susceptibilities of the metals in question as was pointed out in Chapter III. Therefore a short review of our current knowledge and understanding of the relevant electron spin susceptibilities may be appropriate before a discussion of the frequency shifts is attempted. Secondly one has to consider wether they are strongly modified by diffusion and trapping at impurities. The discussion of EFG's in Cu and Al will follow at the end of this chapter.

6.1.1. *Electron spin susceptibilities*

The elecron spin susceptibility can be obtained in a number of direct and indirect ways. Direct measurements, which involve the techniques of conduction electron spin resonance (CESR), spin wave excitations, de Haas van Alphen effect, have only been successful so far in the alkalis and in Be, Cu and Al. In all other instances the electron spin susceptibility has to be extracted indirectly from total susceptibility data, from electronic specific heat data and in a few examples, from host Knight shift measurements.

The conduction electron spin resonance (CESR) method involves the measurement of the area under a CESR absorption curve which is proportional to χ_p. Unfortunately this most direct method, which is free of any ambiguities has only proven possible in Li [131], Na [132] and Be [133]. The value quoted for Be has to be taken as a very preliminary result. The CESR-measurement in Cu [134] made use of the transmission electron spin resonance (TESR) technique in conjunction with the presence of a small amount of Cr-ions. It involves the measurement of the g-shift which is a function of χ_d/χ_p, where χ_d is the impurity local moment susceptibility, which is determined separately, and hence χ_p can be extracted.

The TESR-technique can also be used to induce spin waves which manifest themselves as more or less resolved satellite lines to the CESR-signal. The excitation of spin waves is a cooperative phenomenon in an electron gas which is based on the presence of electron–electron interations or 'many body' effects. The position of the spin wave signals with respect to the CESR signal allows to

determine the zeroth order Landau parameter B_0, which enters into the expression equation (3.1.11) for the spin susceptibility.

$$\chi_p = \chi_F \cdot \frac{m^*}{m} \cdot \frac{1}{1+B_0} \tag{6.1.1}$$

The actual analysis of the spin wave data involves a number of approximations and the absolute accuracy in the final numbers is therefore somewhat limited [137, 139, 140, 145].

A very elegant method to extract χ_p/χ_F directly is to study the amplitude of the rth harmonic of the oscillatory de Haas van Alphen signal which is given by

$$G_T = \cos\left(\tfrac{1}{2}\pi r g \frac{m^*}{m}\right) \tag{6.1.2}$$

where g is the average Landé spin splitting factor of the electrons in the extremal orbit of the Fermi surface considered.

$$g = g_s \frac{1}{1+B_0} \tag{6.1.3}$$

g_s is the conduction electron g-factor as determined by CESR-measurements. With equation (6.1.2) one obtains

$$G_r = \cos\left(\tfrac{1}{2}\pi r g_s \frac{\chi_p}{\chi_F}\right) \tag{6.1.4}$$

Because the amplitude is a cosine expression there are many possible results for χ_p/χ_F. To restrict the number of possible results at least the absolute phase of the dHvA oscillations should be known. Some further guidance is necessary, e.g. approximate values for χ_p/χ_F should help to make some definite choice [141, 144].

It is found that for most of the alkalis all results, irrespective of the method by which they have been obtained, agree fairly well with each other. There is some ambiguity concerning the results for Cs [141]. The dHvA measurements provide two possible numbers, one of which is consistent with the value extracted from the total susceptibility [138] and the other one is in agreement with the value deduced from the Cs-Knight shift [142].

Concerning Cu one is also faced with an inconsistency. The CESR result [134] is significantly smaller than the dHvA result [144] and the number extracted from the total susceptibility. Results for Al are again in fair agreement [145, 138].

Indirectly χ_p^{exp} can be determined from total susceptibility measurements:

$$\chi_{tot} = \chi_{ion} + \chi_p + \chi_L \tag{6.1.5}$$

where χ_{ion} is the diamagnetic susceptibility of the ion core electrons and χ_L is the diamagnetic orbital Landau conduction electron susceptibility. In the free noninteracting electron gas approximation $\chi_L = -\frac{1}{3}\chi_p$.

The problem is, that χ_{tot} is often not very reliably known and that χ_{ion} needs to be calculated or estimated in other ways [138, 143]. χ_p^{exp} can also be obtained indirectly from host NMR Knight shift measurements, sometimes by combination with $T_{1,e}$-data using the Korringa relation [135, 142]. The problem here is usually the lack of a precise knowledge of $\langle|\psi|^2\rangle_F$.

One can also correlate the spin susceptibility with the electronic specific heat γ_{cp} because both are proportional to the density of states at the Fermi energy:

$$\chi_p = 3\left(\frac{\mu_B}{\pi k_B}\right)^2 \gamma_{cp} = 3\left(\frac{\mu_B}{\pi k_B}\right)^2 \frac{m^*}{m} \gamma_{cp,F} \tag{6.1.6}$$

$\gamma_{cp,F}$ is the free electron gas value and m^* is the effective electron mass, which is obtained empirically from the ratio $\gamma_{cp}/\gamma_{cp,F}$ [78, 136]. The so calculated χ_p is an underestimate since exchange enhancement effects are not included. This is indeed indicated in all instances, except Be, where a direct measurement of χ_p was possible [133], which shows that

$$\chi_p^{exp} \gtrsim \frac{m^*}{m} \chi_F$$

Equation (6.1.5) was used to calculate lower limits for χ_p in Mg, Ca, Sr, Ba, Ag, Pb, Hg and Ga [136] (see Table 12).

The total susceptibilities of Ca and Sr are positive and quite large ($\chi_{tot}(Ca) = 1.53 \times 10^{-6}$ emu/cm^3, $\chi_{tot}(Sr) = 2.71 \cdot 10^{-6}$ emu/cm^3) as compared to the other alkali and alkaline earth metals. Neglecting the diamagnetic terms these numbers can be likewise used as lower limits on χ_p. In the further discussion we will always refer to the largest of these lower limits.

There are many theoretical calculations of the electron spin susceptibility in simple metals. Experimental numbers seem to be best reproduced by calculations

Table 12
Compilation of experimentally derived spin susceptibilities used in the analysis. The uncertainties on the directly measured values are of the order of 5–10%. In all other instance the numbers present lower limits

Element	$\chi_p\left(\frac{\text{emu}}{\text{cm}^3}\right) \cdot 10^6$	$\chi_p\left(\frac{\text{emu}}{\text{mole}}\right) \cdot 10^6$	source method	Ref.	other Refs. of interest
Li	2.10	26.8	CESR	131	137, 138, 150
Na	1.09	24.8	CESR	132	139, 138, 135, 147, 150
K	0.90	38.7	dHvA	141	139, 138, 142, 147, 150
Kb	0.86	45.1	dHvA	141	140, 138, 142, 147, 150
Cs	0.81 or 1.03	54.1 or 68.8	dHvA	141	138, 142, 147, 150
Cu	1.36	9.67	dHvA	144	134, 138, 127, 146
Ag	~0.876	~8.7	γ_{cp}	136	
Be	~0.2	~0.99	CESR	133	126
Mg	~1.58	~22.1	total χ	143	151
Ca	~1.58	~41.5	γ_{cp}	136	151
Sr	>2.69	>91.3	total χ		151
Ba	~0.99	~37.8	γ_{cp}	136	
Hg solid	~1.73	~25.5	γ_{cp}	136	
Hg liquid	~1.77	~26.1	total χ	136	
Al	1.77	17.6	spin wave	145	138, 151, 152
Ga solid	~0.698	~8.24	γ_{cp}	136	
Ga liquid	~2.8	~33.0	total χ	136	
Pb	~2.36	~43	γ_{cp}	136	

which take crystalline effects into account, either by refering to the pseudo potential formalism (Borchi and Gennaro [146], S. K. Lai et al. [147]) or to self consistent calculations on the basis of a functional formalism introduced by Kohn and Sham [148] and by Vosko and Perdew [149] (S. H. Vosko et al. [150], J. F. Janak [151]).

Table 12 contains a compilaton of experimental spin susceptibility data, which are thought to be the most reliable ones. These numbers are used throughout the further analysis.

6.1.2. *Possible role of muon diffusion and trapping*

Let us first consider the influence of intrinsic diffusion between equivalent sites on the Knight shift. Here one does not expect any effect. Since the residence time at some interstitial site is assumed to exceed always by far the jump time [153] it is actually of no consequence wether the muon will move or rest. The static Knight shift will be the same as the motional average. This is indeed supported by the data obtained in Cu, which were shown in Fig. 11. It is known, that below ~80 K the muon is frozen in at the octahedral interstitial site while at roomtemperature the residence time has decreased to ~0.05 μsec, corresponding to about 40 jumps during its lifetime. The data do not indicate any change of the Knight shift with temperature.

On the other hand, it is known that trapping has a pronounced impact on the μ^+ diffusion rate, particularly in bcc-metals [10, 11]. In the high temperature limit, approximately realized in the roomtemperature measurements, the trap escape rate ν_e is given by the pre-exponential factor ν_0 of the Arrhenius law

$$\frac{1}{\tau_e} = \nu_e = \nu_0 \exp(-E_t/kT) \tag{6.1.2.1}$$

while the residence time at some undistorted interstitial site is estimated to be of the order of 10^{-13} sec (for hydrogen ~10^{-12} sec[8]). The relative fraction of time spent in a trap, $(\Delta t_{\text{trap}}/\Delta t_{\text{intr.}})$, is then roughly estimated to be $(c/\nu_0) \cdot 10^{13}$ where c is the concentration of traps in atomic −%. Some number for ν_0 are: $\nu_0(\text{Be}) = 10^{10}\,\text{sec}^{-1}$ [154], $\nu_0(\text{Nb}) \simeq 10^9\,\text{sec}^{-1}$ [155], $\nu_0(\text{Ta}) \simeq 10^9\,\text{sec}^{-1}$ [17]. Unfortunately no such numbers are available in almost all of the other metals in which the muon Knight shift has been measured. We therefore take these numbers as typical ones.

In order that $\Delta t_{\text{trap}}/\Delta t_{\text{intr}} < 1$, i.e. muons spent most of their time in an undisturbed part of the crystal, the concentration of traps must be of the order of less than (100–1000) ppm. Looking at Table 5 it is realized that this condition is in most cases only marginally or not at all granted, if all impurities would act as traps. On the other hand the example of Be has shown that the Knight shift was not changed by going from a sample with 10 000 ppm total impurity content to a sample with 600 ppm, which should have made a big difference. Apparently the total amount of impurities is indeed not a relevant number. Rather only certain impurities act as traps and their relative abundance, which certainly is a smaller number, would have to be considered. μ^+ diffusion studies in Al, doped with Mn impurities [15] have been interpreted to the effect that these impurities facilitate self trapping of the μ^+ by lattice strain. The μ^+ is localized thereby at an ordinary (tetrahedral) site somewhere in the vicinity of the impurity, but the immediate environment is that of the pure host. Similarly μ^+ trapping in Nb seems to happen

at a tetrahedral interstitial site, whereby one of the four nearest neighbors is replaced by an impurity, e.g. Ta [156]. In both cases it can be expected that the local electronic structure will not change drastically since type and symmetry of the interstitial site are unchanged. If these possibilities would be the prevailing trapping configurations also in other metals and if the involved impurities would not possess any magnetic properties, e.g. local magnetic moments, it can be expected that also the Knight shift will be largely unchanged from the pure host value.

On the basis of these considerations it is judged that the presented Knight shift data reflect largely intrinsic properties of the muon-host metal complex. It is planned to further corroborate this assumption by future measurements.

6.1.3. *Discussion of the μ^+-Knight shift*

6.1.3.1. *Comparison of the data with theoretical predictions*

We begin by displaying the data in two different plots, which allow an overall comparison of the results. In the first plot (Fig. 16) the Knight shift data are plotted versus the main quantum number of the outer electrons of the host atoms.

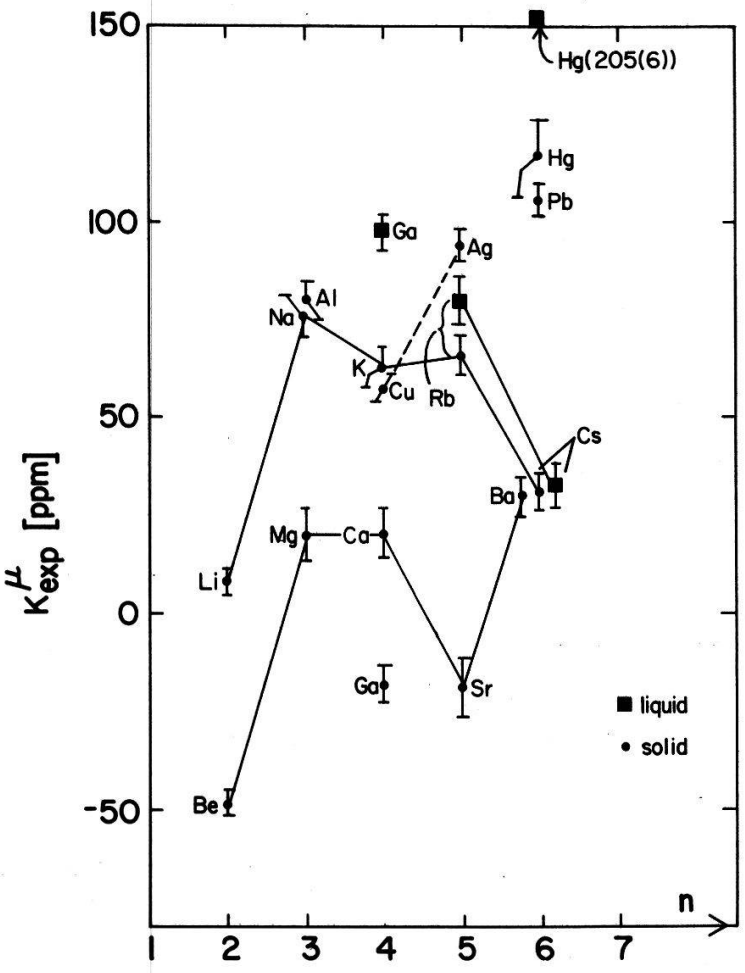

Figure 16
μ^+-Knight shift results in nontransition metals plotted versus the main quantum number n of the valence electrons.

This allows to display possible correlations with the position of the host atom in the periodic table. Such correlations are not indicated except for a certain parallelity in the data obtained in the alkali and alkaline earth metals series.

Generally the Knight shift in the liquid phase is larger than in the solid phase. Most remarkable are the change from a negative Knight shift in solid Ga to a positive Knight shift in liquid Ga, and the huge jump of the Knight shift in Hg upon melting. In Cs and less so in Rb, the Knight shift increases only little upon melting. Figure 16 shows further that a negative Knight shift is observed in Be, Sr and in Ga. This fact demonstrates that it is not sufficient to consider the direct Knight shift (equation 3.1.9) alone, but that indeed diamagnetic screening and core polarization effects have to be taken into consideration.

In the second plot (Fig. 17) the Knight shift data are plotted versus the electron density parameter $r_s = ((3/4\pi)(1/n))^{1/3} a_B$, where n is the average conduction electron density, and a_B the Bohr radius. Again no systematic trends are detected.

Next we calculate Knight shift constants from the nonlinear screening jellium results discussed in Chapter IV and listed in Table 2 using consistently only the experimental susceptibility results listed in Table 12. The Knight shift is either calculated according to equation (3.1.12) or equation (3.1.22). We use average values for $\eta_F(r_\mu)$ and $\rho_s(r_\mu)$ obtained by interpolation from the numbers in Table 2. The predictions thus obtained neglecting at this stage diamagnetic shielding,

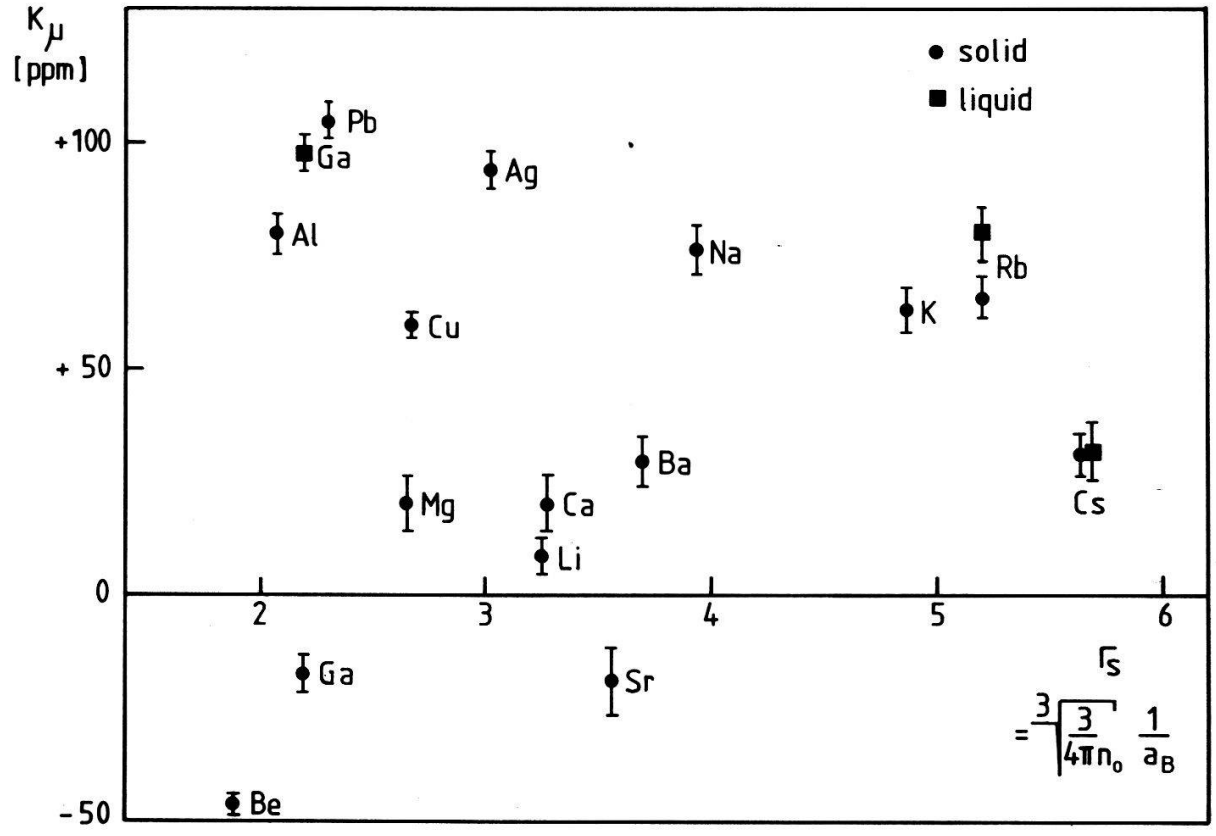

Figure 17
Plot of the μ^+-Knight shift data from nontransition metals versus the electron density parameter $r_s = \sqrt[3]{(3/4\pi)(1/n)} \cdot a_B$, where n is the density of the conduction electrons.

are displayed in Fig. 18 for the alkali and alkaline earth metals. The upper values are obtained by using $\eta_F(r_\mu)$ the lower ones by using $\rho_s(r_\mu)$.

To further facilitate the comparison, Fig. 19 shows a plot of K_{exp} versus K_{theor}, where K_{theor} is calculated by use of $\rho_s(r_\mu)$ for all the investigated simple host metals. Figures 18 and 19 reveal that the overall distribution of the data are only poorly reproduced by the jellium predictions. Generally, with the exception of Ag and solid Hg, the experimental values are always smaller than the theoretical ones. Interestingly the deviation is largest in those metals that possess the largest spin susceptibility constants.

The negative Knight shift values found in Be, Sr and Ga are in principle outside the predictive frame of the jellium model approach. It should be noted,

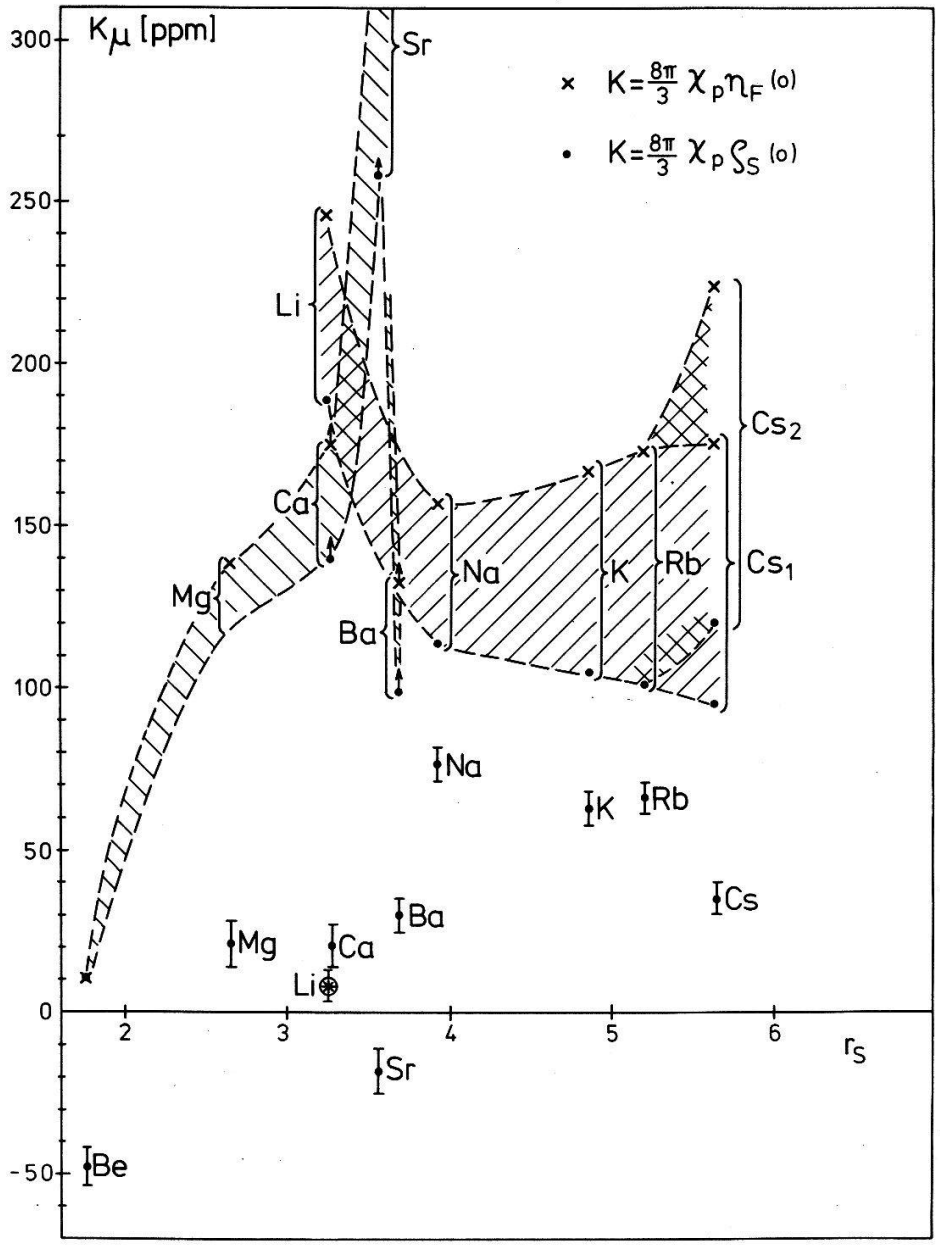

Figure 18
Comparison of nonlinear jellium calculations and experimental μ^+-Knight shift data in the alkali and alkaline earth metals series. The upper curve is obtained by using the theoretical charge density enhancement factor $\eta_F(r_\mu)$ (see equation (3.1.12)), the lower curve by using the spin density enhancement factor $\rho_s(r_\mu)$ (see equation (3.1.22)).

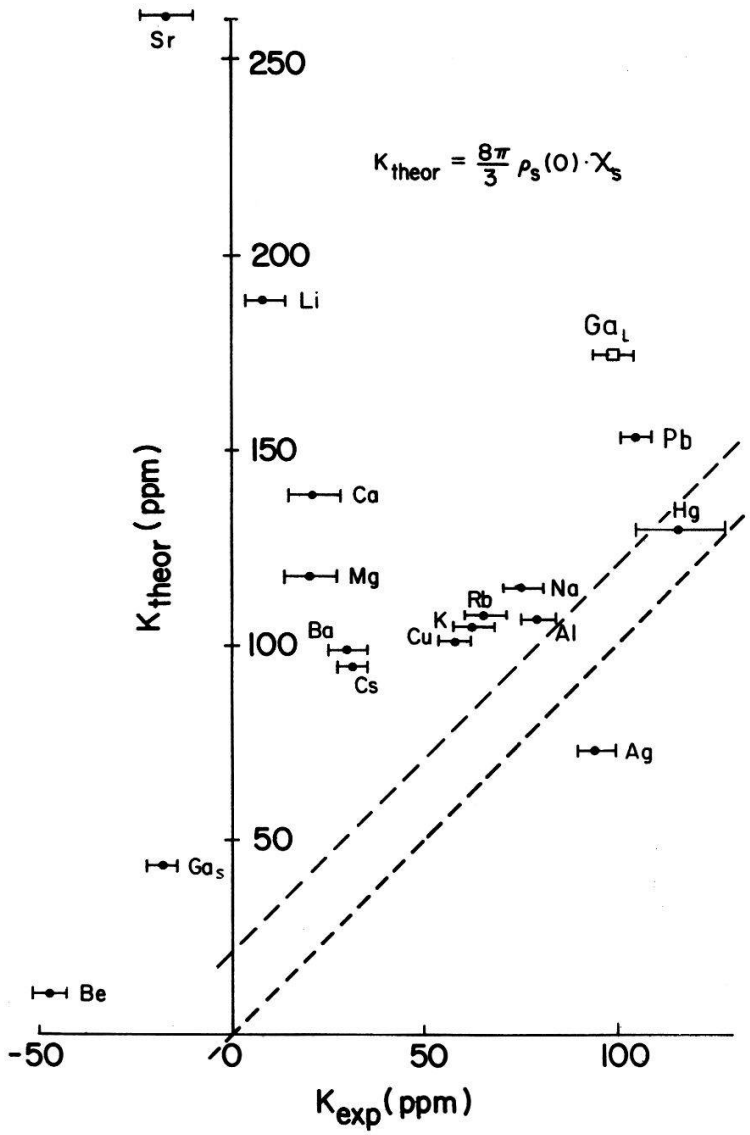

Figure 19
Plot of experimental Knight shift data K_{exp} versus theoretical numbers K_{theor}, calculated from equation (3.1.22) (jellium model). Taking a −20 ppm diamagnetic contribution into account one would expect the data to fall on the upper dashed straight line.

however, that the difference $\Delta K = K_{theor} - K_{exp}$ for Be and, e.g., for Cu is roughly the same despite the different sign of K_{exp}.

This may be taken as an indication that diamagnetic screening, adding a negative contribution to the total Knight shift may be partially responsible for the deviations between experiment and jellium theory. Including now the theoretical values for the diamagnetic shielding from Ref. 108, which are all in the vicinity of ~ -20 ppm, the total theoretical predictions are somewhat lower (e.g. in Be K_{theor} becomes negative!) but of course the overall distribution of the data is still not reproduced.

Available results from SSM, cluster and band structure calculations are collected in Table 13 together with the experimental numbers. The SSM predictions, including a diamagnetic contribution, are in fact quite close to the experimental numbers in Na and in Al, when placing the muon in the latter case in the octahedral interstitial site. This, however, is inconsistent with proton channelling

[14] and muon diffusion and trapping studies [15] in Al which both suggest a tetrahedral site occupation of protons and muons in Al. For Cu it would seem that a tetrahedral site assignment is also the more favorable one with respect to the Knight shift. In Cu it is, however, well known, that muons occupy the octahedral interstitial site [13]. One has to conclude that on the basis of the present limited possibilities of comparison it is hard to evaluate the merits of the SSM calculations with respect to their ability to predict correctly the muon Knight shift. The SSM calculations are, of course, still very approximate in that the neighbor ions enter only into the problem via spherically averaged potentials. Since the electrons of the host atoms are not appearing explicitly all those aspects that involve the formation of bonding states and the overlap of muon centered and host atom centered wave functions are not accounted for.

From this point of view cluster calculations hold much more promise. Indeed as is seen from Table 13 the predicted Knight shift for Cu (Castro et al. [127, 128]) is in quite good agreement with experiment. The authors used for χ a theoretical value of $1.46 \cdot 10^{-6}$ emu/cm^3 which is close to the experimental value in Table 12. It is also interesting to note that the diamagnetic contribution (Lambterm) originating from the localized cluster states amounts only to -7 ppm. A further contribution of -3 ppm is ascribed to band magnetism. Compared with the atomic hydrogen value of -17.8 ppm and -16 ppm from Ref. 108 it appears that the charge density distribution around a μ^+ in Cu does no longer resemble closely that of a hydrogen atom.

Cluster calculations in Be (Keller and Schenck [126]) yielded a small positive result for the direct Knight shift ($\sim$9 ppm, using again χ_p^{exp}). In addition the diamagnetic shielding produced by the doubly occupied low lying bonding state was calculated according to equation (3.1.27) yielding $\sigma = -27$ ppm. This is now a very typical value for the chemical shift of protons in molecules. The total

Table 13
Theoretical KS predictions from SSM, cluster and band structure calculations. Values in parentheses include diamagnetic shielding

		Na	Cu	Be	Al
	K_{exp} [ppm]	76.5(5.0)	59.6(2.3)	−46.7(3.0)	79.6(4.0)
K_{theor} [ppm]	Spherical solid model (SSM) (103) calculated with use of ρ_s (r_μ) and experimental χ (Table 12) (Diamangetic corrections from Ref. 108)	[1] 91.3 (71.3)	[1] 118.5 (102.5)		[1] 93.4 (78.4)
		[2] 91.3 (71.3)	[2] 98.0 (82.0)		[2] 50.4 (35.4)
	Cellular cluster (128, 126)	[1]	[1] +71 (+61)	+9 (−18)	
	KKR-CPA band structure (63)		[1,2] 55		

[1] Octahedral site
[2] Tetrahedral site

frequency shift is then predicted to be −18 ppm. This value deviates from the measured one still considerably, namely by −30 ppm, but inclusion of the effect of diamagnetic shielding can at least produce a negative total shift.

Finally, we comment on the value for K in Cu obtained by a band structure calculation in the coherent potential approximation (CPA) [63]. As in the cluster calculations local bonding states are formed which provide to a large extent the screening charge around the μ^+. The value of +55 ppm (Table 13) appears to be somewhat on the low side in view of the fact that inclusion of diamagnetic shielding would reduce it further down in comparision with the experimental value.

The large negative shift in Be suggests strongly that other negative contributions might be present in addition to the diamagnetic shielding. Following a suggestion by Fukai and Kazama [27] it is tempting to consider the possibility that the localized bonding-state would be capable of producing an internal field by core polarization and, in the case of *d*-metals, by transferred hyperfine fields. We have discussed before how spin dependent exchange and correlation potentials could lead to nonzero spin densities at the muon or proton. It is therefore conceivable that the bonding states could become polarized by an antiferromagnetic exchange interaction with the conduction electrons which in turn are polarized by the external field. Other possible mechanisms have been discussed by Das [157, 158].

To interpret the large negative Knight shift on that basis alone appears, however, questionable in view of the results obtained in solid and liquid Ga. The nuclear Knight shift in Ga changes upon melting by roughly the same relative amount as the spin susceptibility [136]. We therefore assume that also the change of the muon Knight shift in Ga upon melting is due to only the change in χ_p as is also suggested by the position of the Ga data in Fig. 19. We write

$$K = \frac{1}{\mu_B} B_{hf}^{\Omega_a}(r_\mu)\Omega_a \chi_p + K_{dia} \qquad (6.1.3.1)$$

Using for χ_p the values given in Table 13 one arrives at:

$$B_{hf}^{\Omega_a}(r_\mu) \simeq 2.6 \cdot 10^4 \text{ Gauss}/\mu_B/\text{atom}, \; K_{dia} \simeq -55 \text{ ppm}.$$

The constant diamagnetic term is surprisingly large and exceeds the calculated value [108] by about a factor of two. This negative value compares in size with the negative muon Knight shift in Be, particularly if corrected for the small positive contribution associated with the small spin susceptibility.

To conclude we have to consider the possibility that in certain cases the diamagnetic contribution can assume large values and that the observation of a large negative muon Knight shift may not at all reflect core polarization. On the other hand there is the theoretical task of explaining a diamagnetic contribution of the order of ~ -50 ppm which, after all may still be related to local (cluster) bonding states.

Completely incomprehensible for the time being is the huge positive Knight shift in liquid Hg. Nuclear Knight shift measurements do not show any change from the solid to the liquid phase, indicating that also the spin susceptibility remains uneffected. Apparently the local electronic structure of the muon-metal complex differs considerably in the two phases.

To summarize on the comparison of theory with experiment the following points are listed.

(1) The nonlinear response jellium calculations do not describe the bulk of the data, in particular the trend of the Knight shift in the alkaline earth metals is not reproduced. For all metals with the only exception of Ag the predictions are larger than the experimental numbers.

(2) Inclusion of diamagnetic screening shifts the jellium predictions somewhat closer to the experimental numbers, but does not improve on the systematics.

(3) Improved jellium calculations on the basis of the spherical solid model in Na, Cu and Al yield values quite close to the experimental ones, implying, however, site assignments for the muon in Cu and Al which are in contradiction with other measurements.

(4) Microscopic first principles calculation are available for muons in Cu and Be. Large differences in diamagnetic shielding are indicated in qualitative agreement with experiment. The local electronic structure is characterized by the formation of muon-host bonding states.

(5) The more refined calculations (SSM-jellium, microscopic theories) were unfortunately only applied to systems (Cu, Al, Na – exception Be) where already the simple jellium predictions provide adequate numbers (including diamagnetic screening). The more in this respect exotic behavior of the muon Knight shift in, e.g. the alkaline earth metals and in Li and Cs was not treated on the basis of these refined theories.

Consequently no clear picture emerges from this comparison, neither on the relative merits of the various approaches nor on specific features of the local electronic structure, as related, e.g. to the presence of covalent bonding states.

6.1.3.2. *On the systematics of the data in cubic metals*

It would be therefore very important to find out, whether the systematics of the data themselves could hint on the possible physics involved. In the course of trying to correlate the Knight shift data with other properties of the host metals we have indeed found a strong correlation in the *cubic* metals between the molar electronic heat γ_{cp}^{m} and the induced hyperfine field per unpaired electron per atom (atomic volume) $B_{hf}^{\Omega_a}(r_\mu)$ as defined in equations (3.1.18) and (3.1.19). This strong correlation is seen in Fig. 20 where the logarithm of $B_{hf}^{\Omega_a}(r_\mu)$ is plotted versus γ_{cp}^{m}. In order to calculate $B_{hf}^{\Omega_a}(r_\mu)$ from the measured Knight shift values these values had first to be corrected for diamagnetic shielding. For all metals a shielding constant of $-(25 \pm 5)$ ppm was chosen on the basis of Refs. 108 and 126. In view of the results in Ga and Be this assumption is of course questionable. It seems, however, to be justified, at least roughly, by the outcome of this procedure. On the other hand, ignoring diamagnetic shielding totally, does not alter principally the findings to be discussed now.

The plot in Fig. 20 shows that $B_{hf}^{\Omega_a}(r_\mu)$ depends exponentially on the molar electronic heat. Since the molar electronic heat can be considered a measure of the density of states at the Fermi energy per atom ($N^a(\varepsilon_F)$) it appears that it is really this quantity which governs the behavior of $B_{hf}^{\Omega_a}(r_\mu)$. Using the free electron gas expression for γ_{cp}^{m} the data in Fig. 20 can be described by

$$B_{hf}^{\Omega_a}(r_\mu) \simeq B_{hf,0}^{\Omega_a}(r_\mu) \cdot \exp\left(-2.35 \cdot N^a(\varepsilon_F)\right) \qquad (6.1.3.2)$$

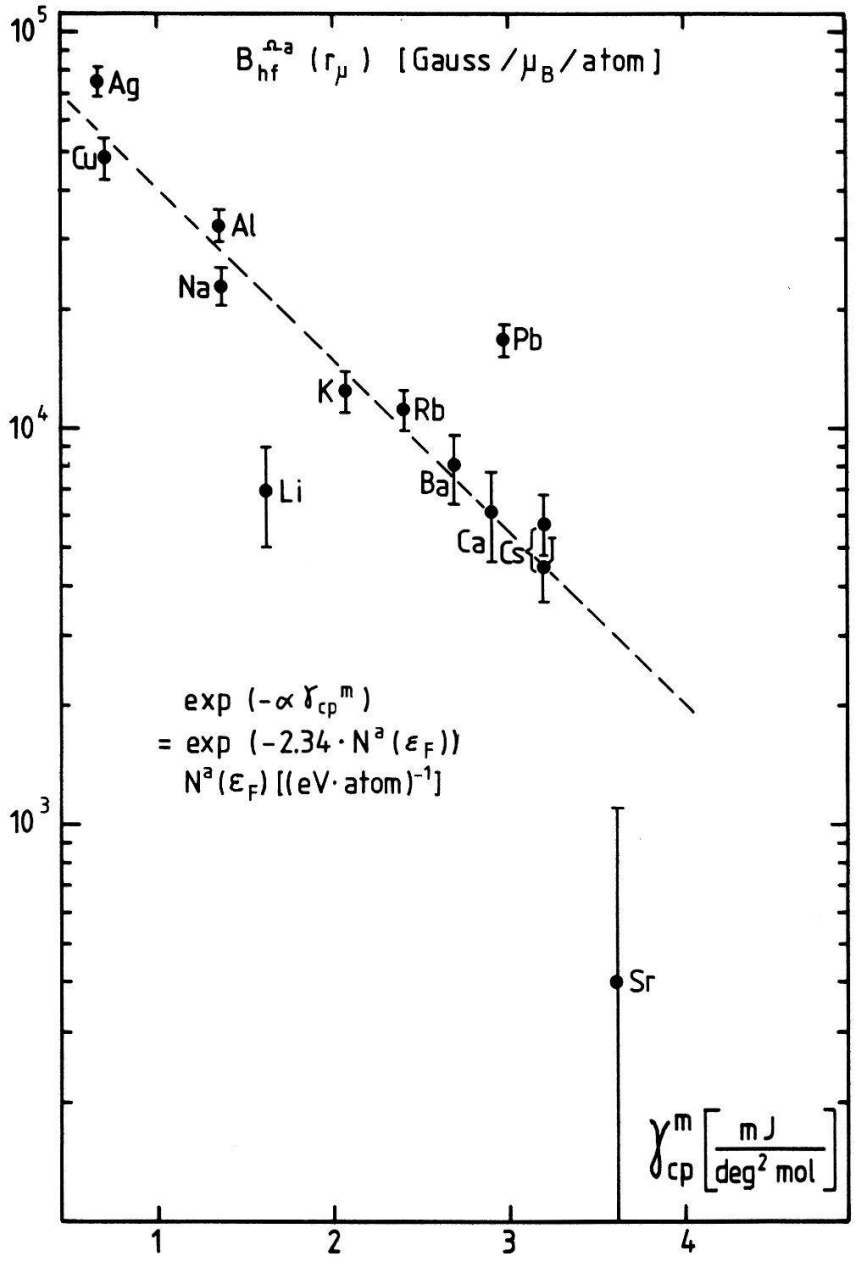

Figure 20
Semilogarithmic plot of induced hyperfine fields per μ_B per atom, $B_{hf}^{\Omega_a}(r_\nu)$, calculated from the KS data with equation (3.1.18), versus the molar electronic specific heat γ_{cp}^{m}.

with $B_{hf,0}^{\Omega_a}(r_\mu) \simeq 1.1 \cdot 10^5$ Gauss/μ_B/atom. The (effective) atomic density of states at ε_F: $N(\varepsilon_F)$ is measured in [(ev)$^{-1}$/atom].

Clear exceptions from this empirical relationship are the results obtained in Li and Pb, while the result from Sr appears reasonably represented in view of the fact that the total Knight shift is small and negative and that therefore $B_{hf}^{\Omega_a}(r_\mu)$ is quite critically dependent on the diamagnetic correction applied. The result for Pb suffers from the absence of a realiable value for the spin susceptibility. In calculating $B_{hf}^{\Omega_a}(r_\mu)$ from K (equation (3.1.18)), the spin susceptibility extracted from the electronic specific heat was used (Table 13). As discussed in Section 6.1.1 this number is an underestimation since exchange enhancement effects are not included. Including such effects would increase χ_p and would shift

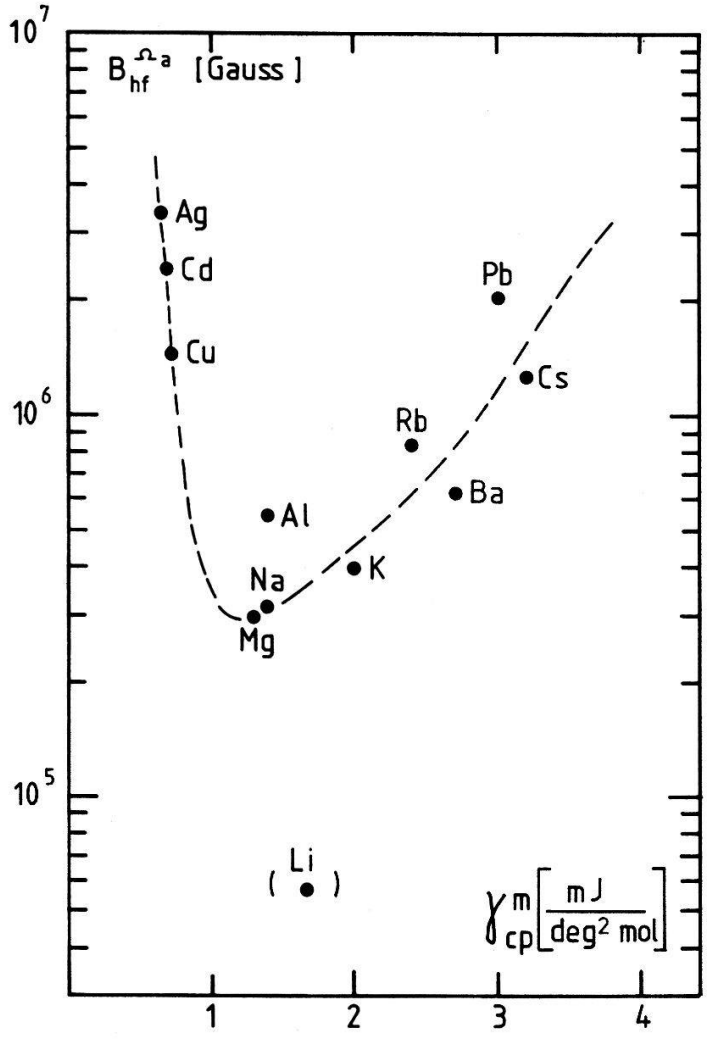

Figure 21
Semilogarithmic plot of induced hyperfine fields per μ_B per atom at nuclei, calculated from nuclear KS data, versus the molar electronic specific heat γ_{cp}^{m}. The dashed line is intended to guide the eye only.

$B_{hf}^{\Omega_a}(r_\mu)$ closer to the empirical curve. Such arguments cannot be applied to the result for Li, since the spin susceptibility has been measured directly and there cannot be any doubt on its value. Interestingly the nuclear Knight shift of Li deviates in the same fashion when compared with other nuclear Knight shifts. In Fig. 21 the induced hyperfine field per μ_B per atom, now calculated from nuclear Knight shift data, is plotted versus γ_{cp}^{m} analogous to the plot in Fig. 20. Again it seems that there is an empirical correlation, indicated by the dashed line, from which the Li value deviates in the same direction and by the same relative order of magnitude as in Fig. 20. We believe that this is due to a large p-electron contribution to the density of states at ε_F which increases the spin susceptibility considerably over the value stemming only from s-electrons. Since the s-electrons are mainly responsible for the Knight shift it appears that the experimental spin-susceptibility is not a good quantity in relation to it.

Note that in Fig. 21 also results from hcp metals are included. Concerning the μSR results in the noncubic metals it is found that they cannot be accommodated by the relation equation (6.1.3.2). In view of recent results on the muon Knight shift in single crystals of hcp Cd and Zn, which display extremely large and

temperature dependent anisotropics [31], indicating effects of a different origin, this may not be too surprising. No attempts are therefore made to include noncubic metals in this analysis.

The empricial correlation encompasses both bcc and fcc metals. Since the muon sites in these metals are the tetrahedral or octahedral interstitial sites, it also appears that the actual site of residence is of no concern. These two facts may be taken as an indication that, after all, some kind of jellium picture may still be relevant. This is supported in a sense by the observation that the Knight shift does not significantly change in Rb and Cs upon melting, implying little structural influence. This observation is particularly interesting for Cs, where the deviation between experiment and the present day SDF-jellium predictions are most obvious (see Fig. 19).

On the other hand the empirical correlation involves the atomic density of states which can assume the same value for different conduction electron densities in metals of different valency. Therefore the actual conduction electron density cannot be the (only) relevant parameter as it is in the ordinary jellium theories. In order to display more clearly the difference between the SDF-jellium predictions and what is implied by the empirical correlation we calculate from the empirical relation equation (6.1.3.2) a spin-density enhancement factor $\rho_s(r_\mu)$ by use of equation (3.1.18) and equation (3.1.22)

$$K = \frac{8\pi}{3}\rho_s(r_\mu)\chi_p = \frac{1}{\mu_B} B_{hf}^{\Omega_a}(r_\mu)\Omega_a\chi_p$$

and

$$\rho_s(r_\mu) = \frac{3}{8\pi}\Omega_a \frac{1}{\mu_B} B_{hf,0}^{\Omega_a}(r_\mu)\exp(-2.35N^a(\varepsilon_F)) \tag{6.1.3.3}$$

with

$$\Omega_a = z \cdot \frac{4\pi}{3} r_s^3 a_0^3$$

In terms of the electron density parameter r_s (free electron gas) and the electron effective mass ratio m^*/m, $N^a(\varepsilon_F)$ is given by

$$N^a(\varepsilon_F) = \frac{m^*}{m} z \cdot \frac{3}{\hbar^2}\left(\frac{4}{9\pi}\right)^{3/2} a_0^2 r_s^2 \quad (a_0 = \text{Bohr radius},\ z = \text{valency}) \tag{6.1.3.4}$$

Figure 22 shows a plot of measured γ_{cp}^m versus zr_s^2. It is seen that for all alkalis (except Li), Cu, Ba and Al roughly the same linear dependence on zr_s^2 is realized, implying very similar m^*/m. For these metals γ_{cp}^m and therefore also $N^a(\varepsilon_F)$ is simply a function of r_s and z only. Consequently for these metals the empirical spin density enhancement factor $\rho_s(r_\mu)$ (equation (6.1.3.3)) is also only dependent on r_s and z. Using the slope of the solid line in Fig. 22 we can now calculate $\rho_s(r_\mu)$ as a function of r_s for mono, di- and trivalent metals. The results are displayed in Fig. 23. For the metals in question the spin density enhancement factor was also calculated directly from the individual Knight shift values and is shown in Fig. 23 too. Furthermore Fig. 23 shows also the theoretical $\rho_s(r_\mu)$ from the SDF-jellium calculations.

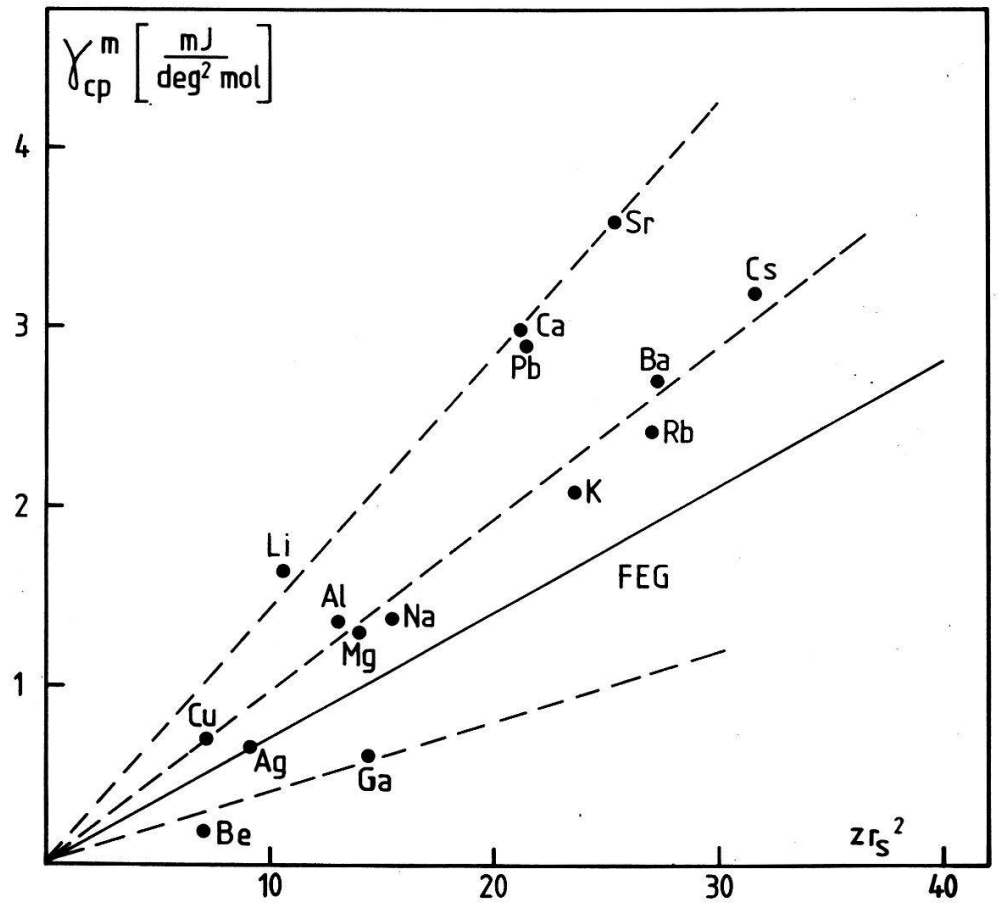

Figure 22
Plot of experimental molar electronic specific heat data versus $z\,r_s^2$, where z is the valency of the metal and r_s the conduction electron density parameter. The solid line indicates the free electron gas (FEG) prediction with $m^*/m = 1$.

Several interesting observations can be made:

(i) For high density (low r_s) metals the empirical $\rho_s(r_\mu)$ are in close agreement with the SDF-jellium predictions and almost independent of the valency z. In fact the jellium predictions seem to envelop the family of curves for different z on the low r_s side, providing an upper bound on the spin density-enhancement factor.

(ii) There is a low density (large r_s) region where the empirical spin density enhancement factor decreases, a behavior which is not at all forseen by the jellium calculations.

(iii) The beginning of the 'low density' regime is shifted to smaller r_s with increasing valency z. Also, for a given r_s (for $r_s \gtrsim 3$) the spin density enhancement factor decreases strongly with rising z.

These observations lead to the following speculations.

(1) Since the high density regime and the low density regime are distinguished by the relative importance of exchange and correlation energies on one side and the kinetic energy of the conduction electrons on the other side, it is suggestive to speculate that the listed observations are also correlated with the relative importance of exchange and correlation effects. In particular the decrease of the spin density enhancement factor at large r_s must then be attributed to strong exchange and correlation mechanisms not accounted for in the usual

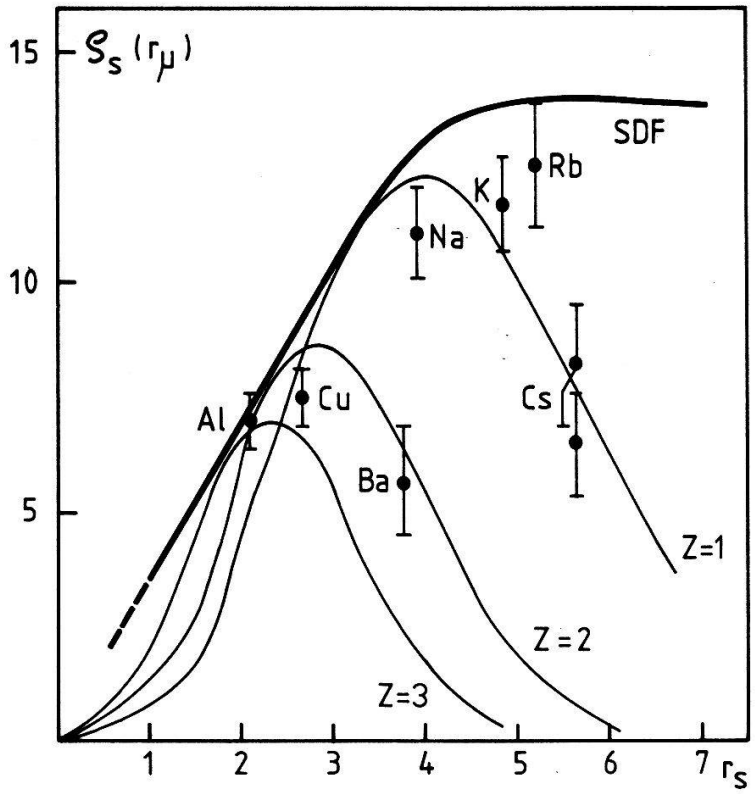

Figure 23
Plot of the spin density enhancement factor $\rho_s(r)$, following from the SDF jellium calculations (heavy solid line) and from the empirical correlation equation (6.1.3.2) (narrow solid lines), versus the conduction electron density parameter r_s. In the latter case different valencies z lead to different curves. The curves shown correspond to $m^*/m = 1.34$.

jellium approaches. This does, however, not explain how the z-dependence is established. We conjecture that this z dependence may be of the following origin.

(2) The z-dependence, or the more basic fact, that the empirical correlation involves the atomic density of states, suggests that the induced hyperfine field at the muon is to some extent coupled to mechanisms at the atomic sites. It should be remembered in this respect that the conduction electrons in a real metal are not described by plane waves but by Bloch wave functions, which are peaked at the atomic sites. It can therefore be expected that electron–electron interactions are particularly important in the immediate vicinity of the atomic sites and that these electron–electron interactions are dependent on the valency of the host atoms. In effect we are argueing that the deviation from the SDF-jellium predictions at lower electron densities (larger r_s) and the apparent set-on of a z-dependency is to be explained on the basis of exchange and correlation effects that take place not at the muon site but at the host atom site.

One such mechanism would be the analogue to the famous RKKY interaction which was already considered in Chapter III. The local moment is replaced by a quasi local moment which is induced by the external field at the host atom site. This quasi local moment would then be the source of RKKY-type spin density oscillations. Indeed Estreicher and Meier [159] have tried to explain the properties of the spontaneous hyperfine field at positive muons in ferromagnetic Ni, Fe, Co and Gd by such a mechanism with some success. Recent calculations by Zaremba and Zobin [160] on the nuclear Knight shift in simple metals also

show that the metal ions are the source of spin density oscillations. The presence of the muon's own potential will certainly modify the 'transferred' spin density, perhaps enhancing it. One effect of the muon potential will be that not only electrons at the Fermi surface carry spin polarization but also states below ε_F due to spin dependent radial wave function distortions [159]. This is very reminiscent of what was discussed before under the heading of core polarization. More appropriate to the muon case one should speak of transferred hyperfine fields.

(3) Quite a different speculation may start from a consideration of the actual distribution of Fermi-surface electrons in a real lattice. At high electron densities and independent of z one may assume a largely uniform distribution of Fermi surface electrons, a situation resembling the jellium hypothesis. However, at lower densities and increased nearest neighbor distances the actual conduction electron distribution will be certainly far from uniform. The deviation of the experimental data from the jellium predictions at larger r_s may then be interpreted as following in particular from a depletion of Fermi surface electrons in the interstitial volume, which effect is enhanced even further by an increased valency. The presence of the muon potential may be another cause of reducing the Fermi surface electron density by lowering states in energy and by the formation of local bonding states below ε_F.

(4) Finally, disregarding the empirical correlation as fortuitous and only considering the results in the monovalent metals, particularly in the alkalis, one may attribute the behavior of the experimental $\rho_s(r_\mu)$ at large r_s (e.g. in Cs) as due to some unknown properties of the interacting electron gas at low concentrations. It is indeed interesting to speculate on what will happen if the free electron density is decreased by orders of magnitude. We will come back to this point in Section 6.2.2 where we discuss briefly results obtained in a semi-metal.

6.1.4. *Electric field gradients* (EFG) *in* Al *and* Cu

As emphasized earlier, EFG's at the muons nearest neighbor host nuclei are a consequence of the spatial charge distribution around the muon and/or of the loss of cubic symmetry due to a lattice distortion by the muon (size effect). Before comparing the experimental results with theory we have to assess the importance of the latter contribution.

An estimate of the EFG due to the size effect for muons in Cu is obtained by using equation (4.3.16), $\lambda = -5$ [110] and $\Delta V = 0.26(a/4)^3$ [18] with the result $q_{zz} = 0.46\,\text{Å}^{-3}$.

This value is about 50% larger than the measured value. It could be used to calculate now the contribution from the screening cloud around the μ^+ (valence effect). Since the sign of the EFG is not determined one obtains two possible values:

$$q_{zz} = (-0.46 \mp 0.3) = -0.16 \quad \text{or} \quad -0.76\text{Å}^{-3}$$

Theoretical predictions for the valence effect from the jellium, SSM-jellium and cluster calculations are listed in Table 14. As can be seen the jellium results for $\delta n(r)$ together with the Bloch enhancement factor of Jena et al. [114] reproduce the experimental value in Cu quite well, if one would neglect any size effect contribution. Use of the Kohn–Vosko enhancement factor, on the other hand, reproduces roughly the larger negative estimated value, when the size effect is included. The smaller estimated value of $-0.16\,\text{Å}^{-3}$ is in good agreement with

Table 14
Electric field gradient q produced by a positive muon at the nearest neighbor nuclei in Al and Cu (valence effect)

	μ^+-Pos.	Bloch factor $\alpha(\mathbf{k}_F)$ Ref. 114	Ref. 112	$\delta n(r_{nn})$ (Å^{-3}) jellium Ref. 93	SSM Ref. 102, 103	cluster Ref. 128	q(Å^{-3})$_{\text{theor}}$ jellium Ref. 93	SSM Ref. 102, 103	cluster Ref. 128	$\lvert q(\text{Å}^{-})\rvert$ exp
Cu	octahedral	−6.5	25.6	−0.0049	−0.0046	+0.0033	+0.26 −1.05	+0.25 −0.98	0.18 +0.72	0.30 ±0.03
	tetrahedral	−8.2			−0.005			+0.27		
		Ref. 119								
Al	octahedral	6.4		0.0024	0.0013		+0.13	+0.07		~0.18
	tetrahedral	8.3			0.0006			+0.04		

the cluster model predictions, when the Jena enhancement factor is used. In view of the uncertainty in α and in the estimation of the size effect it is impossible to draw any firm conclusion from this comparison.

Since the size effect leads also to EFG components perpendicular to the radius vector muon-host atom it should be attempted in future experiments to distinguish between the two possible contributions by trying to uncover non-radially directed EFG's.

Interpretation of the results in Al lacks from the same deficiencies. For completeness the jellium predictions are also listed in Table 14 but will not be discussed further here.

6.2. *Muons in transition metals*

6.2.1. μ^+ *Knight shift in group* V *B metals*

The behavior of hydrogen in the group V *B* metals and the properties of the corresponding metal hydrides are among the most extensively studied of all hydrogen-metal systems. This is mainly a consequence of the ability of these metals to absorb large quantities of hydrogen.

The study of the muon Knight shift in these metals is particularly interesting since also the proton Knight shift has been measured very reliably in all members of the V *B* group (V, Nb, Ta) by NMR [27]. The results of these measurements are compared with the μ^+SR results in Table 15 and Fig. 24. The proton data were obtained in the temperature range 100–200°C, i.e. in the α-phase of the hydrides, and were found to be independent of temperature. The numbers quoted in Table 15 are extrapolations to zero hydrogen concentration, corresponding to the situation in the μ^+SR experiments. Table 15 lists also values for the spin susceptibility as calculated from the electronic specific heat data [136]. As emphasized before these numbers underestimate the true ones, since exchange enhancement effects are not included. It is striking that despite the relatively large spin susceptibility numbers as compared with simple metals, the proton and muon Knight shift data are relatively small. They are also negative with the possible exception of Ta. The μ^+SR data follow the trend of the proton NMR data and are in fact quite close to these. Interestingly in Nb and Ta the μ^+-Knight shift is slightly more positive while in V the μ^+-Knight shift is clearly more negative than the proton Knight shift. In view of the absence of any temperature dependence of the μ^+-Knight shift in Nb (see Table 11), the observed temperature independence of the susceptibility in α-VH_x α-NbH_x and α-TaH_x [27] and the smooth and weak dependence of the proton Knight shift on the hydrogen concentration x it is

Table 15
Comparison of μ^+ *and proton Knight shift data in group* V *B* metals

Element	$\chi_p\left[\frac{\text{emu}}{\text{mol}}\right]$ (from Ref. 136)	K_μ [ppm]	K_p [ppm] (from Ref. 27)
V	$133 \cdot 10^{-6}$	$-(88 \pm 8)$	-66
Nb	$109 \cdot 10^{-6}$	$-(15.6 \pm 3)$	-25
Ta	$83 \cdot 10^{-6}$	$+(5.5 \pm 10)$	~ 0

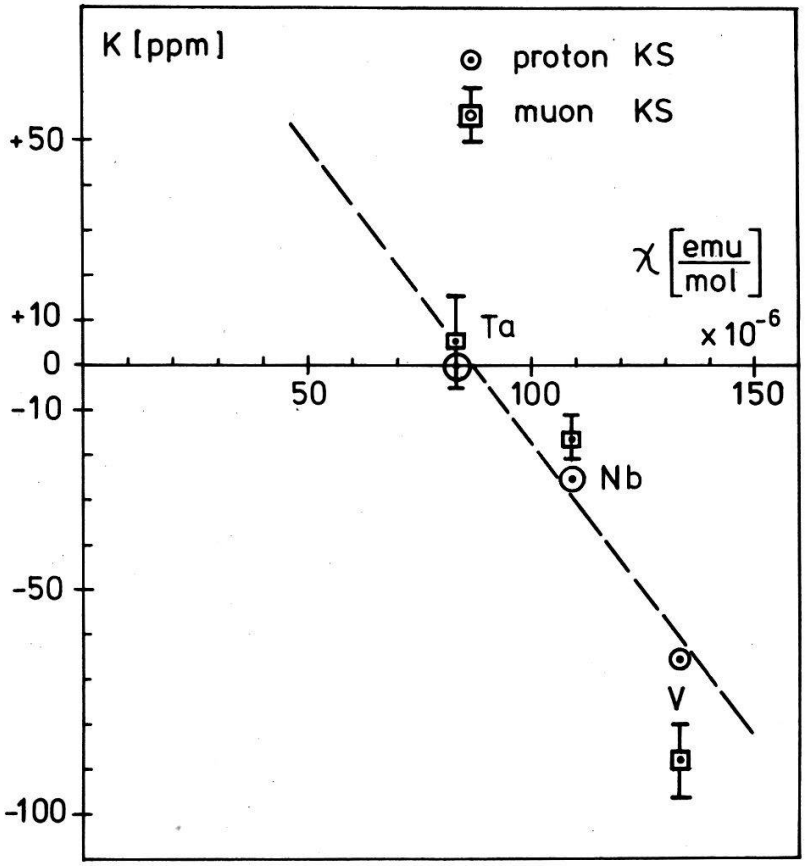

Figure 24
Comparision of proton and muon Knight shift data in V, Nb and Ta. The data are plotted versus the molar spin susceptibility.

concluded that the difference between the μ^+- and the proton Knight shift must reflect an isotope effect. It is not the result of an erroneous extrapolation to zero hydrogen concentration, nor of the different temperatures used in the experiments, nor of trapping and diffusion of the μ^+. Apparently then, size and sign of an isotope effect can vary considerably pointing to quite complex mechanisms. On the other hand μ^+ and proton Knight shift carry the same sign and/or are of the same absolute size which is taken as evidence that basically both particles sample the same electronic environment, i.e. are subject to the same local electronic structure.

In contrast to the nontransition metals one has now to consider also the influence of the d-electrons on the μ^+ or proton Knight shift. This is usually done by considering s-electrons and d-electrons separately and by writing the Knight shift constant as

$$K = K_s + K_d + K_{\text{dia}}$$
$$= \frac{\Omega_a}{\mu_B}\left(B^{\Omega_a}_{hf,s}(r_\mu)\chi_s + B^{\Omega_a}_{hf,d}(r_\mu)\chi_d\right) + K_{\text{dia}} \qquad (6.2.1)$$

The first term is due to the Fermi contact interaction with conduction s-electrons at the Fermi surface, χ_s is the s-electron spin susceptibility. The second term is induced by the d-electrons and χ_d is the d-electron spin susceptibility. The third term, as usual, encompasses all diamagnetic contributions. The second term may

be due to core polarization or transferred hyperfine fields or to a direct contact interaction with the tails of the d-wave functions at the interstitial site (see Chapter III). All three terms may display an isotope effect of different magnitude. It is obvious that a detailed understanding of the total isotope-effect is coupled to quite a detailed understanding of the various relevant aspects of the established local electronic structure which, in fact, makes the observation of isotope effects an important tool in testing theoretical models. Unfortunately detailed theoretical models and calculations which address themselves to all aspects of isotope effects are so far not available.

Concerning the negative sign of the proton/muon Knight shift in V, and Nb Kazama–Fukai [27] suggested that this is partially due to an *a priori* negative interstitial spin density as observed by neutron diffraction in many transition metals, and partially due to a contribution from H induced bonding states by means of core polarization. Indeed soft x-ray emission spectroscopy on NbH_x [161] and VH_x 162 have presented evidence for the formation of states below the bottom of the d-band, as anticipated in some of the theoretical calculations mentioned in Chapter IV.

In view of the relative smallness of the Knight shift numbers and after applying a diamagnetic correction of $-(20–30)$ ppm it is obvious that the positive s-electron induced Knight shift and the negative d-electron induced Knight shift must be of the same order of magnitude, almost canceling each other as in Nb. To get a hint on the order of magnitude involved we estimate K_s to be $\sim+60$ ppm, i.e. similar to K_s in Cu, and $K_d \simeq -60$ ppm. Assuming further that the quoted spin susceptibility for Nb in Table 15 is mostly due to d-electrons we calculate an induced hyperfine field per unpaired d-electron per atom of $B^{\Omega_0}_{hf,d}(r_\mu) \simeq -3\ \mathrm{kG}/\mu_B$. This compares well with the results for the corresponding hyperfine fields in Pd and paramagnetic Ni (see next section).

6.2.2. μ^+-*Knight shift in paramagnetic* Ni *and* Pd

As can be seen from Figs. 12 and 13 the μ^+-Knight shift displays a pronounced temperature dependence in both Pd and paramagnetic Ni. The features of the temperature dependence, particularly in Pd, are reminiscent of the temperature dependence of the magnetic susceptibility of these metals. Indeed when plotting the Knight shift versus the susceptibility with the temperature as an implicit parameter (see Figs. 25 and 26) one finds a linear relationship between the two quantities. For paramagnetic Ni the susceptibility has been taken from Refs. 163, 164 and for Pd from Ref. 165. The total magnetic susceptibility is usually assumed to be expressable as a sum of independent terms by treating s/p- and d-electrons as distinguishable fractions (two band model). One writes

$$\chi_t = \chi_s + \chi_d(T) + \chi_{vv} + \chi_{\mathrm{dia}} \tag{6.2.2}$$

χ_s, χ_d were explained before, χ_{vv} = orbital or Van Vleck susceptibility, χ_{dia} = diamagnetic (ionic) susceptibility. The Landau diamagnetic term is neglected. Only the d-electron term is temperature dependent and displays a Curie-like behavior except for temperatures close to T_c in Ni and below $\sim$200 K in Pd. For high temperatures χ_d vanishes like $1/T$ and in that limit $\chi_t(T\to\infty) = \chi_s + \chi_{vv} + \chi_{\mathrm{dia}}$. However, over most of the temperature range $\chi_t \approx \chi_d(T)$.

The linear dependence of the Knight shift on the total susceptibility, as shown in Figs. 25 and 26 allows now to separate the d-electron induced and

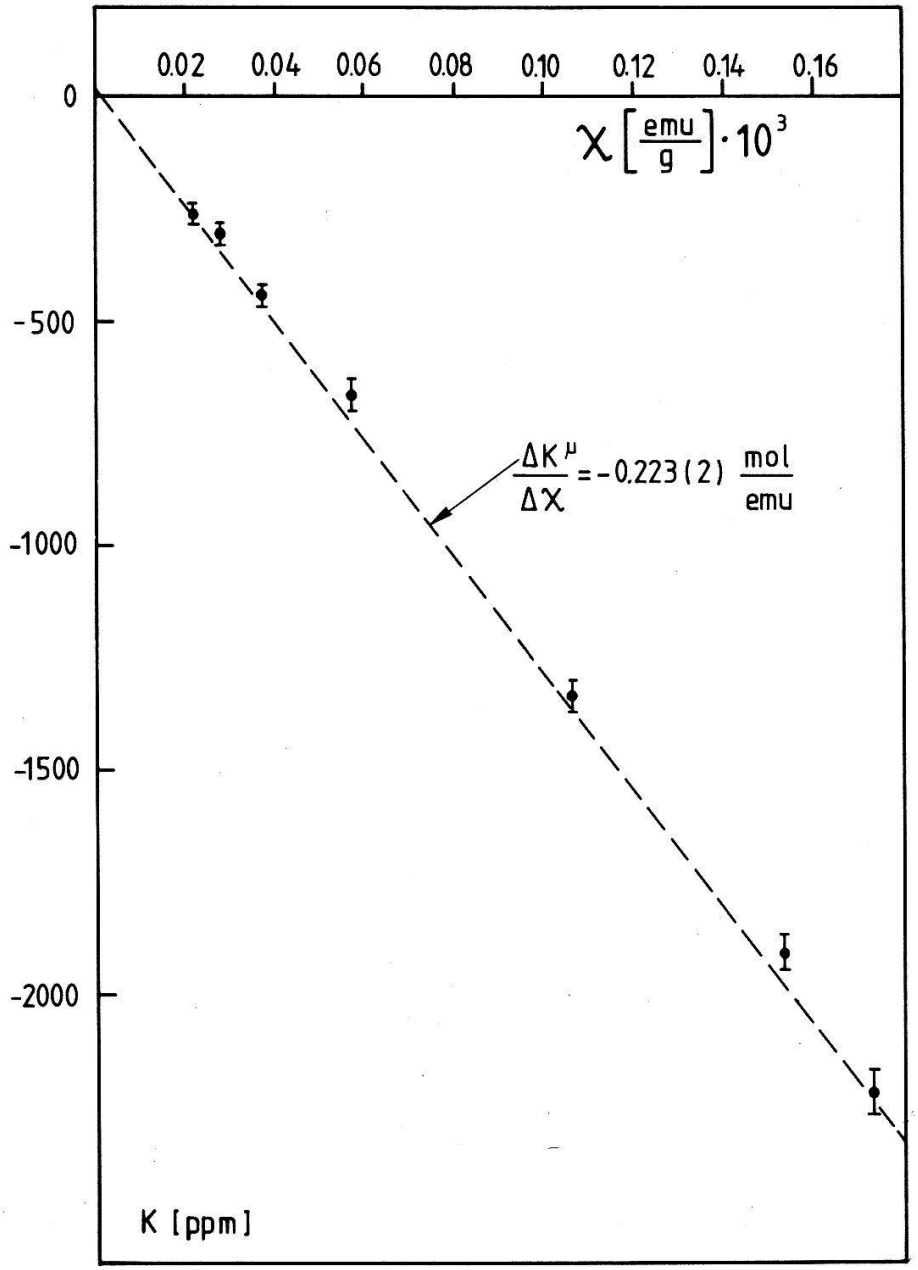

Figure 25
Plot of μ^+ Knight shift in paramagnetic Ni versus the bulk magnetic susceptibility with temperature as an implicit parameter. The straight dashed line represents a least square fit including the data closer to the Curie temperature, not shown in this figure.

temperature dependent contribution to the Knight shift from the sum of the other temperature independent contributions by fitting equation (6.2.1) to the data [166]. One obtains

$$\text{Ni: } K[\text{ppm}] = +18(13) - 0.223(1) \cdot 10^6 \cdot \chi_t\left[\frac{\text{emu}}{\text{mol}}\right] \tag{6.2.3}$$

$$\text{Pd: } K[\text{ppm}] = +45(10) - 0.428(15) \cdot 10^6 \cdot \chi_t\left[\frac{\text{emu}}{\text{mol}}\right] \tag{6.2.4}$$

The numbers in parenthesis are statistical errors from the fit.

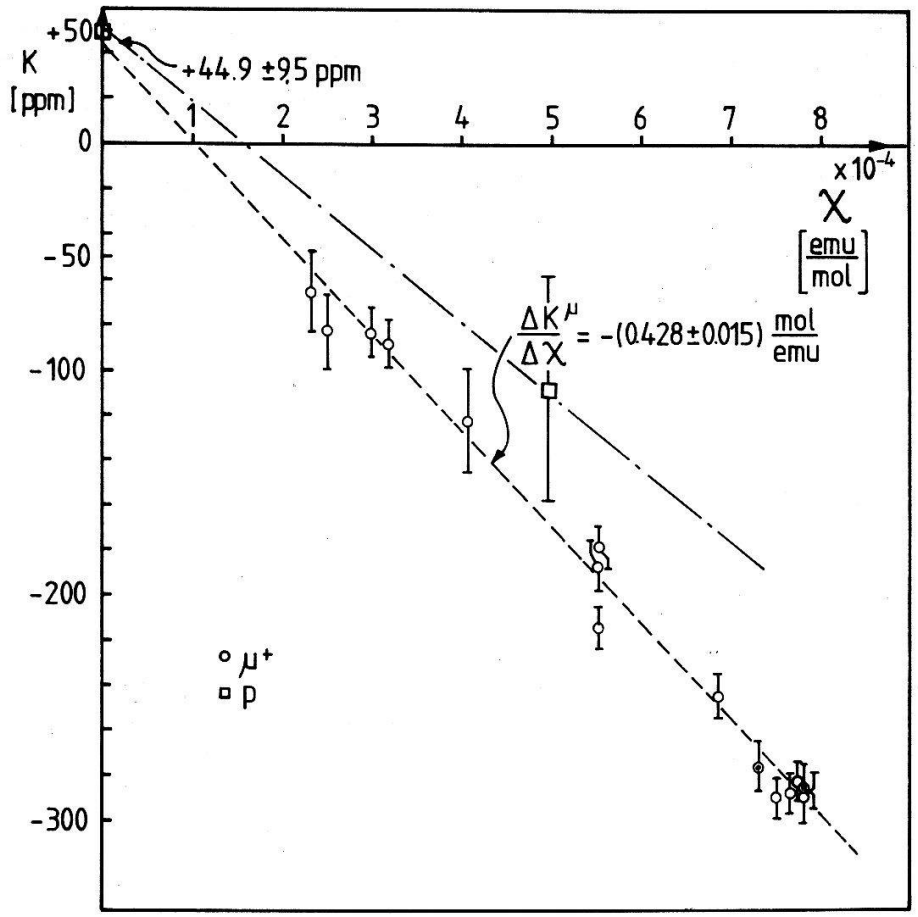

Figure 26
Plot of μ^+ Knight shift in Pd versus the bulk magnetic susceptibility, with temperature as an implicit parameter. The dashed straight line represents a least square fit to the data. Also shown is the proton KS result of Voigtländer et al. [26] and, for $\chi \to 0$, a temperature independent term calculated from a T_{le} measurement in Pd H [60] by use of the Korringa relation.

From the slopes one can calculate the induced hyperfine field per unpaired d-electron per atom according to equation (3.1.21). The result is

Ni: $B_{hf,d}^{\Omega_a}(r_\mu) = -1.246(6)\ \mathrm{kG}/\mu_B/\mathrm{atom}$

Pd: $B_{hf,d}^{\Omega_a}(r_\mu) = -2.39(11)\ \mathrm{kG}/\mu_B/\mathrm{atom}$

The induced hyperfine field at the μ^+ in paramagnetic Ni can be compared with the corresponding spontaneous hyperfine field in ferromagnetic Ni. Using the most recent value for the actual hyperfine field at a μ^+ in ferromagnetic Ni, extrapolated to 0 K, of $B_{hf}(r_\mu) = -707(10)$ G [167] and a saturation magnetization of $M_s(0\ \mathrm{K}) = 528$ G one obtains: $B_{hf}^{\Omega_a}(r_\mu) = B_{hf}(r_\mu)/M_s = -1.14(2)\ \mathrm{kG}/\mu_B/\mathrm{atom}$. This value is slightly but significantly smaller than the paramagnetic value. Interestingly the same relative deviation is observed for the hyperfine fields at the Ni-nucleus in the paramagnetic and ferromagnetic phases [168, 169]. Since the deviation is small it will not be considered further, rather by and large it appears as if the induced hyperfine field per unpaired d-electron per atom is independent of whether the d-spin polarization is induced by an external magnetic field or whether it results from exchange coupling in the ferromagnetic phase.

In order to find $K_s + K_{dia}$ one has to know $\chi_s + \chi_{VV} + \chi_{dia}$. From Ni-host Knight shift measurements Segransan et al. [168] and Shaham et al. [168] have deduced a temperature independent orbital susceptibility of $\chi_{orb} = 1.6 \cdot 10^{-6}$ emu/g and $\chi_{orb} = 3.23 \cdot 10^{-6}$ emu/g, respectively. Other temperature independent contributions [168] are the diamagnetic susceptibility ($\chi_{dia} \approx 0.34 \cdot 10^{-6}$ emu/g) and the s-electron Pauli spin susceptibility ($\chi_s \approx 0.07 \cdot 10^{-6}$ emu/g). The total temperature independent susceptibility may therefore vary between $3 \cdot 10^{-6}$ emu/g and $1.4 \cdot 10^{-6}$ emu/g. Inserting this into equation (6.2.3) one obtains

$$\text{Ni: } K_s + K_{dia} = -11(23) \text{ ppm}$$

For Pd $\chi_s + \chi_{vv} + \chi_{dia}$ has been estimated to be smaller than 10^{-5} emu/mol [166]. It follows that:

$$\text{Pd: } K_s + K_{dia} = +42(13) \text{ ppm}$$

The temperature independent μ^+-Knight shift in Ni is surprisingly small (compatible with zero). Assuming that $K_{dia} \simeq -(20-30)$ ppm one estimates a K_s of 0–42 ppm. Because of the similarity of the electronic band and crystal structure of Cu and Ni it was anticipated that K_s in Ni might correspond to K_s in Cu properly scaled by the ratio of the spin susceptibilities in Ni and Cu, i.e. $K_s(\text{Ni}) = K_s(\text{Cu}) \cdot \chi_s(\text{Ni})/\chi_s(\text{Cu}) \simeq 39$ ppm. This value is not incompatible with the estimated range for K_s in Ni.

The same consideration applied to the results in Pd and Ag yields $K_s(\text{Pd}) = K_s(\text{Ag}) \cdot (\chi_s(\text{Pd})/\chi_s(\text{Ag}) \simeq 76$ ppm (with $\chi_s(\text{Pd}) = 6.2 \cdot 10^{-6}$ emu/mol [166]) which compares quite favorably with the estimate following from the experiment, i.e. $K_s(\text{Pd}) \simeq +42(13) + (20\text{–}30) \simeq 67 \pm 18$ ppm. It is therefore not unreasonable to assume that, as far as the s-electron induced Knight shift is concerned, corresponding properties of the local electronic structure are quite similar in Cu and Ni and in Ag and Pd, respectively. The new information is contained in the d-electron induced part of the Knight shift. This part could be the result of

(i) a significant direct contribution of $3d$-electrons to the spin density at the muon site (Petzinger and Munjal [97])

(ii) some admixture of d-wave functions to the electron states around the μ^+ (e.g. as a consequence of the formation of bonding states [61, 170]).

(iii) a strong exchange interaction between the d-electrons, centered at the Ni-sites, and the electrons (mainly $4s$) contributing to the screening of the μ^+ (Patterson and Falicov [68], Estreicher and Meier [159], Manninen and Nieminen [171]). Because of the negative sign of the Knight shift this exchange coupling must be of an antiferromagnetic type.

Most interesting from the point of view of the local electronic structure is the possibility that the negative spin polarization at the muon site induced by the d-electrons is a consequence of the formation of bonding states.

Indeed of all theoretical calculations mentioned in Chapter IV the prediction of Katayama et al. [61] comes closest to the experimental value (see Table 16 for a compilation of theoretical numbers). As was discussed there the negative hyperfine field at a μ^+ was due to a dominating negative spin polarization of the doubly occupied local bonding states.

Table 16
Compilation of theoretical predictions for the hyperfine field at μ^+ in ferromagnetic Ni

Source	B_{hf} [Gauss]
Daniel-Friedel model Jena [172]	−600
Cellular cluster model Keller et al. [125, 176]	−680
KKR-XPA-band structure calcu. Katayama et al.	−720
Supercell band structure calc. Jepsen et al. [64]	−463
Experiment ferromag. Ni [167]	−710 (10)
paramag. Ni [34]	(−770 (3))*

*) Calculated from $B_{hf}^{\Omega}(r_\mu)$

Of the many other theoretical attempts to calculate the hyperfine field at a positive muon in ferromagnetic Ni (Patterson and Falicov [68], Jena [172], Petzinger and Munjal [97], Jena et al. [96]) we mention only the cluster calculations in the multiple scattering cellular approach by Patterson and Keller [125] and more recently by Castro and Keller [170]. In the latter work the total interstitial charge density at the octahedral position in pure ferromagnetic Ni was calculated to be 0.096 electrons/Å^3, carrying a spin polarization of −2.2%. These numbers are constant within a radius of 1.26 Å. Implantation of a positive muon at the octahedral site leads to the formation of a set of bonding-states 1.85 eV below the bottom of the conduction band, which are composed of 1s-hydrogenlike and 3d-Ni wave functions, forming part of the A_{1g} symmetry local orbitals band of the μ^+-6 Ni cluster. These segregated states contribute about 0.65 electrons to the screening of the μ^+. The computed hyperfine field at the muon is −680 Gauss in excellent agreement with the experimental result. The authors do not present an analysis which tells which of the electronic states contribute to the hyperfine field, but it appears reasonable to assume, that the bonding states which account for a large fraction of the screening charge and involve 3d-Ni-electrons are largely responsible for the calculated and observed hyperfine field.

We note that the d-electron induced hyperfine fields/μ_B/atom in Ni, Pd and the estimated value in Nb are of the same order of magnitude. It seems therefore very likely that in all instances this is an indication for the formation of bonding levels.

Finally, we can compare the μSR results obtained in Pd with some proton NMR experiments in Pd. Wiley et al. [60] have measured the Korringa relaxation time T_{1e} in PdH. Assuming that the s-electron density of states at the Fermi surface is not changed very much in going from pure Pd to PdH one can apply the Korringa relation (equation (4.2.1)) to calculate the related Knight shift for protons in the α-phase in dilute PdH. Using the results of Ref. 60 one obtains

$K_s \simeq 74$ ppm. This number agrees well with the estimated K_s for muons in Pd. In absolute value it is somewhat larger than the μSR-value. If this statistically nonsignificant difference, for the sake of argument, is taken seriously, it might actually be again a reflection of an isotope effect. Interestingly the indicated trend is in agreement with the other result of Wiley et al. [60] which shows that the s-electron spin density is slightly larger at the deuteron in PdD than at the proton in PdH. Generally speaking the s-electron induced Knight shift seems to increase with increasing mass of the 'hydrogen' isotopes. This was also found in a jellium type calculation by Jena et al. [173]. As discussed in Section 4.2 the Korringa product $T_{1e} \cdot T$ for protons in PdH was calculated by Freeman and Gupta [59] and found to be in excellent agreement with experiment.

The Knight shift of protons in Pd has been measured at 75°C by Brill and Voitländer [26]. Extrapolating their data to zero hydrogen concentration a value of $K = -110(50)$ ppm is observed. This result is also displayed in Fig. 26. It is somewhat more positive than the corresponding muon Knight shift at this temperature. This would be in accordance with the possible trend observed in the high temperature limit where K_s(proton) seems to be larger than $K_s(\mu^+)$. It is, however, also seen that the slope of the straight line connecting the high temperature estimate for the proton Knight shift with the experimental number at 75°C is less steep than the corresponding slope for the μSR data. Since the slopes correspond to the induced hyperfine fields per unpaired d-electron per atom we have found here a first indication for a separate isotope effect concerning the d-electron induced Knight shift. In contrast to the isotope effect for K_s the latter one seems to decrease with increasing isotopic mass.

A naive interpretation of this fact would be that the particle with the smaller mass and a larger zero point vibration amplitude approaches more closely the host atoms thereby being exposed to a greater density of d-electrons resulting in an increased d-electron induced negative hyperfine field. The reduced distance to d-electrons might also result in an increased strength of the predicted H-1s/Pd-3d bonding states.

6.3. *Muon Knight shift in antimony* (Sb)

Antimony presents insofar a special case as it is actually a semimetal with a conduction electron density of $5 \cdot 10^{19}/\text{cm}^3$, which is about three orders of magnitude smaller than in ordinary metals. In this respect antimony may be considered as an intermediate between a semiconductor and an ordinary metal.

μSR-measurements in the semiconductors Si [174, 175] and Ge [176, 177] have revealed that muons are present in the form of deep and shallow muonium-states, i.e. paramagnetic states involving one unpaired electron. In ordinary metals, on the other side, as we have seen, no paramagnetic muoniumstates are formed; instead covalent bonding states with the neighbor host atoms may exist. It is therefore extremely interesting to study the electronic states associated with a positive muon or proton in an intermediate situation, in order to learn more about the conditions that favour either the formation of some paramagnetic entity or the complex and diamagnetic structure present in ordinary metals.

The anisotropy of the frequency shift observed by μSR in a single crystal of Sb is displayed in Fig. 27. The temperature dependence for two different external fields is shown in Fig. 28 (Hartmann et al. [35]).

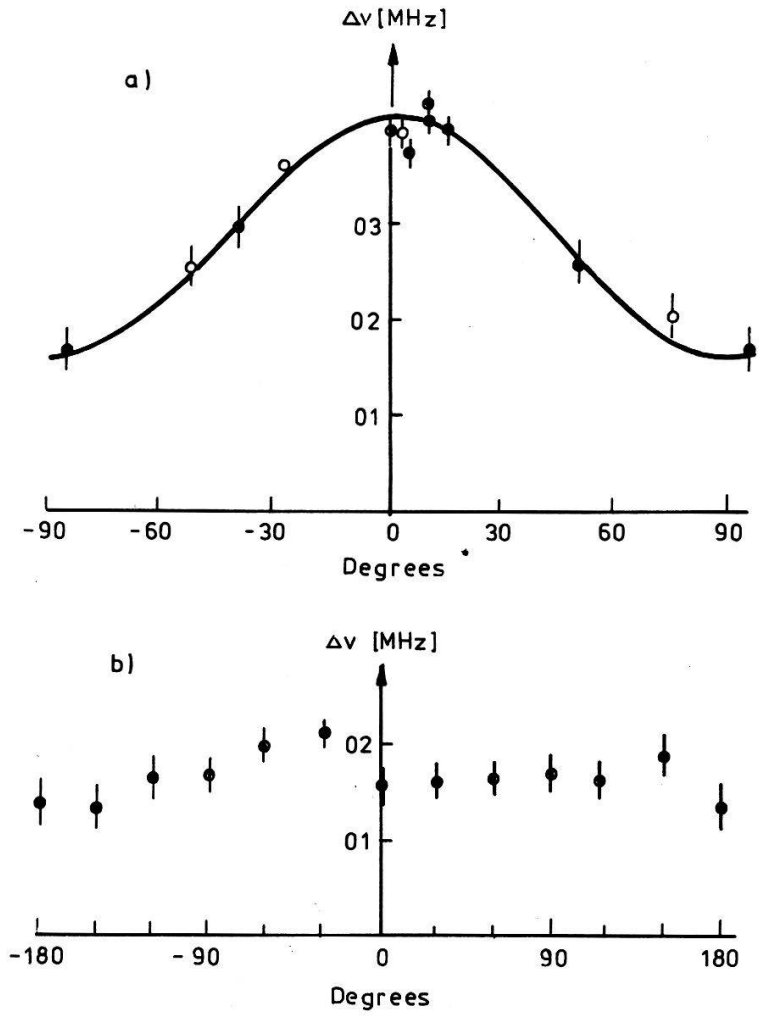

Figure 27
Angular dependence of the frequency shift in single crystal Sb with (a) B_{ext} in the xz-plane, (b) B_{ext} in the xy-plane (z-axis = crystalline c-axis) (from Ref. 35).

The temperature dependence is reminiscent of a local paramagnetic moment and of the effective hyperfine field in a paramagnetic atom. The data can indeed be fitted by a Brillouin function with $J=\frac{1}{2}$ (or possibly $J=\frac{3}{2}$) resulting in an exchange field of ~320 KGauss for the high field data points [35]. The different saturation values for $\Delta\nu$ at low temperature for differrent applied fields could be the result of a field dependence of the localized wavefunction associated with the local paramagnetic moment. The anisotropy of $\Delta\nu$ would imply a large fraction of p-character in the electronic state around the muon.

The occurrence of a localized paramagnetic state with a sizeable p-character (anisotropy in the hyperfine field) resembles very much the results for the Mu*-state found in Si [175] as well as in Ge [177]. The state in Sb, however, must be much more shallow in view of the very small hyperfine field of the order of 10 Gauss that is produced at the muon.

Finally, it is interesting to note, that a search for large frequency shifts in the semimetals As and Bi has yielded no significant result [35].

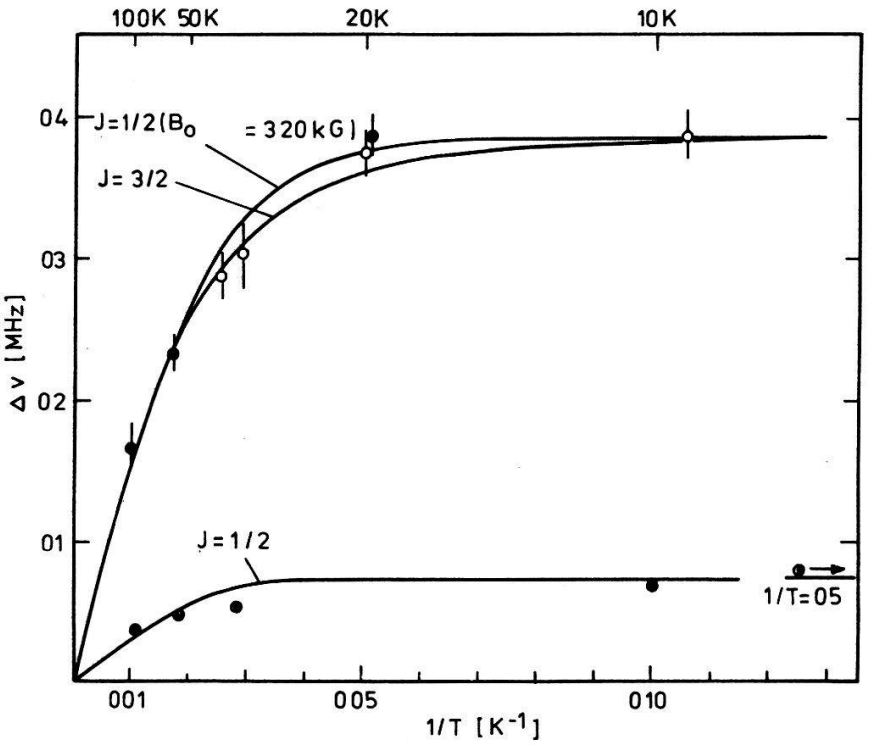

Figure 28
Temperature dependence of the muon frequency shift in Sb at about $B_0 = 2$ KGauss (upper curve) and $B_0 = 0.4$ KGauss (lower curve). The solid lines represent fitted Brillouin functions (from Ref. 35).

VII. Summary

In the preceding chapters we have discussed results of μSR Knight-shifts-measurements in elemental simple and transition metals. In addition, information on electric field gradients at nearest neighbors in Cu and Al has been reviewed. The results have been compared with theoretical calculations on the electronic structure of hydrogen in metals, in particular with nonlinear response jellium calculations. The comparision has shown that the data are not reproduced, neither in magnitude nor in their systematic behavior by the jellium predictions. Cluster and band structure calculations tend to be more in agreement with the data, but since only a few such calculations have been performed, their ability to reproduce systematic trends is not tested yet.

The data itself suggest that mechanisms usually not considered so far in relation to hydrogen in metals, have to be included in the theoretical calculations. This is notably indicated by the negative values for the muon Knight shift in Be, Ga and Sr. A negative Knight shift is outside the frame of the usual Knight shift theory in simple metals. Additional mechanisms such as diamagnetic shielding and 'core polarization' in connection with the formation of bonding states could be very important. In this respect the systematic disagreement between experiment and jellium predictions (see Fig. 19) may be extremely informative concerning the electronic structure problem. Band structure as well as the multiple scattering cellular cluster calculation do predict deep lying bonding states, but their possible contribution to the Knight shift has not been considered in any theoretical calculation so far, with the exception of Be, in which the diamagnetic shielding of the muon due to cluster bonding states has been evaluated, and of Cu.

Quite a remarkable result of the analysis of most of the Knight shift data in the nontransition metals of cubic symmetry was the exponential correlation with the molar electronic specific heat and therefore with the density of states at the Fermi energy, irrespective of crystal structure and muon site. This result is not understood at present. But, if generally valid, it teaches that the spin density and with that the electronic structure around a positive muon is not that sensitive to particular details, but depends in an as yet hidden but systematic fashion on some more integral properties of the crystalline state.

From a comparison of the emprical correlation with the corresponding jellium predictions it was speculated that exchange and correlation effects at the atomic sites are rather important.

Hints on the composition of the electronic structure around a positive muon or proton are perhaps best deduced from the results obtained in Pd and paramagnetic Ni, which seem to allow to distinguish between s- and d-electron contributions to the spin density at the muon site. The negative hyperfine field in ferromagnetic Ni and the negative Knight shift in paramagnetic Ni must be related to d-electrons in view of their correspondence with d-electron associated bulk-properties (saturation magnetization, magnetic susceptibility). Both types of host electrons are in one way or another involved in the formation of the electronic structure around a positive muon or proton.

In V, Nb, Ta and Pd it was possible to compare the muon Knight shift data with proton Knight shift data, obtained under almost identical conditions. It was found that they correspond closely to each other, indicating that both particles are really associated with the same local electronic structure. But it was also evident that isotope effects are present and, most interesting, it seems to appear that the isotope effect on the s-electron induced Knight shift and the d-electron induced Knight shift are of opposite direction.

Finally, the results obtained in Sb, which is a semimetal, are of a completely different kind and may perhaps more adequately be compared with the results obtained in the semiconductors Si and Ge.

The interpretation of the measured electric field gradients in Cu and Al is at present hampered by a lack of detailed theoretical understanding of the so called size effect and by some principal doubts on the validity of the Kohn–Vosko approximation involving the Bloch enhancement factor in relation to the μSR-results.

In summary μSR-studies have increased the amount of experimental data, pertaining to the local electronic structure of hydrogen in metals, considerably over what was available before. The μSR-data certainly can serve as a key to a deeper understanding of the electronic structure problem. This poses a challenge to theorists who now must come up with more refined, complete and realistic calculations. Hints on what direction should be taken are perhaps suggested by the systematics of the Knight shift data. It is also this aspect which will certainly be pursued further in future experimental μSR-work.

Acknowledgements

This paper could not have been written without the enormous involvement and help of my collaborators and colleagues from ETH Zürich in performing the

experiments at SIN. My warm thanks are due to Drs. Mario Camani, Fred N. Gygax, Alphons Hintermann, Walter Rüegg, Hugo Schilling and Dipl. Phys. Walter Studer. In addition I have to thank Prof. Eberhart Klempt and Drs. Rainer Schulze and Hartmut Wolf and Dipl. Phys. Hermann Wehr from the University of Mainz who contributed a lot to the development of the stroboscopic method and the apparatus and who participated in collecting a number of the Knight shift data.

Numerous discussions with many physicists around the world have played an essential part in motivating the experiments and in providing hints on how to understand the data. I am particularly indebted to Prof. W. Baltensperger, ETH Zürich, Prof. Jaime Keller, UNAM Mexico City, Prof. A. J. Freeman, Evanston, Prof. D. Ll. Williams, UBC Vancouver, Prof. J. Voitländer, München, Prof. Y. Fukai, Chuo University Tokyo, Dr. L. Schlapbach, ETH Zürich, Prof. N. Kaplan, Jerusalem, Dr. P. F. Meier, Zürich, and Dr. M. Stoneham, Harwell. Finally I have to thank Profs. D. Ll. Williams, N. Kaplan and H.-J. Gerber, ETH Zürich, for the careful reading of the manuscript at various stages of completion and for many critical and useful comments.

REFERENCES

[1] A. SCHENCK and K. M. CROWE, CERN-REPORT 74–8 (1974).
[2] J. H. BREWER, K. M. CROWE, F. N. GYGAX and A. SCHENCK: in *Muon Physics*, Vol. III, eds. V. W. Hughes and C. S. Wu, Academic Press (1975).
[3] A. SCHENCK: in *Nuclear and Particle Physics at Intermediate Energies*, ed. J. B. Warren, Plenum (1976).
[4] A. SCHENCK, Proceed. Int. School Physics Exotic Atoms I, Erice, Italy (1977).
[5] J. H. BREWER and K. M. CROWE in Ann. Rev. Nucl. Part. Sci. *28*, 239 (1978).
[6] A. SCHENCK, Hyperfine Interactions *4*, 282 (1977).
[7] A. T. FIORY, Hyperfine Interactions *6*, 63 (1979).
[8] *Hydrogen in Metals*, 2 Vol. eds. G. Alefeld and J. Völkl, Topics in Appl. Phys. *Vol. 28*, Springer (1978).
[9] A. SEEGER, in: Ref. 8, Vol. 1.
[10] Proc. First Int. Top. Meet. Muon Spin Rotation, eds. F. N. Gygax, W. Kündig and P. F. Meier, Hyperfine Interactions *6* (1979).
[11] Proc. Second Int. Top. Meet. Muon Spin Rotation, eds. F. H. Brewer and P. W. Percival, Hyperfine Interactions *8*, p. 307–841 (1981).
[12] W. R. WAMPLER and B. LENGELER, Phys. Rev. *B15*, 4616 (1977).
[13] M. CAMANI, F. N. GYGAX, W. RÜEGG, A. SCHENCK and H. SCHILLING, Phys. Rev. Lett. *39*, 836 (1977).
[14] J. P. BUGEAT, A. C. CHAMI and E. LIGEON, Phys. Lett. *A58*, 127 (1976) and J. P. Bugeat and E. Ligeon, Phys. Lett. *71A*, 93 (1979).
[15] O. HARTMANN, E. KARLSSON, L. O. NORLIN, D. RICHTER and T. O. NIINIKOSKI, Phys. Rev. Lett. *41*, 1055 (1978).
[16] H. K. BIRNBAUM, M. CAMANI, A. T. FIORY, F. N. GYGAX, W. J. KOSSLER, W. RÜEGG, A. SCHENCK and H. SCHILLING, Phys. Rev. *B17*, 4143 (1978).
[17] H. SCHILLING, M. CAMANI, F. N. GYGAX, W. RÜEGG and A. SCHENCK, Phys. Lett. *67A*, 231 (1978).
[18] H. SCHILLING, M. CAMANI, F. N. GYGAX, W. RÜEGG and A. SCHENCK, Hyperfine Interactions *8*, 675 (1981) and J. Phys. *F12* (1982).
[19] C. P. FLYNN and A. M. STONEHAM, Phys. Rev. *B1*, 3966 (1970) and Y. Kagan and M. I. Klinger, J. Phys. *C7*, 2971 (1974).
[20] W. KEHR, see Ref. 8, Vol. 1.
[21] H. SUGIMOTO and Y. FUKAI, Phys. Rev. *B22*, 670 (1980).
[22] D. E. EASTMAN, J. K. CASHION and A. C. SWITENDICK, Phys. Rev. Lett. *27*, 35 (1971) and F. Antonageli, A. Balzarotti, A. Blanconi, E. Burratini, F. Perfetti and N. Nistico, Phys. Lett. *55A*, 309 (1975).

[23] E. GILBERG, Phys. Stat. Sol. (b) *69*, 477 (1975).
[24] Y. FUKAI, S. KAZAMA, K. TANAKA and M. MATSUMOTO, Solid State Commun. *19*, (1976).
[25] See e.g. R. N. COTTS, in Ref. 8, Vol. 1.
[26] P. BRILL and J. VOITLÄNDER, Ber. Bunsenges, Phys. Chem. *77*, 1097 (1973) and private communication (1980).
[27] S. KAZAMA and Y. FUKAI, J. Less.-Common. Met. *54*, 25 (1977).
[28] R. G. BARNES, W. C. HARPER, S. O. NELSON, D. K. THOME and D. R. TORGESON, J. Less-Common Met. *49*, 483 (1976).
[29] M. CAMANI, F. N. GYGAX, E. KLEMPT, W. RÜEGG, A. SCHENCK, H. SCHILLING, R. SCHULZE and H. WOLF, Phys. Rev. Lett. *42*, 679 (1979).
[30] A. SCHENCK, Ref. 11, p. 445.
[31] F. N. GYGAX, A. HINTERMAN, W. RÜEGG, A. SCHENCK, W. STUDER and H. WEHR, Ref. 11, p. 479.
[32] F. N. GYGAX et al., to be published.
[33] F. N. GYGAX, A. HINTERMANN, W. RÜEGG, A. SCHENCK and W. STUDER, Solid State Commun. *38*, 1245 (1981).
[34] F. N. GYGAX, W. RÜEGG, A. SCHENCK, H. SCHILLING, W. STUDER and R. SCHULZE, Proc. of ICM 79, (München 1979), J.M.M.M. *15–18*, 1191 (1980).
[35] O. HARTMANN, E. KARLSON, L.-O. NORLIN and K. PERNESTÅL, Hyperfine Interactions *4*, 828 (1978).
[36] M. CAMANI, F. N. GYGAX, W. RÜEGG, A. SCHENK, H. SCHILLING, F. STUCKI and L. SCHLAPBACH, in *Recent developments in condensed matter physics*. Vol 2, Eds. F. T. Devreese et al. (Plenum Press, 1981).
[37] H. YASUOKA, R. HAYANO, N. NISHIDA, K. NAGAMINE, T. YAMAZAKI and Y. ISHIKAWA, Solid State Commun. *26*, 745 (1978).
[38] H. WEHR, K. KNORR, F. N. GYGAX, A. SCHENCK and W. STUDER, Phys Rev. B. *24*, 4041 (1981).
[39] J. M. CASSELS, T. W. O'KEEFFE, M. RIGBY, A. M. WETHERELL and J. R. WORMALD, Proc. Phys. Soc. *A*70, 451 (1957).
[40] K. M. CROWE, J. F. HAGUE, J. E. ROTHBERG, A. SCHENCK, D. L. WILLIAMS, R. W. WILLIAMS and K. K. YOUNG, Phys. Rev. *D5*, 2145 (1972).
[41] J. CHRISTIANSEN, H. E. MAHNKE, E. RECKNAGEL, D. RIEGEL, G. SCHATZ, G. WEBER and W. WITTHUHN, Phys. Rev. *C1*, 613 (1970).
[42] M. CAMANI, F. N. GYGAX, E. KLEMPT, W. RÜEGG, A. SCHENCK, H. SCHILLING, R. SCHULZE and H. WOLF, Phys. Lett. *77B*, 326 (1978).
[43] M. CAMANI, F. N. GYGAX, E. KLEMPT, W. RÜEGG, A. SCHENCK, H. SCHILLING, R. SCHULZE and H. WOLF, to be published in Phys. Rev. D.
[44] See e.g. A. ABRAGAM, *The Principles of Nuclear Magnetism*, Clarendon, Oxford (1970).
[45] J. H. VAN VLECK, Phys. Rev. *74*, 1168 (1948).
[46] P. F. MEIER, in Exotic Atoms '79, eds. K. M. Crowe, J. Duclos, G. Fiorentini, G. Torelli, Plenum, 1980.
[47] O. HARTMANN, Phys. Rev. Lett. *39*, 832 (1977).
[48] See e.g. J. WINTER, *Magnetic Resonance in Metals*, Clarendon, Oxford (1971).
[49] K. YOSIDA, Phys. Rev. *106*, 893 (1957).
[50] See e.g. D. W. DAVIES, *The Theory of the electric and magnetic properties of molecules*, John Wiley (1967).
[51] See e.g. W. M. MUELLER, J. P. BLACKLEDGE, and G. G. LIBOWITZ, *Metal Hydrides*, Chapter 6, Academic (1968).
[52] G. G. LIBOWITZ, *The Solid State Chemistry of Binary Metal* Hydrides, Chapter 1, Benhamin (1965).
[53] A. C. SWITENDICK, Ref. 8, Vol. 1, Chapter 5.
[54] A. C. SWITENDICK, Solid State Commun. *8*, 1463 (1970).
[55] J. S. FAULKNER, Phys. Rev. *B13*, 2391 (1976).
[56] D. A. PAPACONSTANTOPOULOS, B. M. KLEIN, J. S. FAULKNER, L. L. BOYER, Phys. Rev. *B18*, 2784 (1978).
[57] C. D. GELATT, H. EHRENREICH and J. A. WEISS, Phys. Rev. *B17*, 1940 (1978).
[58] P. SOVEN, Phys. Rev. *156*, 809 (1967).
[59] M. GUPTA and A. J. FREEMAN, Phys. Rev. *B17*, 3029 (1978).
[60] C. L. WILEY and F. Y. FRADIN, Phys. Rev. *B17*, 3462 (1978).
[61] H. KATAYAMA, K. TERAKURA and J. KANAMORI, Solid State Commun. *29*, 431 (1979).

[62] K. TERAKURA, J. Phys. F: Metal Phys. *7*, 1773 (1977).
[63] J. KANAMORI, H. K. YOSHIDA and K. TERAKURA, Ref. 11, p. 573.
[64] O. JEPSEN, R. M. NIEMINEN and J. MADSEN, Solid State Commun. *34*, 575 (1980).
[65] N. F. MOTT and H. JONES, *Metals and Alloys*, Oxford (1936).
[66] J. FRIEDEL, Philos, Mag. *43*, 153 (1952).
[67] L. C. R. ALDRED, Phys. Lett. *50A*, 73 (1974).
[68] B. D. PATTERSON and L. M. FALICOV, Solid State Commun. *15*, 1509 (1974).
[69] Z. D. POPOVIC and M. J. STOTT, Phys. Rev. Lett. *33*, 1164 (1974).
[70] S. PRAKASH, Phys. Lett. *61A*, 405 (1977).
[71] J. LINDHARD, Kgl. Danske Videnskab. Selskab. Mat.-fys. Medd. *28*, no. 8 (1954).
[72] K. S. SINGWI, M. P. TOSI, R. H. LAND and A. SJÖLANDER, Phys. Rev. *176*, 589 (1968).
[73] K. S. SINGWI, A. SJÖLANDER, M. P. TOSI and R. H. LAND, Phys. Rev. *B1*, 1044 (1970).
[74] J. HUBBARD, Proc. Roy Soc. A243, 336 (1957), Phys. Lett. *25A*, 709 (1967).
[75] L. I. SHAM, Proc. Roy Soc. *A283*, 33 (1965).
[76] P. VASHISHTA and K. S. SINGWI, Phys. Rev. *B6*, 875 (1972) and ref. therein.
[77] L. C. R. ALDRED, Phys. Lett. *46A*, 65 (1973).
[78] C. KITTEL, *Introduction to Solid State Physics*, Wiley (1971) p. 278 ff.
[79] P. F. MEIER, Helv. Phys. Acta *48*, 227 (1975).
[80] D. J. KIM, Phys. Lett. *96A*, 177 (1973).
[81] D. J. KIM, B. B. SCHWARTZ and H. C. PRADDAUDE, Phys. Rev. *B7*, 205 (1973).
[82] A. SJÖLANDER and M. J. STOTT, Phys. Rev. *B5*, 2109 (1972).
[83] P. BHATTACHARYYA and K. S. SINGWI, Phys. Rev. Lett. *29*, 22 (1972).
[84] P. HOHENBERG and W. KOHN, Phys. Rev. *136*, B864 (1964).
[85] W. KOHN and L. J. SHAM, Phys. Rev. *140*, A1133 (1965).
[86] U. VON BARTH and L. HEDIN, J. Phys. *C5*, 1629 (1972).
[87] A. K. RAJAGOPAL and J. CALLAWAY, Phys. Rev. *B7*, 1912 (1973).
[88] O. GUNNARSSON and B. I. LUNDQUIST, Phys. Rev. *B13*, 4274 (1976).
[89] J. FRIEDEL, Adv. Phys. *3*, 446 (1954). Nuovo Cim. Suppl. *7*, 287 (1958).
[90] L. HEDIN and B. I. LUNDQUIST, J. Phys. *C4*, 2064 (1971).
[91] C. O. ALMBLADH, U. VON BARTH, Z. D. POPOVIC and M. J. STOTT, Phys. Rev. *B14*, 2250 (1976).
[92] E. ZAREMBA, L. M. SANDER, H. B. SHORE and J. H. ROSE, J. Phys. *F7*, 1763 (1977).
[93] P. JENA and K. S. SINGWI, Phys. Rev. *B17*, 3518 (1978).
[94] M. RASOLT and D. J. W. GELDART, Phys. Rev. Lett. *35*, 1234 (1975).
[95] R. JOST, Helv. Phys. Acta *20*, 256 (1947).
[96] P. JENA, K. S. SINGWI and R. M. NIEMINEN, Phys. Rev. *B17*, 301 (1978).
[97] K. G. PETZINGER and R. L. MUNJAL, Phys. Rev. *B15*, 1560 (1977).
[98] R. L. MUNJAL and K. G. PETZINGER, Hyperfine Interactions *4*, 301 (1978).
[99] O. GUNNARSON, B. I. LUNDQUIST and J. W. WILKINS, Phys. Rev. *B10*, 1319 (1974).
[100] P. JENA, Hyperfine Interactions *6*, 5 (1979).
[101] P. F. MEIER, Hyperfine Interactions *6*, 29 (1979).
[102] R. M. NIEMINEN and M. MANNINEN, Hyperfine Interactions *6*, 25 (1979).
[103] M. MANNINEN and R. M. NIEMINEN, J. Phys. F: Metal Phys. *9*, 1333 (1978).
[104] C. O. ALMBLADH and U. VON BARTH, Phys. Rev. *B13*, 3307 (1976).
[105] N. W. ASHCROFT and D. C. LANGRETH, Phys. Rev. *155*, 682 (1967).
[106] W. V. EICHENAUER, Z. Metallkd. *59*, 613 (1968).
[107] P. JENA, F. Y. FRADIN and D. E. ELLIS, Phys. Rev. *B20*, 3543 (1979).
[108] E. ZAREMBA and D. ZOBIN, Phys. Rev. *B22*, 5490 (1980).
[109] M. T. BÉAL-MONOD and W. KOHN, J. Phys. Chem. Solids *29*, 1877 (1968).
[110] P. L. SAGALYN and M. N. ALEXANDER, Phys. Rev. *B15*, 5581 (1977).
[111] I am indebted to D. LL. WILLIAMS for advice on this.
[112] W. KOHN and S. H. VOSKO, Phys. Rev. *119*, 912 (1960).
[113] R. H. STERNHEIMER and H. M. FOLEY, Phys. Rev. *102*, 731 (1956).
[114] P. JENA, S. G. DAS and K. S. SINGWI, Phys. Rev. Lett. *40*, 264 (1978).
[115] G. A. BURDICK, Phys. Rev. *129*, 138 (1963).
[116] D. LL. WILLIAMS, private communication.
[117] B. L. JENSEN, R. NEWALD and D. LL. WILLIAMS, J. Phys. F *2*, 169 (1972) and R. Nevald, B. L. Jensen and P. B. Fynboo, J. Phys. F *4*, 1320 (1974).
[118] Y. FUKAI, Phys. Lett. *34A*, 425 (1971) and Y. Fukai and K. Watanabe, Phys. Rev. *B2*, 2353 (1970); Phys. Rev. *B10*, 3015 (1974).
[119] P. M. HOLTHAM and P. JENA, J. Phys. F *5*, 1649 (1975).

[120] A. MAINWOOD and A. M. STONEHAM, J. Less-Comm. Met. *49*, 271 (1976).
[121] A. MAINWOOD, thesis (AERE, Harwell, TP 684, 1976).
[122] H. ADACHI, S. IMOTO, T. TANABE and M. TSUKADA, J. Phys. Soc. Japan *44*, 1039 (1978).
[123] J. KELLER, in *Computational Methods for Large Molecules and Localized States in Solids*, eds. F. Hermann, A. D. McLean and R. K. Nesbett, p. 341, Plenum (1972) and refs. therein.
[124] J. KELLER, Hyperfine Interactions *6*, 15 (1979) and refs. therein.
[125] B. D. PATTERSON and J. KELLER, Hyperfine Interactions *6*, 73 (1979).
[126] J. KELLER and A. SCHENCK, Hyperfine Interactions *6*, 39 (1979).
[127] M. CASTRO, J. KELLER and H. SCHILLING, Hyperfine Interactions *6*, 43 (1979).
[128] J. KELLER, M. CASTRO and H. SCHILLING, submitted to J. Phys. F.
[129] D. P. HUTCHINSON, J. MENES, G. SHAPIRO and A. M. PATLACH, Phys. Rev. *131*, 1351 (1963).
[130] J. IMAZATO, Y. J. UEMURO, N. NISHIDA, R. S. HAYANO, K. NAGAMINE and T. YAMAZAKI, J. Phys. Soc. Japan *48*, 1153 (1980).
[131] J. E. KETTELER, W. L. SHANHOLTZER and W. E. VEHSE, J. Phys. Chem. Solids *30*, 665 (1969).
[132] T. KUSHIDA, J. C. MURPHY and M. HANABUSA, Sol. State Commun. *15*, 1217 (1974).
[133] G. FEHER and A. F. KIPP, Phys. Rev. *98*, 337 (1955).
[134] P. MONOD and S. SCHULTZ, Phys. Rev. *173*, 645 (1968).
[135] See R. T. SCHUMACHER and W. E. VEHSE, J. Phys. Chem. Solids *24*, 297 (1963).
[136] G. G. CARTER, L. H. BENNETT, D. J. KAHAN, *Metallic shifts in NMR, Part I*, Progr. Mat. Sci. Vol. 20 (Pergamon Press, 1977).
[137] L. D. FLESNER and S. SCHULTZ, Phys. Rev. *B14*, 4759 (1976).
[138] R. DUPREE and E. F. W. SEYMOUR, Phys. Kondens. Materie *12*, 97 (1970).
[139] G. L. DUNIFER, D. PINKEL and S. SCHULTZ, Phys. Rev. *B10*, 3159 (1974).
[140] D. PINKEL and S. SCHULTZ, quoted in Ref. 141.
[141] B. KNECHT, J. Low Temp. Phys. *21*, 619 (1975).
[142] J. A. KAECK, Phys. Rev. *175*, 897 (1968).
[143] P. JENA, T. P. DAS and S. D. MAHANTI, Phys. Rev. *B1*, 432 (1970).
[144] D. LUBZENS, M. R. SHANABURGER and S. SCHULTZ, Phys. Rev. Lett. *29*, 1387 (1972) and D. L. Randles, Proc. Roy, Soc. A *331*, 85 (1972).
[145] G. L. DUNIFER, M. R. PATTISON and T. M. HSU, Phys. Rev. *B15*, 315 (1977).
[146] E. BORCHI and S. DE GENNARO, Phys. Rev. *B5*, 4761 (1972).
[147] S. K. LAI, S. WANG and C. B. SO, J. Phys. F *8*, 883 (1978).
[148] W. KOHN and L. J. SHAM, Phys. Rev. *140*, A1133 (1965).
[149] S. H. VOSKO and J. P. PERDEW, Can. J. Phys. *53*, 1385 (1975).
[150] S. H. VOSKO, J. P. PERDEW and A. H. MACDONALD, Phys. Rev. Lett. *35*, 1726 (1975).
[151] J. F. JANAK, Phys. Rev. *B16*, 255 (1977).
[152] J. P. TIMBIE and R. M. WHITE, Phys. Rev. *B1*, 2409 (1970).
[153] See e.g. W. GISSLER, Ber. Bunsenges. Phys. Chem. *76*, 770 (1972).
[154] H. METZ, H. ORTH, G. ZU PUTLITZ, A. SEEGER, H. TEICHLER, J. VETTER, W. WAHL, M. WIGAND, K. DORENBURG, M. GLADISCH and D. HERLACH, Ref. 10, p. 271.
[155] M. BORGHINI, T. O. NIINIKOSKI, J. C. SONLIÉ, O. HARTMANN, E. KARLSSON, L. O. NORLIN, K. PERNESTÅL, K. W. KEHR and D. RICHTER, Phys. Rev. Lett. *40*, 1723 (1978).
[156] O. HARTMANN et al., Proc. Int. Symp. Elect. Struct. a. Prop. Hydrogen in Metals, Richmond, USA (1982), to be published.
[157] S. H. MAHANTI, L. TTERLIKKIS and T. P. DAS, in *Magnetic Resonance*, ed. C. K. Coogan et al. (Plenum Press, 1970),
[158] S. D. MAHANTI and T. P. DAS, Phys. Rev. *B3*, 1599 (1971). See comment on p. 37, Ref. 10.
[159] S. ESTREICHER, A. B. DENISON and P. F. MEIER, Ref. 11, p. 601
[160] E. ZAREMBA and D. ZOBIN, Phys. Rev. Lett. *44*, 175 (1980).
[161] E. GILBERG, Phys. Stat. Sol. (6) *69*, 477 (1975).
[162] Y. FUKAI, S. KAZAMA, K. TANAKA and M. MATSUMOTO, Solid State Commun. *19*, 507 (1976).
[163] J. S. KOUVEL and M. E. FISHER, Phys. Rev. *136*, A1626 (1964).
[164] S. ARAJS and R. V. COLVIN, J. Phys. Chem. Solids *24*, 1233 (1963).
[165] W. SÄNDER and J. VOIGTLÄNDER, Z. Physik *B31*, 13 (1978).
[166] J. A. SEITCHIK, A. C. GOSSARD and V. JACCARINO, Phys. Rev. *136*, A1119 (1964).
[167] A. B. DENISON, H. GRAF, W. KÜNDIG and P. F. MEIER, Helv. Phys. Act. *52*, 460 (1979).
[168] P. J. SEGRANSAN, W. G. CLARK, Y. CHABRE and G. C. CARTER, J. Phys. F: Metal Phys. *6*, L153 (1976).
[169] M. SHAHAM, J. BARAK, E. EL-HANANY and W. W. WARREN, JR. Phys. Rev. Lett. *39*, 570 (1977).
[170] J. KELLER and M. CASTRO, preprint, 1979.

[171] M. MANNINEN and R. M. NIEMINEN, J. Phys. F: *11*, 1213 (1981).
[172] P. JENA, Solid State Comm. *15*, 1509 (1974).
[173] P. JENA, C. L. WILEY and F. Y. FRADIN, Phys. Rev. Lett. *40*, 578 (1978).
[174] J. H. BREWER, K. M. CROWE, F. N. GYGAX, R. F. JOHNSON, B. D. PATTERSON, D. G. FLEMING and A. SCHENCK, Phys. Rev. Lett. *31*, 143 (1973).
[175] B. D. PATTERSON, A. HINTERMANN, W. KÜNDIG, P. F. MEIER, F. WALDNER, H. GRAF, E. RECKNAGEL, A. WEIDINGER and TH. WICHERT, Phys. Rev. Lett. *40*, 1347 (1978).
[176] I. I. GUREVICH, I. G. IVANTER, E. A. MELESHKO, B. A. NIKOLSKY, V. S. ROGANOV, V. I. SELIVANOV, V. P. SMILGA, B. V. SOKOLOV and V. D. SHESTAKOV, Sov. Phys. JETP *33*, 253 (1971).
[177] H. GRAF, E. HOLZSCHUH, E. RECKNAGEL, A. WEIDINGER and TH. WICHERT, Hyperfine Interactions *6*, 177 (1979).
[178] G. H. FRULLER and V. W. COHEN, Nucl. Data, Sect. *A5*, 433 (1969).